A FUZZY-LOGIC APPROACH FOR DEVELOPING A UNIVERSAL PERFORMANCE-BASED RATING SYSTEM FOR EVALUATION OF CONCRETE BRIDGES VIA VISUAL INSPECTION

by

Sahand Salili

Submitted in partial fulfillment of the requirements
for the degree of Master of Applied Science

at

Dalhousie University
Halifax, Nova Scotia

February 2024

Dalhousie University is located in Mi'kma'ki, the ancestral and unceded territory of the Mi'kmaq. We are all Treaty people.

DEDICATION

I dedicate this thesis to the unwavering love and support of four remarkable individuals who have been my pillars of strength throughout this academic journey. To my beloved mother, Soosan, whose boundless encouragement and sacrifices have nurtured my dreams and aspirations, I am forever grateful. To my father, Saeed, whose wisdom, guidance, and belief in my abilities have inspired me to persevere through challenges and reach for excellence, thank you from the depths of my heart. To all my friends in Halifax, whose constant companionship, understanding, and motivation have infused joy and camaraderie into every step of this pursuit.

TABLE OF CONTENTS

LIST OF TABLES

LIST OF FIGURES

ABSTRACT

Recognized for its cost-effectiveness and ease of implementation, visual inspection-based rating systems are widely adopted for preliminary bridge condition assessment. Periodic visual inspections of bridges are important to detect any potential deterioration and determine the need for further actions, such as rehabilitation or replacement. However, visual inspection only offers qualitative ratings of visible defects, such as concrete cracks and spalling, categorized into levels (e.g., moderate, or severe defects) given inspection guidelines. This makes it challenging to quantitatively discern the load capacity of bridges, especially because these ratings are subjective to the inspectors' judgement. Thus, traditional visual inspection-based rating systems fall short in providing quantitative measures for bridge performance, lowering the reliability of subsequent decisions, and deriving decision-makers towards more budget-consuming assessment techniques.

To address these gaps, this study proposes a new performance-based rating system that is called the universal performance rating system (UPRS) that enables decision-makers to estimate the remaining load capacity given visual data. The methodology includes fuzzy logic analysis with damage models and structural analysis to predict the remaining capacity of deteriorated elements, where the UPRS was coded in a MATLAB® platform. First, visible defects are mapped to losses in mechanical properties via fuzzy membership functions. The reduced properties are then entered into a numerical model to estimate the capacity, which is subsequently linked to the visible defects via a calibrated condition index. The end-product of this approach is performance graphs for the inspected elements, allowing engineers to map visual observations directly into capacity measures. For illustration, the proposed rating system is applied to: (I) a reinforced concrete bridge girder affected by corrosion, and (II) an in-service prestressed concrete bridge girder affected by corrosion and alkali-silica reaction (ASR) in Nova Scotia

LIST OF ABBREVIATIONS USED

AASHTO	American Association of State Highway and Transportation Officials
ACI	American Concrete Institute
AHP	Analytical Hierarchy Process
ASCE	American Society of Civil Engineers
ASME	American Society of Mechanical Engineers
ASR	Alkali-Silica Reaction
BDCI	Bridge Deck Condition Index
BIM	Building Information Modeling
BMS	Bridge Management System
BRIMS	Bridge Information Management System
CI	Condition Index
CSA	Canadian Standards Association
CSCE	Canadian Society for Civil Engineering
D1	Dead loads of factory-made components
D2	Dead load of cast-in-place concrete
D3	Dead load of asphalt concrete
DAF	Displacement Amplification Factor
FAHP	Fuzzy Analytical Hierarchy Process
FDDS	Fire Damage Diagnosis System
FEM	Finite Element Method
FHWA	Federal Highway Administration
FS	Fused Silica

FSE	Fuzzy Synthetic Evaluation
GPR	Ground-Penetrating Radar
I_D	Dynamic load allowance
IRT	Infrared Thermography
NBIS	National Bridge Inspection Standards
n	Maximum number of design lanes
NDT	Non-Destructive Testing
NS	Nova Scotia
L	Live load
$LLCF$	Live Load Capacity Factor
PC	Prestressed Concrete
R^2	Coefficient of determination
RBSM	Rigid Body Spring Modeling
RMSE	Root Mean Squared Error
RC	Reinforced Concrete
U	Resistance adjustment factor
VI	Visual Inspection
w_l	Lane width, mm
Δ_a	Allowable deflection, mm
Δ_{max}	Maximum deflection due to service loads, mm
f_{yp}	Yielding tensile strength of undamaged strands, MPa
$f_{yp}{}^*$	Yielding tensile strength of corroded strands, MPa
$E_{sp}{}^*$	Modulus of Elasticity of corroded strands, MPa

E_{sp}	Modulus of Elasticity of undamaged strands, MPa
L	Girder length, m
L_{ij}	Length of damage *i* at location *j,* mm
M_f	Moment due to factored loads, kN.m.
M_r	Ultimate moment resistance, kN.m.
R_r	Ultimate member resistance, kN.m. or kN
$r_{corrosion}$	The loss ratio of the cross-sectional area of the rebar due to corrosion
$r_{concrete}$	Ratio of compressive strength of damaged concrete to undamaged one
s_{bar}	Reinforcement spacing, mm
$U_{d,Damaged}$	Maximum displacement utilization ratio for damaged girder
$U_{d,Undamaged}$	Maximum displacement utilization ratio for undamaged girder
V_f	Shear due to factored loads, kN
V_r	Ultimate shear resistance, kN
w_{cr}	Crack width, mm
W_{ij}	Weight of the damage *i* at location *j*
$\alpha(t)$	Percentage area loss of strand by corrosion at time *t*
α_A	Load factor for force effects due to additional loads (creep, shrinkage, etc.)
α_D	Load factor for force effects due to dead loads
α_L	Load factor for force effects due to live loads
β	Reliability index
ε_{so}	Concrete strain at peak compressive stress
ε_{ASR}	ASR expansion, %

Ω	Slip compatibility factor
ρ	Loss ratio of strand area due to corrosion

ACKNOWLEDGEMENTS

Completing this thesis has been a journey of growth, learning, and perseverance, and I owe my deepest gratitude to the individuals who have been instrumental in its successful realization.

First and foremost, I extend my heartfelt appreciation to my esteemed supervisor, Dr. Fadi Oudah. His profound knowledge, insightful guidance, and unwavering encouragement have been invaluable throughout this research endeavor. Dr. Oudah's mentorship has not only enriched the quality of this thesis but also enhanced my understanding of the subject matter. I am truly honored to have had the privilege of working under his expert tutelage.

I would like to express my sincere thanks to Dr. Ahmed Abdelmaksoud for his significant contributions to this thesis and for being a co-author of our conference paper, "A Universal Performance-Based Rating System for Existing Structures via Fuzzy Logic: A General Framework," presented at CSCE 2023 (Moncton) and integrated into this thesis. His generous support, thoughtful insights, and expertise in the field have been indispensable. Dr. Ahmed's commitment to fostering academic growth and his dedication to sharing knowledge have made a profound impact on my research journey. I am deeply grateful for his guidance and encouragement.

To all the individuals mentioned above, you have played pivotal roles in shaping the outcome of this thesis, and I am honored to have had your unwavering support. Your contributions, including the use of our conference paper in this thesis, have made this journey meaningful and rewarding. Thank you for being part of this significant achievement.

CHAPTER 1 INTRODUCTION

1.1 BACKGROUND

Bridges are essential elements of the transportation infrastructure, facilitating the movement of people and goods. The deterioration of concrete bridge superstructures has emerged as a significant concern globally, including in Canada. Bridge superstructures that experience structural deterioration often display various signs of damage. These include but are not limited to corrosion of steel reinforcement due to factors such as high humidity, or penetration of chloride ions into the concrete deck that could cause concrete cracking, scaling, and spalling. These issues have a substantial impact on the overall integrity and performance of bridges, which necessitate careful consideration and the implementation of suitable remedial measures (Tee, et al., 1988). However, with resource limitations and the increasing number of deteriorating bridges, it is necessary to develop effective bridge assessments strategies for these remedial measures.

Nova Scotia (NS) has 4100 bridges, most of which are aging, and need regular maintenance (*Five Year Highway Improvement Plan,* 2023). The increasing number of aged and deteriorated bridges not only poses risks to public safety but also exerts a substantial economic burden on governments. In April 2022, NS planned to spend $500 million on road and safety improvement, and bridge maintenance was an important part of the plan. These significant financial resources were allocated toward bridge inspection, maintenance, and rehabilitation activities, diverting funds from other important infrastructure projects (*Five Year Highway Improvement Plan,* 2023). This investment in maintaining bridge infrastructure signifies the importance of ensuring that funding is prioritized where it is most needed for effective maintenance and repair efforts.

To keep roadways safe, governments developed periodic assessments and maintenance systems. Visual inspection (VI) is widely used as the first step of assessment in those systems given its simplicity, cost-effectiveness, and the absence of the need for special equipment or highly skilled personnel (Washer, 2001; ACI Committee 201, 2008). It provides a straightforward mean of assessing the surface condition of bridge components, facilitating regular inspection routines. Despite these benefits, VI is often subjective and imprecise, making it challenging to evaluate bridge conditions solely by relying on the VI report. Factors such as limited access to certain areas, or visual obstructions can hinder its effectiveness, underscoring the need for complementary inspection methods for a comprehensive assessment of bridge condition (Zambon *et al.*, 2019).

Another limitation of the existing VI methods is their qualitative results. Conducting a visual inspection could provide the decision-makers with some descriptive measures of the condition of the bridge. While the terms such as “severely damaged”, “moderately cracked”, and “wide spalling” are common in routine inspection tables, they are highly subjective to the inspectors’ experience and do not provide accurate numeric data for the decision-makers about the bridge’s level of safety or remaining capacity (ACI Committee 201, 2008). The goal of this study is to address the latter drawback of VI systems, specifically for concrete bridges. Reinforced and prestressed concrete bridges have formed the largest portion of the Canadian bridge population given their ability to withstand harsh environmental conditions (Building Bridges That Span a Lifetime; 2015). For example, in Ontario, more than 74% of bridges are concrete (*Ontario Data Catalogue, Bridge Condition*, 2021). In British Columbia, with a moderate climate, the number of concrete bridges is still more than the other types (timber and steel), with 46% of the bridges being built with concrete (Siddiquee and Alam, 2017). As such, deteriorated concrete bridges have been chosen as the focus of this research.

1.2 OBJECTIVES AND SCOPE

The objective of the thesis is to develop and implement a novel universal performance-based rating system (UPRS) that provides quantitative measures of the remaining strength and stiffness of deteriorated bridge superstructure based on the data obtained from VI and using fuzzy logic.

With the help of a unique mixture of fuzzy logic analysis, analytical deterioration models, and structural analysis, this rating system could build a direct link between the VI data and the performance of the damaged bridge. Employing analytical deterioration models, combined with fuzzy logic analysis, enables the mapping of the visible defects in bridge superstructure components into quantitative reductions in mechanical properties while addressing the uncertainties in the measurement of defects. The mapped properties can then be integrated with a numerical structural model to assess the post-defect performance (e.g., remaining capacity and increased deformation). Then, the performance-defect relationships are plotted, forming the core of the proposed performance-based rating system. Using these charts, engineers can swiftly estimate the reduction in the performance of the structure, facilitating informed decisions regarding further evaluation and retrofitting. This method serves as a valuable complement to existing visual inspection methods. It is important to note that this method is not intended as a substitute or alternative to detailed engineering analysis. Instead, it enhances the capabilities of visual inspection, offering a practical and efficient way to improve structural condition assessments without replacing the need for more sophisticated approaches when required. The scope of this research includes:

- Identify common deterioration mechanisms of steel reinforced concrete (RC) girders and review the deterioration processes for typical environmental exposure in Nova Scotia.

- Review the general concept of fuzzy logic and identify its feasibility for developing the proposed rating system.
- Develop the framework of the proposed rating system and code it in MATLAB.
- Apply the framework to generate user-friendly evaluation charts to assess the condition of in-service deteriorated RC girders and demonstrate its application on a real-life bridge assessment in Nova Scotia.

1.3 STRUCTURE OF THE THESIS

This thesis is organized into five chapters, each addressing specific aspects of the research. The following is an overview of the thesis structure:

Chapter 1. *Introduction*: This chapter sheds light on the importance of conducting this research. It also outlines the objective and scope of the thesis.

Chapter 2. *Literature Review*: This chapter offers a comprehensive overview of prior research studies related to visual inspection, as well as corrosion-induced and alkali-silica reaction (ASR)-induced damaged concrete bridges.

Chapter 3. *Development of UPRS Framework*: In this chapter, the methodology for developing the performance-based rating system is presented. The steps involved in integrating fuzzy logic into the assessment framework and the selection of performance indicators are also discussed.

Chapter 4. *A Demonstrative Example of Generating Performance Charts*: This chapter demonstrates the development of the performance charts using a deteriorated reinforced concrete (RC) bridge superstructure.

Chapter 5. *Case Study - Assessing a Damaged Prestressed Concrete Bridge Girder in Nova Scotia*: This chapter offers a case study investigating the condition assessment of a damaged prestressed concrete AASHTO bridge girder located in NS using the proposed rating method.

Chapter 6. *Conclusions and Recommendations*: This chapter provides a summary of the study, concludes the research results, and offers recommendations for further research in this field.

CHAPTER 2 LITERATURE REVIEW

2.1 GENERAL

This chapter presents an overview of the key concepts involved in the development of the proposed fuzzy-logic based performance rating system, followed by presenting the research gaps in literature. The concept review includes review of deterioration mechanisms in concrete bridges, visual inspection (VI) procedures in practice, and fuzzy logic mathematical expressions.

2.2 DETERIORATION MECHANISMS OF CONCRETE BRIDGE SUPERSTRUCTURES

Concrete bridges can be affected by various deterioration mechanisms, each contributing to the overall degradation of the structural integrity over time. In this research, two of the most common deterioration mechanisms are included in the proposed rating system and reviewed herein: (1) corrosion, and (2) alkali-silica reaction (ASR).

2.2.1 Corrosion of Steel Reinforcements and Prestressing Strands

Corrosion is the main and most budget-consuming deterioration mechanism in the bridge industry, significantly impacting the long-term performance and structural integrity of concrete bridge girders (El Aghoury and Galal, 2014; Zhang *et al.*, 2019). Corrosion occurs when the steel reinforcement embedded within the concrete is exposed to aggressive agents, such as moisture, chloride ions, and Oxygen. Over time, these agents penetrate the concrete cover, initiating a chemical reaction that leads to the formation of rust on the surface of the reinforcement. As the rust accumulates, the volume of the steel increases, exerting pressure on the surrounding concrete (Cabrera, 1996; Nürnberger, 2002).

In its initial stages, corrosion might be a hidden problem with little or no visually observable damage states. As the corrosion progresses, the expansion of the corrosion byproduct causes internal stresses in the concrete around the circumference of the reinforcing bar which, in turn, leads to the formation of corrosion induced cracking in concrete. These cracks worsen the integrity of the concrete where more severe consequences may manifest, including delamination and spalling of concrete (Dai *et al.*, 2019; Wang *et al.*, 2019; Oudah, 2023).

Corrosion-induced cracks are distinguished by their shape and color, as they most often follow the paths of embedded steel reinforcements, and are often accompanied by rust-colored staining, indicating the presence of iron oxide, a clear indicator of corrosion (Huang and Yang, 1997; Steware and Rosowsky, 1998). In certain scenarios, specialized tools like borescopes or ground-penetrating radar help inspectors obtain a more comprehensive understanding of the corrosion's extent. Additionally, selective cutting of concrete may be required to gain visual access to the embedded rebars and confirm that the damage is indeed attributable to corrosion (ACI Committee 201, 2008). Figure 1 and Figure 2 show examples of two deteriorated concrete girders of a prestressed concrete bridge in NS suffering from crack and spalling due to corroded prestressing strands (the performance charts of this bridge have been developed in Chapter 5).

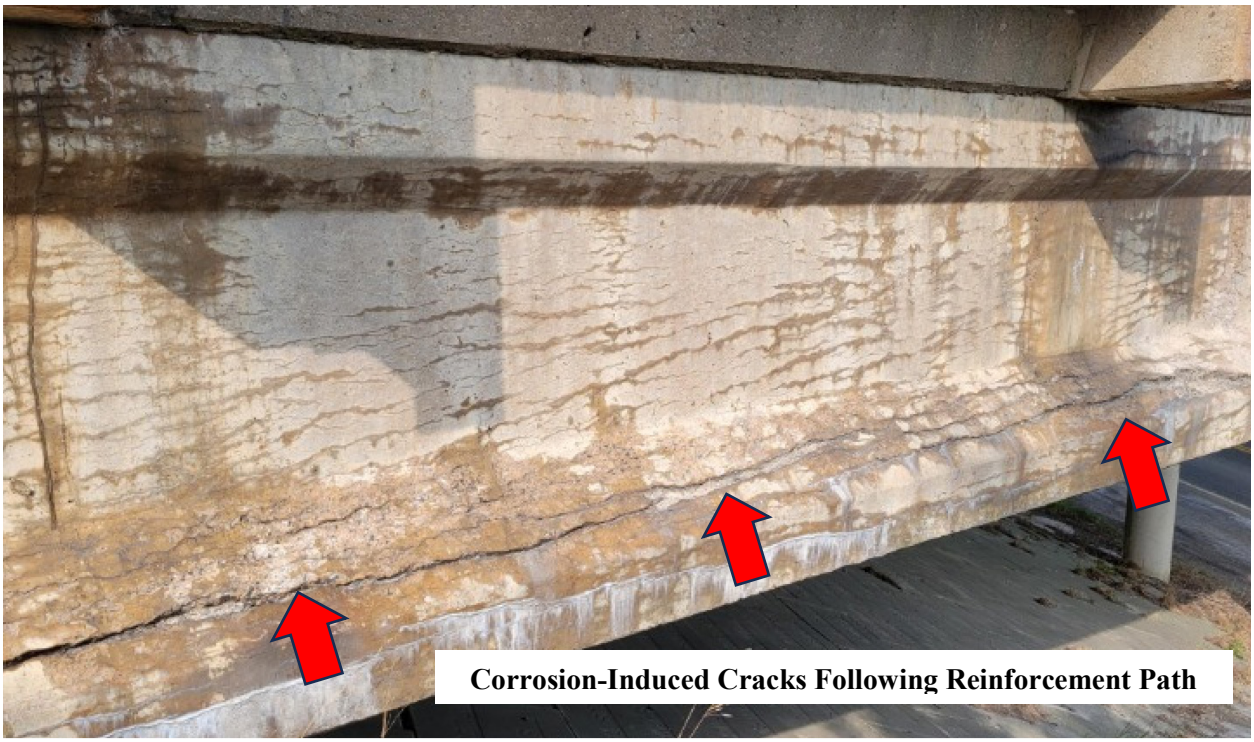

Figure 1- Corrosion-induced cracks on a prestressed bridge girder, NS

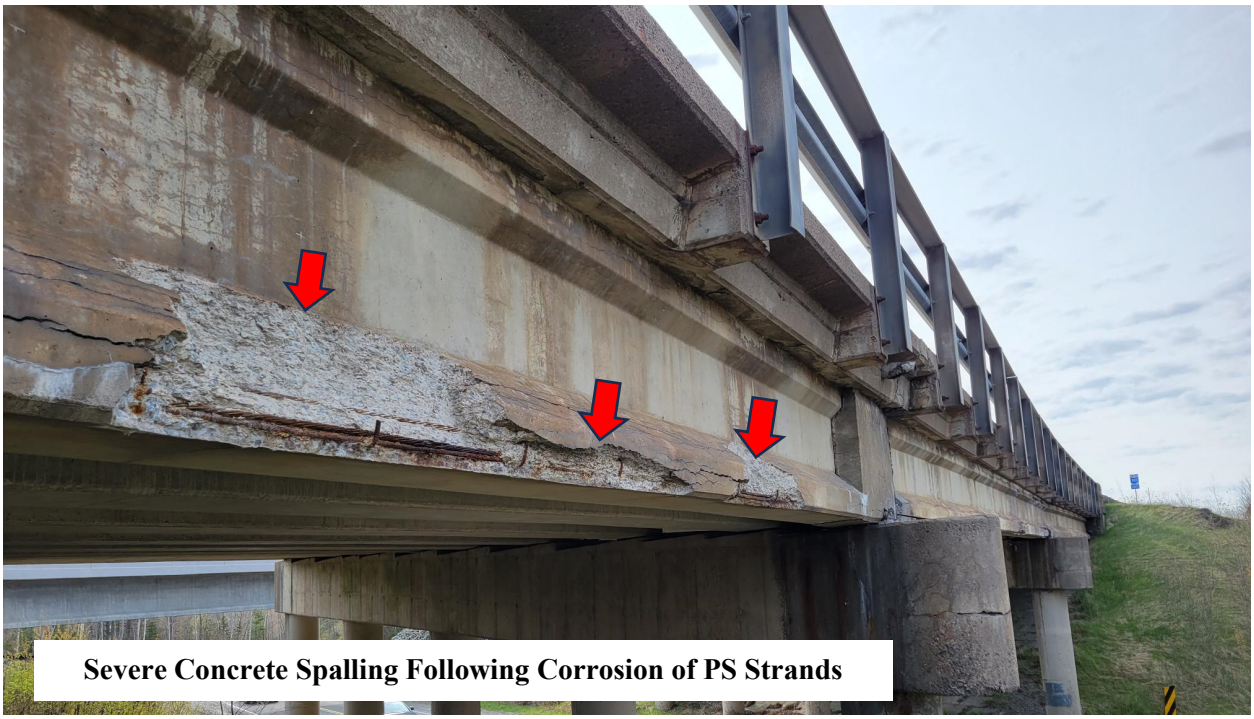

Figure 2- Severe corrosion-induced spalling of a prestressed concrete bridge girder, NS

Due to the importance of this subject, numerous research studies have concentrated on investigating the effects of corrosion on concrete structures. Cabrera (1996) investigated the influence of corrosion rate on the width and patterns of cracks in the concrete and the bond loss due to corrosion. Using accelerated corrosion, the relationships between corrosion level, crack width and patterns, bond loss, and the increase in beam deflection were quantified. It was found that a 9% corrosion resulted in a 50% increase in the beam deflection, and up to a 40% decrease in the concrete-reinforcement bond strength. It was concluded that both the deflection and the bond loss of a concrete beam affected by reinforcement corrosion have a linear relationship to the area percentage of corroded reinforcement.

Yuan and Guo (2020) proposed a method to adjust the steel reinforcing stress-strain relationship, effectively addressing the impact of bond loss caused by corrosion. Introducing a stress pseudo-strain curve, which incorporates the effect of corroded reinforcement's strain lag, suggested that the compatibility of the concrete and steel strains could be assumed to remain valid using that revised stress-strain relationship. To confirm their method, they conducted a seismic cyclic test on a non-uniformly corroded pier. A trial-and-error approach was recommended to identify the length of the plastic hinge, based on the amount of corroded portion of the pier involved.

In a separate study (Dai *et al.*, 2019), the effects of strand corrosion on the flexural capacity of prestressed concrete (PC) beams were examined through an analytical approach. This approach considered factors such as strand cross-section reduction, material deterioration, concrete cracking, and bond degradation, all of which collectively influenced the flexural capacity of corroded PC beams. The proposed systematic calculation procedure allowed for the determination of the ultimate flexural analysis using an iterative approach to account for strain incompatibility and was

subsequently compared with previous test results from various studies. It was found that for corrosion levels less than 7.3%, the bond degradation played a minor role in the ultimate flexural resistance. However, when the corrosion level doubled, bond loss surpassed the influence of strand area loss on the capacity. If strand area loss extended to 30%, bond loss, in this scenario, resulted in twice the damage compared to the area loss itself.

The effect of concrete-reinforcement bond loss due to corrosion, which can lead to strain incompatibility in PC beams, was studied experimentally by Wang et al (2017). The study presented an analytical model aimed at predicting the ultimate flexural capacity of corroded prestressed concrete (PC) beams subjected to strand corrosion. A normalized bond stress of one for corrosion levels below 6% and an exponential reduction in bond stress for corrosion levels exceeding 6% were recommended. A compatibility factor, **Ω**, ranging from 1.0 for corrosion loss of less than 13% and 0.66 for corrosion loss of up to 85% were recommended for calculating the total elongation of the strands in slip regions, where **Ω** is defined as:

$$\Omega = \frac{\varepsilon_p}{\varepsilon_{p,cal}} \quad (1)$$

where ε_p is the strand strain at the mid-span beam section and $\varepsilon_{p,cal}$ is the corresponding strand strain based on the plane section assumption method.

Corrosion of reinforcing rebars or prestressing strands can affect the material properties to the extent that the stress-strain relationship could be different than an undamaged one, with changes in the yielding and the ultimate stresses and strains, and also in the modulus of elasticity (Nürnberger, 2002; Ahmed *et al.*, 2006; Azad, *et al.*, 2007; Wu and Nürnberger, 2009; Mitra *et al.*, 2010; Vereecken *et al.*, 2021). Jeon *et al.* (2019) tested corroded low-relaxation prestressing strands (Grade 270) to find an equivalent material model for corroded strands. Experimental

testing indicated that the ultimate strain dropped from 7.5% for undamaged strands to 2% for strands with 5% corrosion loss. The strain dropped to 0.5% for strands with 20% corrosion loss. On the other hand, corrosion loss of 40% resulted in a drop of 45% in the ultimate stress of the strands (refer to Figure 3).

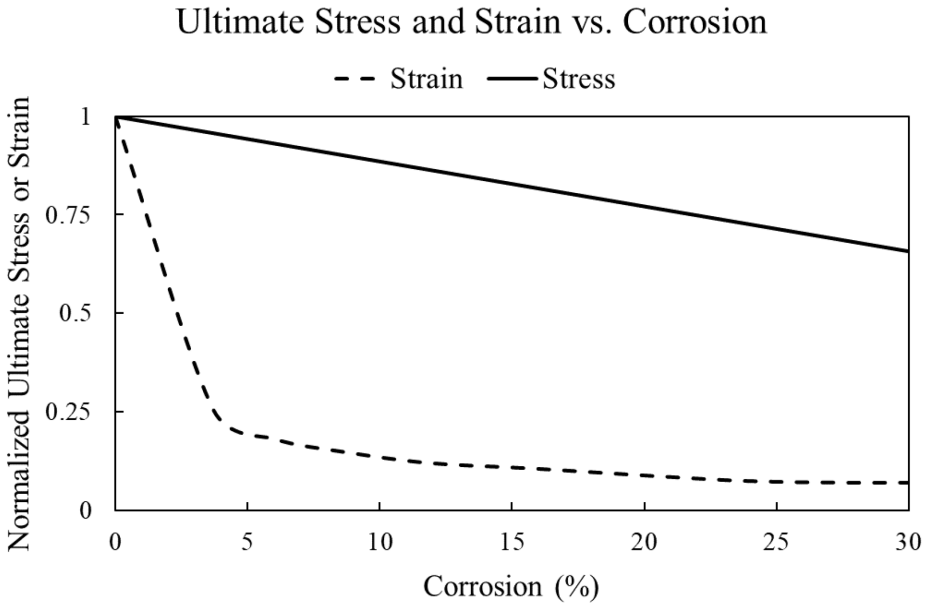

Figure 3- Normalized ultimate stress and strain of corroded prestressing strands (Jeon *et al.*, 2019)

Corrosion can also affect the ductility of reinforcements. A study by Lu *et al.* (2016) found that the strands with about 3% corrosion will loose about half of their energy absorption capacity. At a corrosion level of 12%, the strand loses its ductility entirely and behaves like a brittle material, with no post-yielding deformation capability (refer to Figure 4). In another experimental study on RC beams with corroded steel rebars (Parulekar *et al.*, 2020), a 15% reduction in ultimate flexural strength and a 35% decrease in ductility at 10% rebar corrosion has been reported. These findings emphasize the vital role of corrosion in structural degradation.

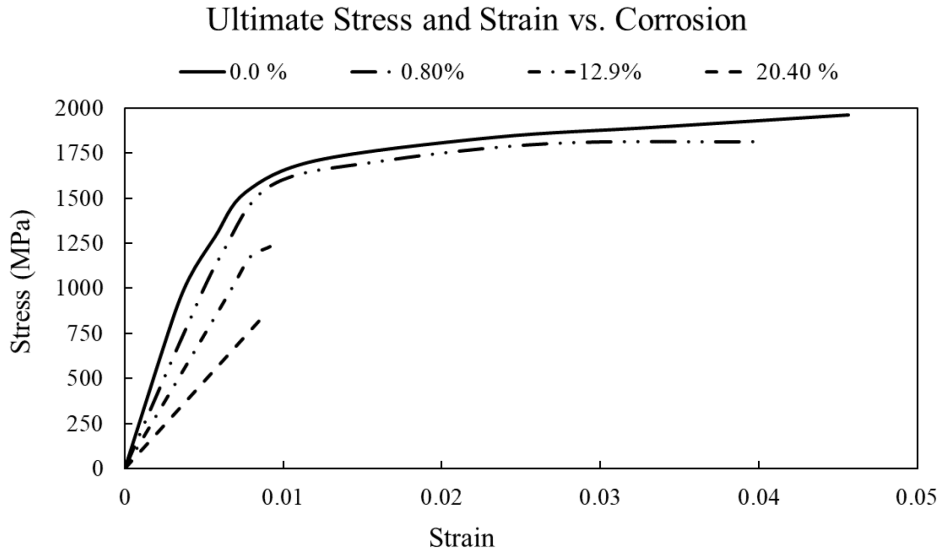

Figure 4- Stress-strain curves for strands with different levels of corrosion (Lu *et al.*, 2016)

2.2.2 Alkali-Silica Reaction (ASR)

Alkali silica reaction (ASR) is a chemical process that occurs within concrete structures when hydroxyl ions in the pore water of concrete interact with certain types of silica found in some aggregates (Jones and Clark, 1998; Karthik, *et al.*, 2020). This interaction produces a gel that has a unique characteristic: it readily absorbs water and swells. When this reaction intensifies, the gel's expansion exerts pressure on the surrounding concrete, leading to the development of micro-cracks and causing the concrete to expand internally (Mohammadi, *et al.*, 2020). To induce ASR in concrete, three key conditions must be met (Thomas *et al.*, 2011):

a. A significant presence of alkali hydroxides in the concrete's pore solution, primarily originating from the cement itself, which contains small quantities of sodium (Na^+) and potassium (K^+). In some instances, additional alkalis may come from various concrete components like aggregates, admixtures, or supplementary cementing materials, as well as external sources such as deicing salts or seawater.

b. An ample quantity of reactive minerals within the aggregate. Reactive minerals mostly encompass repeating units of silica such as ($SiO_2 \cdot nH_2O$), cristobalite, tridymite, volcanic glass, and different forms of microcrystalline, cryptocrystalline, and strained quartz.
c. A high level of moisture. ASR stops when the relative humidity within the concrete falls below 80 percent, but its activity intensifies as humidity levels rise from 80 percent to 100 percent.

In new constructions, ASR could be prevented by avoiding reactive aggregates or using low-alkali cement. In constructed structures affected by ASR, controlling moisture is the best solution (Thomas, *et al.*, 2013). Figure 5 shows the sequence of ASR-induced damage in concrete.

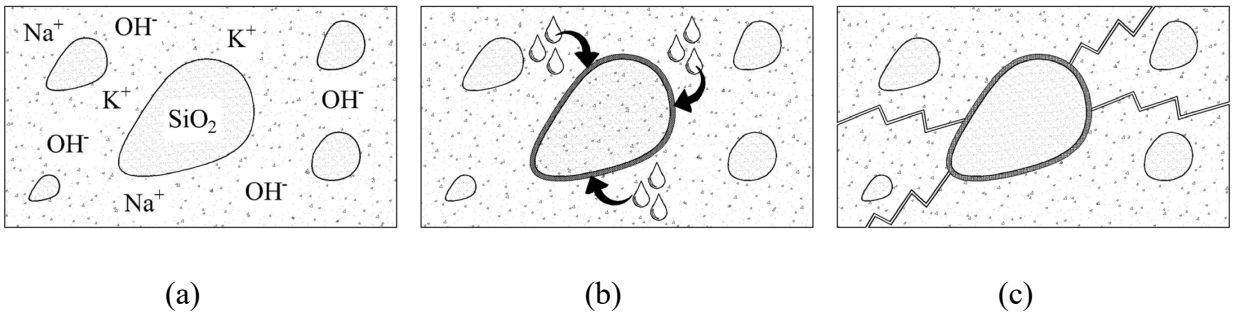

Figure 5- sequence of ASR propagate: (a) reaction between the Na^+, K^+, and OH^- from the cement paste and unstable silica from some types of aggregates, (b) formation of alkali-silica gel that absorbs water from the paste, and (c) expansion of the gel that leads to internal pressure to concrete and eventually, cracking (Thomas *et al.*, 2011)

Visual symptoms of ASR-affected concrete generally consist of (Jones and Clark, 1998; Thomas, *et al.* 2013):

a. Cracks that follow the structure's restraints
b. Expansion causing deformations, relative movements, and displacements, especially measurable in expansion joints
c. Concrete crushing
d. Extrusion of joint sealant material

e. Surface pop-outs and spalling

f. Surface discoloration and gel extrusion

A classic indication of ASR is map cracking, also known as pattern or alligator cracking (Thomas *et al.*, 2011) (Figure 6). These cracks are randomly distributed on the surfaces of concrete elements that can move freely in multiple directions. In some instances, discoloration is noted near the cracks, often caused by gel exudation in their vicinity. However, when expansion is hindered in one or more directions due to factors such as conventional reinforcement, prestressing, or external forces from abutments or nearby structures, the cracks become aligned with the direction of least confinement (Zahedi, et. al, 2022). For instance, in concrete pavements, where expansion is primarily limited in the longitudinal direction, cracks tend to align transversely. In reinforced concrete columns, vertical alignment is common due to restraint from the primary reinforcement and dead load. Meanwhile, in prestressed bridge girders, horizontal alignment is prevalent due to confinement by the prestressing tendons parallel to the beam's axis. Although map cracking is a possible sign of ASR, it should be accompanied by other symptoms, and chemical tests to confirm that the problem has been indeed caused by ASR (Lindgård *et al.*, 2012).

Due to the substantial impact of ASR on concrete structures, numerous researchers have been motivated to investigate the relationships between ASR and the material properties as well as the performance of structures affected by ASR. ASR intensity can be quantified by assessing ASR expansion, ε_{ASR}, which is the elongation of a specimen relative to its original length (Islam and Ghafouri, 2014). Esposito *et al.* (2016) studied the influence of ASR on the engineering properties of concrete, recording the changes for one year. The data was categorized into four reactivity classes based on the ASR expansion they had, namely, nonreactive ($\varepsilon < 0.05\%$), potentially reactive ($0.05\% < \varepsilon < 0.10\%$), reactive ($0.10\% < \varepsilon < 0.50\%$), and extremely reactive ($\varepsilon >$

0.50%), and they provided the results as normalized data, which means dividing the data for each category to the reference (nonreactive) case. In their experiment, the modulus of elasticity followed an exponential-shaped downward path, reaching 20% of its reference value with an expansion of 3%. They identified the elastic modulus to be the best indicator of ASR compared to other concrete properties, correlating to a curve with an error of less than 7%. On the other hand, the compressive strength of concrete was identified as the worst indicator of ASR, showing an upward trend in low expansions, and a downward one afterward. As a result, they suggested a piecewise linear fit for the compressive strength.

Sanchez *et al.* (2017) conducted a set of experimental tests on concrete samples built using different ASR-susceptible aggregates and tracked their changes over one year. They found that with an ASR expansion of 0.3%, the modulus of elasticity could be reduced by 30% to 70% depending on the aggregate type used. With the same level of expansion, compressive strength showed a 15-30% reduction.

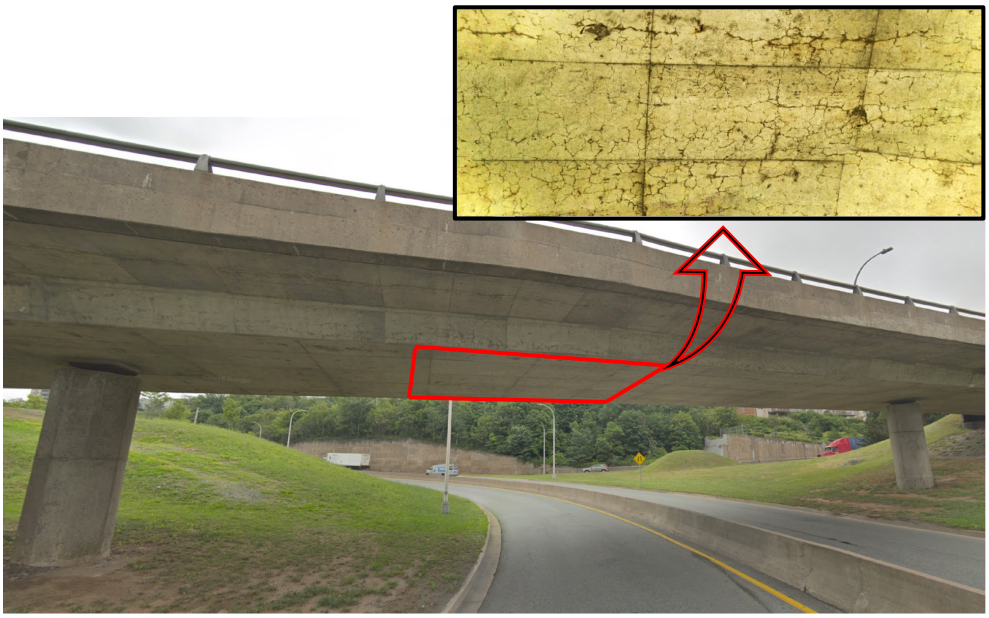

Figure 6- Map cracking on a bridge superstructure in Halifax, NS, possibly caused by ASR (Google Maps , 2021)

Another experimental study (Kongshaug *et al.*, 2020) examined the effect of the restraints on the amount of ASR expansion and hence, the change in modulus of elasticity and the compressive strength of concrete. During the tests, a restraint was added in one direction of some of the specimens to model the restraints that might be present in a real structural configuration. The results showed that the restraint decreased the ASR expansion, and consequently, reduced the decrease in the modulus of elasticity. They have also found a weak correlation between the expansion and the compressive strength, verifying previous studies in that regard. Figure 7 and Figure 8 illustrate the effect of ASR expansion on the compressive strength and the modulus of elasticity of concrete.

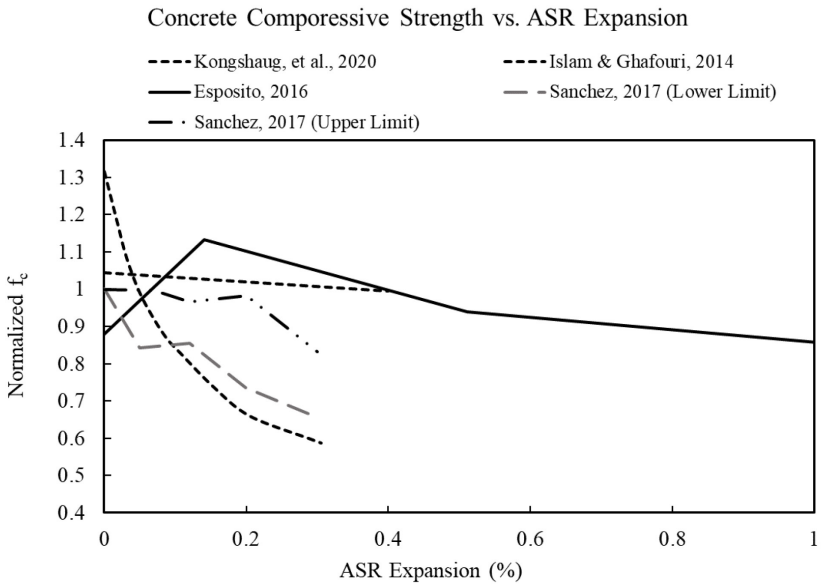

Figure 7- The concrete compressive strength vs. ASR Expansion

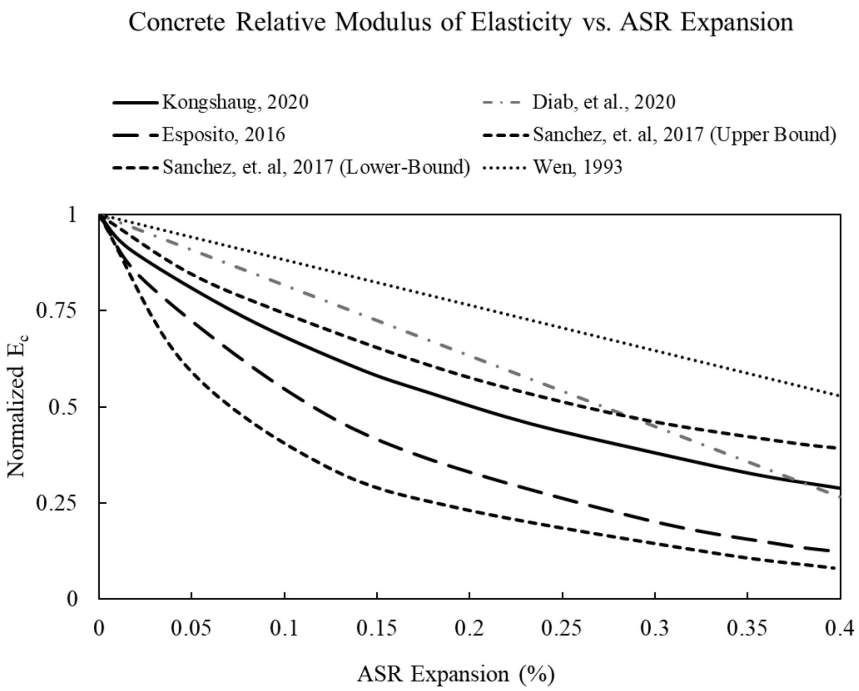

Figure 8- Concrete modulus of elasticity vs. ASR Expansion (Esposito *et al.*, 2016; Sanchez *et al.*, 2016; Diab, Soliman and Nokken, 2020; Kongshaug *et al.*, 2020; Yuan, Guo and Li, 2020)

2.3 VISUAL INSPECTION AND BRIDGE MANAGEMENT SYSTEM (BMS)

2.3.1 Guidelines and Codes for Conducting VI and BMS

Visual inspection (VI) is a fundamental pillar within bridge management systems (BMS), serving as a vital component in assessing the condition of bridges. This meticulous procedure involves a systematic examination of the bridge's visible surfaces, structural elements, and connections, with the primary objective of identifying early signs of deterioration (*Bridge Inspection & Maintenance System BIM Bridge Inspection and Maintenance*, 2008). These signs may encompass various issues, such as cracks, spalling, corrosion, and deformations.

To ensure the thoroughness and consistency of this assessment process, inspectors typically follow specific guidelines established by authoritative bodies. In the United States, the Federal

Highway Administration (FHWA) provides comprehensive guidelines for bridge inspection through the *National Bridge Inspection Standards (NBIS)*. In the USA, *the AASHTO Manual for Bridge Evaluation* (2018) serves as the main federal source of BMS rules. Chapter 3 and 4 of this manual develop general principles of BMS and VI, while for practical purposes, AASHTO's other book (*AASHTO Bridge Element Inspection Guide Manual*, 2010) provide valuable information about detailed element-by-element inspection methods. Most of the states have their own set of guidelines or codes for bridge inspection as well (i.e., Bridge Inspection Field Manual, Minnesota Department of Transportation, 2016). In addition to the aforementioned guides and codes, the *Guide for Conducting a Visual Inspection of Concrete in Service* (ACI Committee 201. , 2008a), provides valuable insights into various deterioration mechanisms and their observable manifestations on concrete surfaces.

In Canada, the Canadian Standards Association (CSA) provides the inspection and BMS general rules in the 14th chapter of *the Canadian Highway Bridge Design Code*, CSA S6 (CSA Group, 2019), while the detailed methodologies are left to the rules set by provinces based on their specific conditions (i.e., Alberta Transport's Bridge Inspection & Maintenance System (BIM)-Bridge Inspection and Maintenance, 2008)).

2.3.2 Common Practice in Conducting VI

Inspectors often employ a structured approach during VI, utilizing forms and tables designed to document their observations systematically (i.e., refer to tables in the AASHTO Bridge Element Inspection Guide Manual, 2010). These documents help ensure that critical details about the bridge's condition are not overlooked. They provide a standardized framework for recording the location and extent of any observed issues, along with their severity. This standardized data collection process is invaluable, as it allows for the comparison of bridge conditions over time and

between different structures. Consequently, adherence to these guidelines and the diligent completion of inspection forms and tables are essential aspects of an effective BMS.

To carry out VI effectively, various guidelines and standards offer specific methodologies for grading the apparent bridge condition. For instance, AASHTO employs a 10-point scale to grade the level of surface deterioration in different components of a bridge (*AASHTO Bridge Element Inspection Guide Manual*, 2010). This scale enables inspectors to assign numerical values to observed defects, helping them to quantify the severity and progression of deterioration. Furthermore, guidelines often provide inspection frequencies, indicating how often different types of bridges should be inspected based on their importance and usage, ensuring that inspections are conducted at appropriate intervals to monitor changes in condition effectively. Such guidelines and their meticulous application are vital in maintaining safe and reliable bridges within transportation networks. Canadian Bridge Inspection Manual (2010) defines 4 levels of damage states including "*very severe*", "*severe*", "*moderately damaged*", and "*minor damage*" for each damage state such as concrete crack and spalling based on the dimensions of damage. It also provides some guidelines for inspectors to identify hazardous damage, i.e., a severe crack due to overstress, from a relatively unimportant one caused by shrinkage.

2.3.3 Limitations of Current VI Practices

While visual inspection (VI) is a crucial tool in assessing the condition of bridges, it primarily relies on qualitative measures and visual indicators to identify signs of deterioration. One of the significant drawbacks of these conventional methods is their limited ability to provide quantitative information on the structural performance of the bridge. VI often detects visible signs of damage, such as cracks, spalling, or corrosion, but it falls short of delivering comprehensive insights into the structural integrity and load-carrying capacity of the bridge. These methods can identify the

presence of issues but may not accurately quantify their severity or their impact on the bridge's overall performance. Consequently, relying solely on qualitative measures can result in a lack of precise data necessary for making informed decisions about maintenance and rehabilitation strategies, potentially leading to suboptimal resource allocation and management practices within bridge management systems.

2.4 FUZZY LOGIC THEORY

Fuzzy Logic Theory is a mathematical framework that deals with uncertainty and imprecision in decision-making processes. First proposed by Prof. Lotfi A. Zadeh in his famous article Fuzzy Sets (Zadeh, 1965), it provides a mean to handle information that is not easily quantifiable. Fuzzy logic allows for the representation and manipulation of vague and ambiguous concepts, enabling more nuanced reasoning and decision-making in complex systems.

Unlike traditional binary logic, which relies on crisp boundaries of true and false, fuzzy logic introduces the concept of partial truth. It acknowledges that many real-world phenomena exist in degrees or shades of truth, rather than strict black-and-white categories. Fuzzy logic provides a way to express and reason with this inherent fuzziness, allowing for more realistic modeling of uncertain or subjective information. At the core of fuzzy logic is the notion of fuzzy sets, which extend the traditional concept of sets by assigning membership degrees to elements. These membership degrees represent the degree of belongingness of an element to a fuzzy set, reflecting the level of truth or relevance. Fuzzy logic also utilizes linguistic variables and fuzzy rules to capture and manipulate knowledge in a human-like manner. The strength of fuzzy logic lies in its ability to handle complex and uncertain systems by incorporating expert knowledge and fuzzy reasoning. It has found applications in various fields, including control systems, artificial

intelligence, decision support systems, and the assessment of superstructures.

2.4.1 Definitions

A definition of a fuzzy set can be formulated as follows: In a space of points (objects) denoted as **X**, with a generic element *x* representing a point in **X**, **X** can be expressed as $\mathbf{X} = \{x\}$. Within this space, a fuzzy set (class) **A** is characterized by a membership function, denoted as $f_A(x)$, which assigns a real number in the range of [0,1] to each point in **X**. The values of $f_A(x)$ at each point, *x* is indicative of the degree of membership of *x* in set **A**. Therefore, the closer the value of $f_A(x)$ is to 1, the higher the degree of membership of *x* in **A**. In other words, the more certainty leads to values of $f_A(x)$ being closer to one, while lower levels of certainty lead to the value of $f_A(x)$ approaching zero (Zadeh, 1965).

As an example, consider a bridge girder assessment report with crisp numbers of zero to 10 representing the level of damage (zero for no damage and 10 for near-collapse damage). One could also assign a level of certainty to each damage level given a bridge scenario ranging from zero to one. Now, if the girder is assessed as "in good shape", the inspector could be more confident that the level of damage is near zero (no damage), and not near 10 (highly damaged). The opposite is true when an inspector sees a near collapse case, where there is more certainty that the high damage levels are correct and not the opposite. Figure 9 shows the idea of "strong" and "weak" support, where strong support means a high level of confidence that a specific outcome is true and the opposite.

While a *binary universe* covers just outcomes of either zero or one, the fuzzy universe accepts the whole range of [0,1]. In this regard, crisp set theory deals with the clear classification of whether something belongs to a precisely defined set or not, and this is achieved through binary

statements (Figure 10-(b)). Fuzzy sets can be considered a generalization form of crisp set theory (Figure 10-(a)), while they could be continuous as well (Figure 10-(c)). A bridge, for example, could be either steel or concrete. One could define two (or more) crisp nonfuzzy sets of **A** and **B** representing "steel bridges" and "concrete bridges", and a bridge could be a member of set **A**, or not (associated with $\mu_A = 1$ or $\mu_A = 0$, respectively). On the other hand, some ideas in engineering are more vague, judgmental, or a matter of personal opinion (Brown et al. (1983). For example, one could say a bridge is in "poor condition". The subset "poor condition" is fuzzy and imprecise; thus, it cannot be assigned to an exact binary set of zero or one.

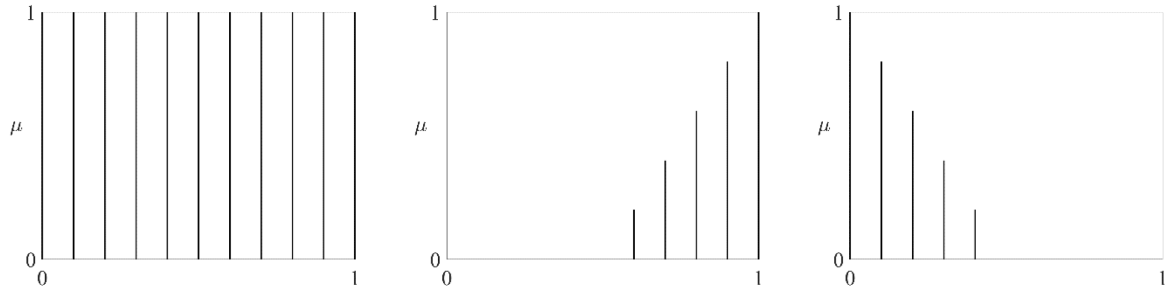

(a) Fuzzy universe (b) Strong support (c) Weak support

Figure 9- Discrete Fuzzy Diagrams (Brown *et al.*, 1983)

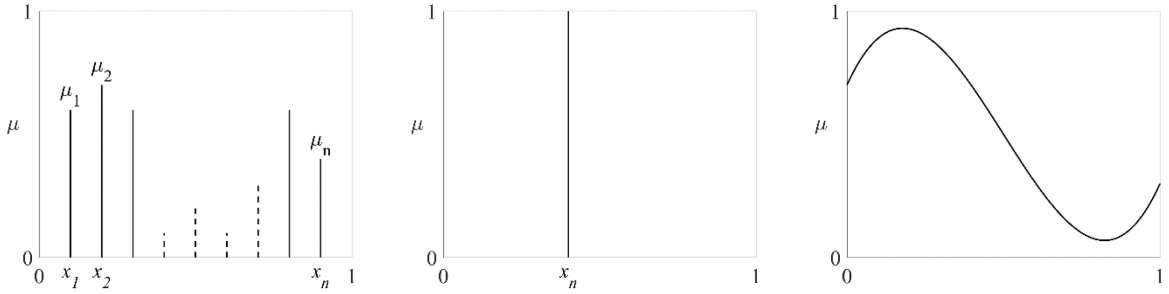

(a) Fuzzy set F (b) Crisp set F (c) Continuous fuzzy set F

Figure 10- Demonstrations of Fuzzy and Crisp Sets (Brown *et al.*, 1983)

For illustrative purposes, Figure 11 presents a simplified representation of how people describe the water temperature of a swimming pool using fuzzy language expressions. These three linguistic

expressions for temperature rating are: "cold," "warm," and "hot." While individuals generally have a sense of these expressions and the approximate temperature ranges associated with them, they are inherently subjective and imprecise.

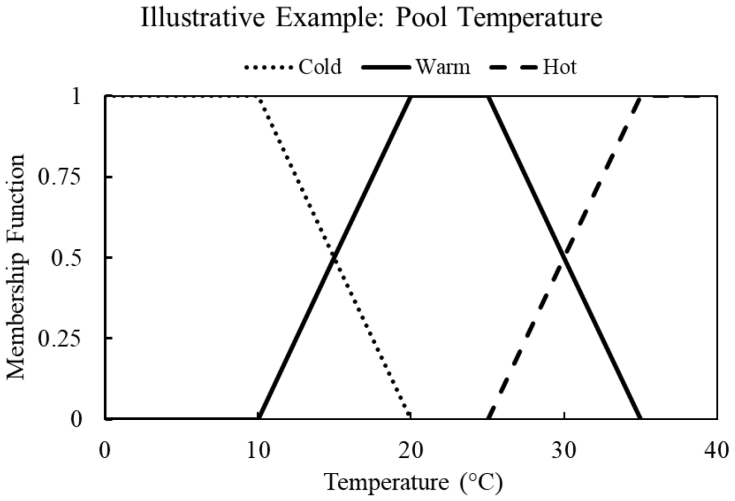

Figure 11- An illustrative example of fuzzy logic usage.

2.4.2 Algebraic Operations on Fuzzy Sets

Zadeh (Zadeh, 1965) defined several mathematical operations that can be applied to fuzzy sets as follows. The complement of a fuzzy set *A*, denoted by *A'*, is defined by

$$f_{A'} = 1 - f_A \tag{2}$$

A is *contained* in B if and only if $f_A \leq f_B$, or

$$A \subset B \iff f_A \leq f_B \tag{3}$$

The *union* of two fuzzy sets f_A and f_B is also a fuzzy set *C*, and is defined as

$$f_C(x) = Max\,[f_A(x), f_A(x)], \qquad x \in X \tag{4}$$

The intersection of two fuzzy sets A and B is a fuzzy set C, written as $C = A \cap B$, defined as:

$$f_C(x) = Min\,[f_A(x), f_A(x)], \qquad x \in X \tag{5}$$

The *algebraic product* of A and B is denoted by AB and is defined by

$$f_{AB} = f_A f_B \tag{6}$$

The *algebraic sum* of A and B is denoted by $A + B$ and is defined by

$$f_{A+B} = f_A + f_B \tag{7}$$

The algebraic sum is meaningful only when $f_A + f_B \leq 1$ is satisfied for all x.

The *absolute difference* of A and B is denoted by $|A - B|$ and is defined by

$$f_{|A-B|} = |f_A - f_B| \tag{8}$$

2.4.3 Fuzzy Logic Theory in Structural Engineering

Modeling deterioration, fire, earthquake, and other similar complex random phenomena has been successfully approached by researchers using fuzzy logic to capture the uncertainty and imprecision inherent in these processes. Markiz and Jrade (2018) used fuzzy logic to address the challenges associated with evaluating bridge conditions and deterioration. Their study focused on integrating fuzzy logic decision support into a Bridge Information Management System (BrIMS) at the conceptual stage of bridge design. This innovative approach aimed to forecast bridge deteriorations and effectively prioritize maintenance, repair, and replacement (MR&R) decisions.

Abdelmaksoud *et al.* (2022) introduced a novel methodology aimed at enhancing bridge management systems (BMSs) by addressing the limitations associated with probabilistic analysis. BMSs traditionally rely on deterioration models derived from probabilistic analyses of field inspection data, which primarily account for aleatoric uncertainty while overlooking epistemic uncertainty tied to subjective or imprecise data. This research recognized the need to bridge this gap and proposed a BMS-compatible approach. Their innovative methodology combines logistic regression to capture aleatoric uncertainty and fuzzy set theory to address epistemic uncertainty.

In particular, the researchers employed membership functions to model subjective or imprecise data, such as bridge condition ratings, as continuous variables rather than discrete values. These continuous variables were then integrated into logistic regression analysis, resulting in logistic models with fuzzy coefficients. What sets this approach apart is its ability to predict a range of possible future bridge conditions, as opposed to providing a discrete condition assessment.

In novel research, Omar *et al.* (2017) introduced an innovative approach to bridge condition rating that sought to mitigate the inherent uncertainties associated with traditional visual inspection reports. To address the challenges resulting from uncertainties of conducting the visual inspection on bridges, the researchers incorporated non-destructive testing (NDT) technologies, such as infrared thermography (IRT) and ground-penetrating radar (GPR), alongside visual inspection, providing a more comprehensive and precise assessment of concrete bridge decks. What makes this method unique is that it utilizes fuzzy math to combine data from different sources. The fuzzy synthetic evaluation (FSE) approach was employed to convert measured defects into fuzzy condition categories. These fuzzy categories were then combined to formulate an overall bridge deck condition index (BDCI). To identify the parameters influencing the integration process, the research team sought input from experienced bridge engineers, benefiting from their extensive knowledge and intuition. The developed rating procedure was put to the test through a case study involving a full-scale reinforced concrete bridge deck. The results of this study highlighted the limitations of relying solely on visual inspection, as such assessments could either overestimate or underestimate the true condition index of a bridge deck.

Andric´ and Lu (2016) introduced a pioneering approach to address the escalating challenges posed by disasters worldwide. In their research, a novel framework for disaster risk assessment that combines the Fuzzy Analytical Hierarchy Process (FAHP) with fuzzy knowledge

representation and fuzzy logic techniques was proposed. A thorough survey of collapsed bridges over the past few decades, identifying potential hazards, was conducted to serve as a basis for the proposed risk assessment framework. FAHP was employed as a systematic, accurate, and effective means of ranking risk factors, surpassing the limitations of the traditional Analytical Hierarchy Process (AHP). Various risk indicators, probabilities of occurrence, potential impacts of disasters, and their consequences, drawing on expert opinions were studied to compute bridge risk, considering the various risk factors and their associated parameters. The approach was proven to be practical and efficient, enabling quick and reliable multi-hazard risk analysis and assessment of bridges.

Meyyappaq et. al (no date) used the fuzzy clustering technique to model uncertainties associated with data collected from bridge health monitoring sensors. Marano and Quaranta (2008) defined the basics for using fuzzy logic in structural optimization. Nieto-Morote and Ruz-Vila (2011) modeled subjective judgment in construction projects with the help of fuzzy logic, and Cho et. al. (2017) developed a novel fire damage diagnosis system (FDDS) based on fuzzy theory.

2.5 RESEARCH GAP

The following outlines identified gaps based on a comprehensive review of existing literature. This review encompasses both existing codes and standards in bridge assessments and conducted research in this field.

Existing codes and standards in bridge assessments offer valuable guidance on structural inspections and evaluation criteria. However, a significant gap within these documents is the absence of specific provisions for conducting quantitative performance assessments based on visual inspection data. These codes predominantly emphasize qualitative assessments,

categorizing defects into states like minor, moderate, or severe, without providing a clear methodology for deriving quantitative estimates of structural performance. While visual inspections yield valuable data such as crack width, quantity, location, or the extent of reinforcement corrosion, these critical details often remain underutilized due to the lack of guidance on how to further translate them into meaningful quantitative assessments.

In the realm of bridge engineering and material degradation modeling, significant progress has been made by researchers to understand how visual damage symptoms, such as crack width, relate to crucial material properties, i.e. compressive strength, modulus of elasticity, and bond loss. However, what remains absent is the integration of this knowledge into the visual inspection. Furthermore, while fuzzy logic has found valuable applications in bridge assessment, it has been mostly used to address uncertainties in decision-making processes or risk assessment of bridges. This untapped potential is a stark gap in current research efforts, as the fusion of fuzzy logic with VI could serve as a powerful tool for accommodating and effectively mitigating the inherent vagueness and imprecision often encountered in visual inspection data. This disconnect between material degradation modeling and visual inspection, alongside the untapped potential of fuzzy logic, calls for focused attention and further exploration in the field. To address this gap, this research proposes a novel *universal performance-based rating system* by integrating fuzzy logic and deterioration models. This combined approach aims to provide a more robust and precise estimation of the remaining capacity of deteriorated structures, thereby enhancing the effectiveness of structural assessments and maintenance decision-making. Deterioration models predict the reduction in capacity by using formulas that relate qualitative damage states and uncertain quantitative visual data to material properties, while fuzzy logic effectively manages the uncertainties inherent in such predictions.

CHAPTER 3 DEVELOPMENT OF UPRS FRAMEWORK

3.1 GENERAL

In the quest to establish a universal performance-based rating system (UPRS) for deteriorated structures using fuzzy logic, this chapter introduces the comprehensive methodology driving this research initiative. Each component within the framework of analysis (methodology) plays a pivotal role in constructing structural performance charts, which can be applied to various types of structures. However, this study focuses on its implementation within the context of corrosion- or ASR-induced damage in steel-reinforced and prestressed concrete bridge girders. The framework was developed using an integrated fuzzy logic approach and programmed in MATLAB® environment. Features of the developed framework and computer code include:

- Structural analysis for modeling and evaluating simply-supported bridge girders (both reinforced and prestressed) and assessing the remaining capacities at various levels of deterioration.
- Material degradation models capable of establishing a connection between visual damage indicators and the material properties, including the properties of reinforcing and prestressing steels, and the concrete-reinforcement bond loss due to corrosion and ASR.
- A random damage model generator that can produce randomly generated damaged girders, with different damage locations and intensities.
- A fuzzy logic engine, advanced in fuzzifying damage states and associating them with relevant material properties, and at the final stage, able to defuzzify the results.
- The structural performance chart generator

3.2 STRUCTURAL PERFORMANCE CRITERIA

The first step in the methodology is determining the performance criteria based on which the investigated structure is to be assessed. These criteria may pertain to specific limit states relevant to the type of the structure or its intended use. For instance, a typical concrete girder could be assessed for its ultimate limit state (i.e., flexural and shear capacity) and the serviceability limit state (i.e., deflection limitations), based on a specific design standard. In this study, the utilization ratios (i.e., the ratio of the ultimate load to the factored resistance) have been used as the representative of the structural performance. One can define the utilization ratios of flexure, shear, and deflection of a girder as follows:

$$U_M = \frac{M_f}{M_r} \tag{9}$$

$$U_S = \frac{V_f}{V_r} \tag{10}$$

$$U_D = \frac{\Delta_{max}}{\Delta_a} \tag{11}$$

where,

M_f = moment due to factored loads;

M_r = ultimate moment resistance;

V_f = shear due to factored loads;

V_r = ultimate shear resistance;

Δ_{max}= maximum deflection due to service loads; and,

Δ_a= the allowable deflection.

The initial values for the utilization ratios at any location (x) along the girder can be calculated

based on the pre-damage girder capacities (M_{ro}, V_{ro}) and maximum deflection (Δ_{max-o}), in which $0 \leq x \leq L$, and L is the length of the girder under assessment.

3.3 CRISP DAMAGE STATES AND MEMBERSHIP FUNCTIONS

A fuzzy logic model of a defect consists of membership function(s) describing the uncertainty in the measurement of this defect during inspections. To develop a fuzzy model, one first needs to define the crisp damage states. As this study focuses on two damage models in concrete structures, namely corrosion and ASR, the crisp damage states have been defined based on crack width and ASR expansion, respectively. The expansion resulting from ASR is typically measured by assessing the increase in concrete specimen length over time as a key indicator of the reaction's progress. Table 1 and Table 2 present the discrete damage states for crack width and ASR expansion in this study.

Given the subjective nature of inspections, precise boundaries between these damage states could not be precisely identified by inspectors on-site. Consequently, an overlapping region has been incorporated to denote the inherent uncertainty (fuzziness) in the defect's measurements. As the uncertainties associated with the inspection increase with the increase in damage severity, the width of overlapping is assumed to increase linearly up to ±20% at the very severe damage state (Abdelmaksoud, *et al.* 2023). Table 1 represents the membership functions defined as a function of the crack width and the ASR expansion for four different damage states.

Table 1- Crisp damage states vs. crack width (Andrade *et al.*, 2016; Tahershamsi *et al.*, 2017)

Severity of damage	Crack width (mm)
Light	Less than 0.5
Medium	0.5 to 1.0
Severe	1.0 to 2.0
Very severe	More than 2.0

Table 2- Crisp damage states vs. ASR Expansion (Diab, *et al.*, 2020; Kongshaug *et al.*, 2020)

Severity of damage	ASR Expansion (%)
Light	Less than 0.1
Medium	0.1 to 0.2
Severe	0.2 to 0.4
Very severe	More than 0.4

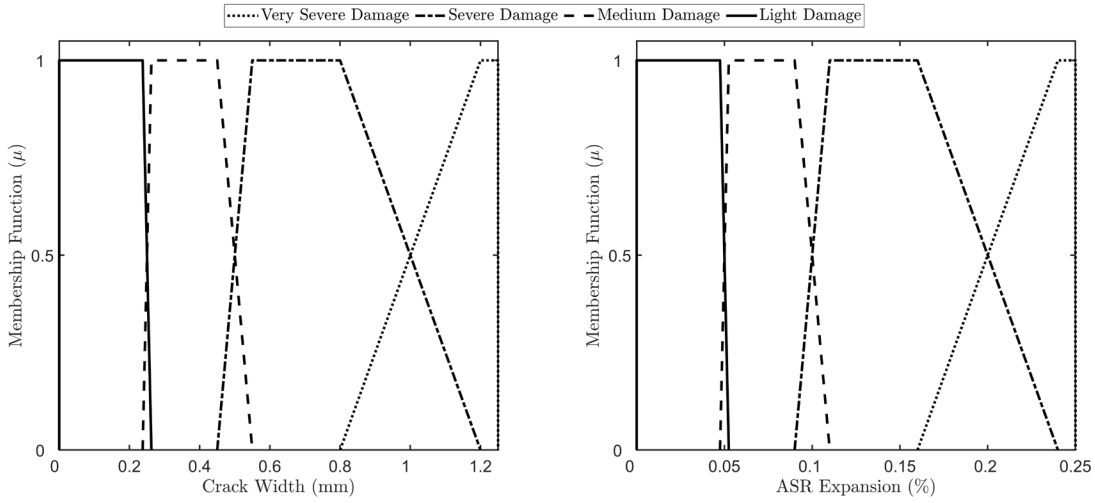

Figure 12-Membership functions of different levels of crack severity

3.4 RANDOMLY-GENERATED DAMAGE MODELS

It is critical to evaluate the impact of a broad spectrum of potential damage scenarios, varying in both severity and location along the girder. Subsequently, a performance-damage relationship can be established through regression analysis. With this goal in mind, *'n'* damage distributions have been built. In this regard, the UPRS framework (interchangeably referred to as the platform) picks a randomly selected mesh and then applies damage of random severity. Furthermore, it extends this damage to neighboring meshes, creating a three-dimensional representation with slightly reduced severity in each direction. Increasing the value of *n* enhances the accuracy of the results, leading to a better curve fit.

The severity of damage is categorized into four distinct crisp limit states, as discussed in section 3.3. In addition to this, the locations of the randomly generated damage have been classified based on their specific influence on the structural elements. In this particular study, corrosion-induced cracks, for instance, are divided into three vertical zones: (a) 'top damage', which primarily impacts negative moment reinforcements; (b) 'bottom damage', affecting positive moment reinforcements; and (c) 'side damage' targeting mainly shear reinforcements.

3.5 MATERIAL DEGRADATION MODELS

The platform leverages material degradation models to estimate the material properties of concrete, steel reinforcements, and prestressing strands, as well as the concrete-reinforcements bond loss, given the visually observable damage symptoms. Damage due to corrosion, ASR, and a combination of them have been addressed. The following section outlines these models employed within the platform for this purpose.

3.5.1 Properties of Corrosion-Induced Damaged Concrete

The following simplified expression relates the residual strength of the concrete to the observed crack widths (Coronelli and Gambarova, 2004):

$$r_{concrete} = 1 - \frac{k \times \frac{1}{s_{bar}} \times w_{cr}}{k \times \frac{1}{s_{bar}} \times w_{cr} + \varepsilon_{so}} \quad (12)$$

where, $r_{concrete}$ is the normalized concrete compressive strength, w_{cr} is the crack width, s_{bar} represents the spacing between reinforcements, the shape factor, *k*, is assigned a value of 0.1, and ε_{so} denotes the strain at peak compressive stress, typically considered as 0.002.

Corrosion-induced cracks in concrete tend to extend to a depth approximately twice that of the concrete cover thickness, resulting in a reduction in the unconfined concrete strength. The extent of crack penetration delineates the region around the cross-section impacted by corrosion (Ghanooni-Bagha, *et al.*, 2016; Shayanfar, *et al.*, 2016).

3.5.2 Properties of Corroded Steel Reinforcements

When reinforcements are affected by corrosion, their condition is marked not only by a reduction in the cross-sectional area but also by changes in their Young's modulus, yielding strength, ultimate strength, and rupture strength (Coronelli and Gambarova, 2004; Azad, Ahmad and Al-Gohi, 2010; Andrade *et al.*, 2016; Jnaid and Aboutaha, 2016; Peng *et al.*, 2022). The reductions in the reinforcement properties can be projected based on the observed crack widths in concrete cover (w_{cr}). Typically, w_{cr} is influenced by various factors such as corrosion depth, rebar diameter, cover-to-rebar diameter ratio, and concrete tensile strength, however; literature shows that it is often acceptable to estimate the crack width by considering the ratio of corrosion depth to the original rebar diameter (Tahershamsi *et al.*, 2017). Assuming uniform corrosion throughout the reinforcement perimeter, the crack width can be approximated using the following equation

(Andrade *et al.*, 2016):

$$w_{cr} = c_1 . r_{corrosion} \tag{13}$$

where c_1 represents an empirical constant, typically assigned a value of 8, and $r_{corrosion}$ denotes the loss ratio of the cross-sectional area of the reinforcement due to corrosion.

The loss in yielding strength, r_{fy}, is assumed to be proportional to the loss ratio of reinforcement cross-sectional area, $r_{corrosion}$ (Du, *et al.*, 2005):

$$r_{fy} = c_2 . r_{corrosion} \tag{14}$$

where c_2 is a constant taken as 0.0012 or 0.005 for ribbed and plain bars, respectively.

The loss in the reinforcement modulus of elasticity, r_{es}, is also proportional to the loss ratio of reinforcement cross-sectional area, $r_{corrosion}$ (Gopinath, *et al.*, 2011):

$$r_{es} = c_3 . r_{corrosion} \tag{15}$$

where the experimental constant c_3 is taken as 0.0075.

3.5.3 Corroded Prestressing Strands

Similar to corroded reinforcing steels, prestressing strands could undergo corrosion due to weathering or being in contact with special chemicals. The amount of corrosion can be related to the observed crack width in concrete cover (w_{cr}) as follows (Dai *et al.*, 2015):

$$w_{cr} = c_4 . r_{corrosion} + c_5 \tag{16}$$

where c_4 and c_5 are empirical constants with values of 0.0515 and – 0.008, respectively.

Vereeken et. al (2021) conducted a comprehensive study on the assessment of prestressed and post-tensioned structures subjected to corrosion, focusing on different corrosion models and their influence on structural behavior. The following relationships for the corroded strand's modulus of

elasticity and yielding stress, respectively, were recommended:

$$E_s = (1 - c_6.r_{corrosion} \times 100)E_{s0} \quad (17)$$

$$f_y = (1 - c_7.r_{corrosion} \times 100)f_{y0} \quad (18)$$

where, E_{s0} and f_{y0} are the modulus of elasticity and yielding stress of undamaged strands. c_6 and c_7 are empirical coefficients equal to 0.00848 and 0.0075.

3.5.4 Concrete-Reinforcement Bond Reduction due to Corrosion

The fundamental assumption in concrete structural design is that planes remain planar throughout the loading process (CSA A23.3:19). It is typically accepted that this assumption remains valid even under extreme loading conditions (Wang *et al.*, 2013). However, when evaluating highly corroded concrete elements, this assumption does not hold as the loss of bond between reinforcements and concrete causes the reinforcement to slip, creating a strain incompatibility between the reinforcements and the concrete (Desnerck, *et al.*, 2015; Feng, *et al.*, 2016; Zhang *et al.*, 2017; Yuan, *et al.*, 2020). In this regard, Zhang et. al (2017) suggested using a *compatibility factor* in the slip regions for modifying the compatibility equation, as follows:

$$\Omega = 0.8099\rho^2 - 1.2271\rho + 1 \quad (19)$$

where ρ is the loss ratio of strand area due to corrosion.

3.5.5 ASR-Damaged Concrete

As mentioned in section 2.2.2, ASR-induced damage can lead to a reduction in concrete strength. In the case of high ASR activity in concrete, the residual strength and the Young's modulus of concrete can be expressed as (Zhychkovska, 2020):

$$r_{concrete-fc} = -0.076 \ln(\varepsilon_{ASR}) + 0.7 \quad (20)$$

$$r_{concrete-ec} = 1 - \frac{\varepsilon_{ASR}}{\varepsilon_{ASR}+0.38} \quad (21)$$

where ε_{ASR} is the ASR expansion (%). $r_{concrete-ec}$ is within the range of 0.6 to 1.

3.5.6 Concrete-Reinforcement Bond Reduction due to ASR

Similar to corrosion, ASR-induced cracks can degrade the bond strength between concrete and steel or prestressing reinforcements. Luo *et al.* (2022) investigated the residual bond strength of ASR-damaged concrete under different confinement conditions as shown in Figure 13. To account for the potential impact on the structural capacities, a compatibility factor was defined as the residual bond ratio. The value of the factor, for a given ε_{ASR}, was derived from Figure 13 by interpolation but capped at unity (equal or less than 1.0).

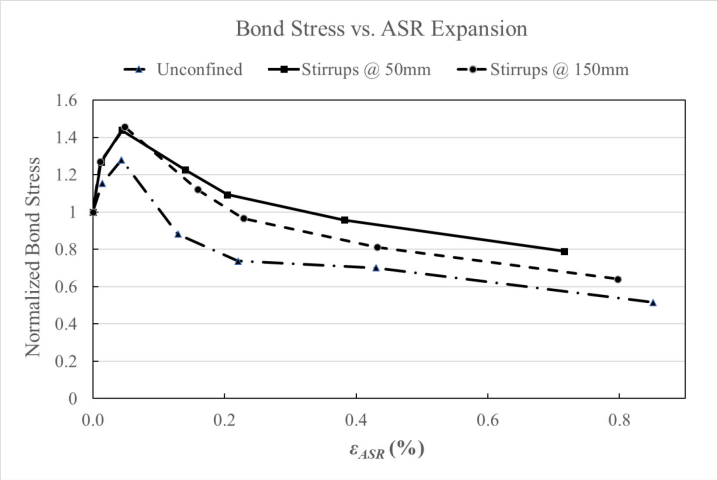

Figure 13- Normalized bond strength vs. ASR Expansion (Luo, *et al.*, 2022)

3.6 DEFUZZIFICATION

Given the fuzzy nature of the deterioration inputted into the numerical analysis, the assessed performance criteria will also be expressed as membership functions. These functions can be further processed or utilized directly by decision-makers. The first approach entails a process named defuzzification. This converts the membership function of a given performance criterion into a single crisp, numerical value that can be readily interpreted and used in engineering

calculations and decision-making processes. The second approach entails assessing the min-max range of values for the performance criteria at a given membership level. This range can used as the basis to estimate the likelihood of the criteria exceeding a pre-determined limit. The results of this study are displayed using both approaches. Note that several defuzzification methods exist, the one adopted here is the centroid method (Chakraverty *et al.*, 2019), which computes the membership function's centroid.

3.7 DEVELOPING STRUCTURAL PERFORMANCE CHARTS

This section illustrates the process of developing user-friendly structural performance charts produced by the UPRS and to be used by the inspector to evaluate the structural performance of the examined bridge. These charts have been developed by grouping the analysis results (in this study; U_M, U_S, *and* U_D) into different pairs of damage severities (from Tables 1 and 2) and damage locations (i.e., midspan, end-span, and top, bottom, or side of the girder). Those user-defined taxonomies could be introduced based on the needs of the project. Considering a simply supported bridge girder in this study, two separate types of performance charts have been generated: (1) strength-based charts, and (2) stiffness-based charts.

3.7.1 Developing Strength-Based Charts

These charts refer to the performance criteria related to the ultimate limit state. In this study, the grouping has been done based on the damage severities defined in Tables 1 and 2, and the damage location taxonomy defined in Table 3, and shown schematically in Figure 14. An initial length discretization for each location taxonomy can be established through engineering judgment, with the option to adjust it after each analysis. A shorter length may encompass only a few damage initiation points, while a longer length could include a greater number of such points, potentially

leading to a wider range of structural responses at one location taxonomy. In both cases, the precision and efficacy of the method could be affected.

Table 3- Damage location taxonomy for developing strength-based charts

Damage Location Definition	Distance to Critical Section / Length
At Critical Section	<10%
Near Critical Section	10-25%
Mid-Far from Critical Section	25-40%
Far from Critical Section	>40%

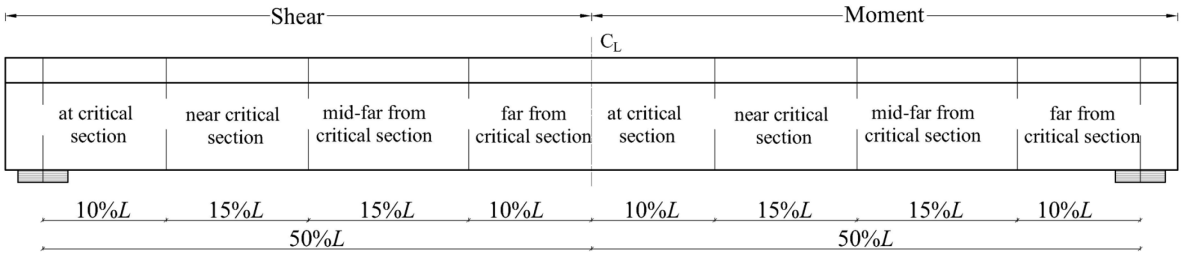

Figure 14- Damage location definition for resistance-based charts

3.7.2 Developing Stiffness-Based Charts

The maximum displacement of a girder depends on the stiffness distribution along its length. As a result, the damage distribution contributes to the maximum displacement of the girder, but with different weights based on the damage location. A damage near the supports has less impact, while a damage near the midspan has a more severe effect on the increase of displacement (Abdelmaksoud, *et al.*, 2022; Salili, *et al.*, 2023). To address this, the damage location groups included in Table 4 and shown in Figure 15 have been considered.

Table 4- Damage location taxonomy for developing stiffness-based charts (Abdelmaksoud, *et al.*, 2022)

Damage Location Definition	Distance to Critical Section / Length
At Critical Section	<25%
Far from Critical Section	>25%

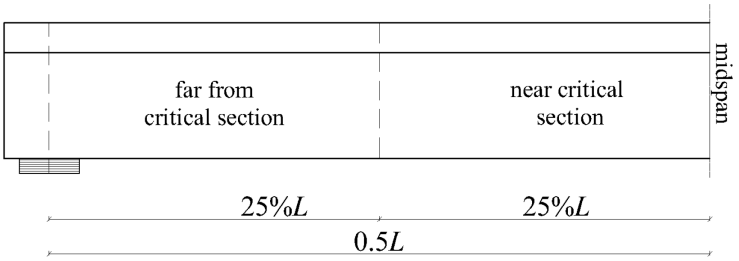

Figure 15- Damage location definition for stiffness-based charts

Another important factor in developing the stiffness-based charts is that the increase in the displacement not only depends on the damage location and its severity but also depends on the length of the damaged part of the girder. To avoid complex charts, a condition index factor, *CI (0~100)* has been introduced which can be related to the performance criteria:

$$CI = \frac{\sum\sum L_{ij} W_{ij}}{\sum L_{ij}} \times 100 \tag{22}$$

where, L_{ij} and W_{ij} are the length and weight of the damage with severity i at location j, respectively. W_{ij} $(0\sim1)$ is a weighing factor relating the damage severity to its effect on the displacement. Conducting a regression analysis, one can find W_{ij} for any given damaged element.

In this study, the increase of the displacement due to damage with respect to the displacement of the undamaged girder is of interest. As such, the Displacement Amplification Factor (DAF) can be defined as:

$$DAF = \frac{U_{d,Damaged}}{U_{d,Undamaged}} \tag{23}$$

where $U_{d,Damaged}$ and $U_{d,Undamaged}$ are the maximum displacement utilization ratios of the damaged and undamaged girders

CHAPTER 4 A DEMONSTRATIVE EXAMPLE OF DEVELOPING PERFORMANCE CHARTS

4.1 GENERAL

In this chapter, generating structural performance charts using the developed UPRS framework is demonstrated on a practical example. A reinforced concrete bridge girder subjected to corrosion is considered where the performance of the damaged girder is investigated. First, a simply supported RC bridge girder with a length of 10 m has been modeled, analyzed, and designed according to the Canadian Highway Bridge Design Code (CSA S6:19). For simplicity, the dead and live loads are considered to be uniformly distributed. Figure 16 shows the girder dimensions and reinforcing details. Figure 17 and Figure 18 illustrate the shear and moment utilization ratios and resistances, respectively. The maximum shear and moment capacity ratios are 0.95 and 0.91, respectively.

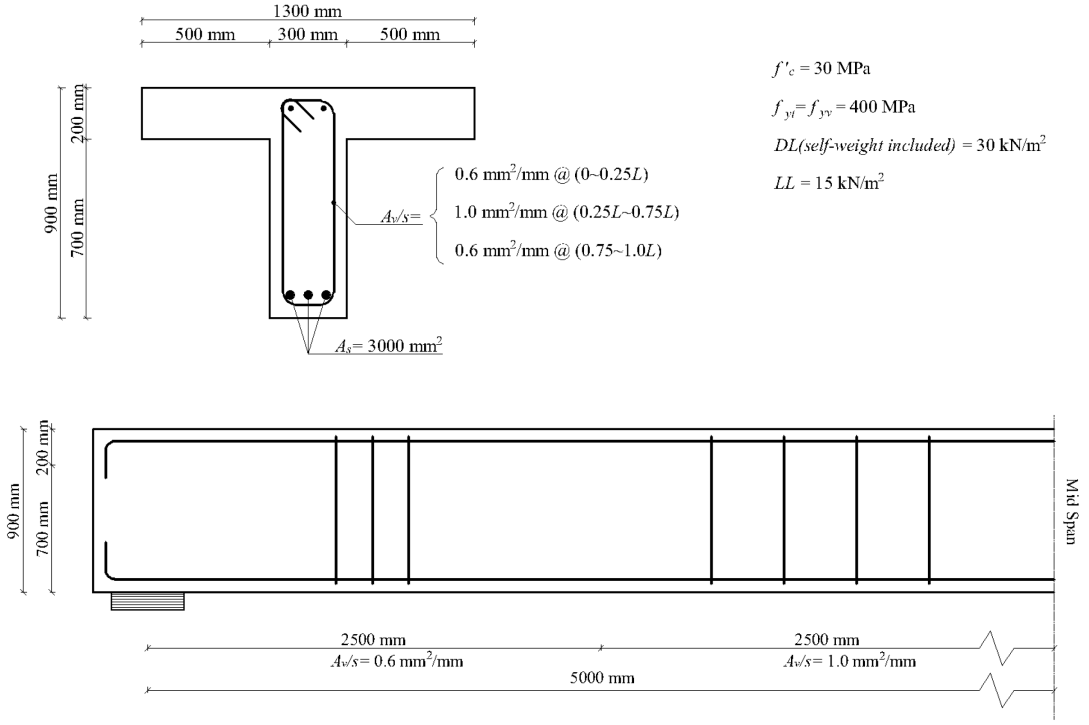

Figure 16- Details of RC Girder

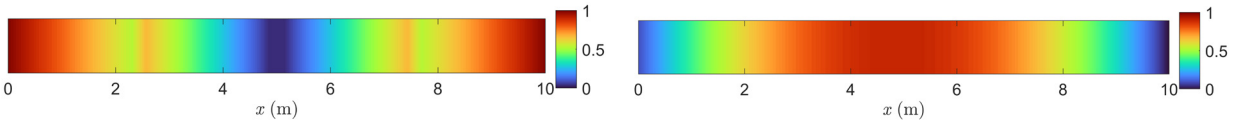

(a) Shear (b) Moment

Figure 17- The utilization ratio contours of the undamaged RC girder

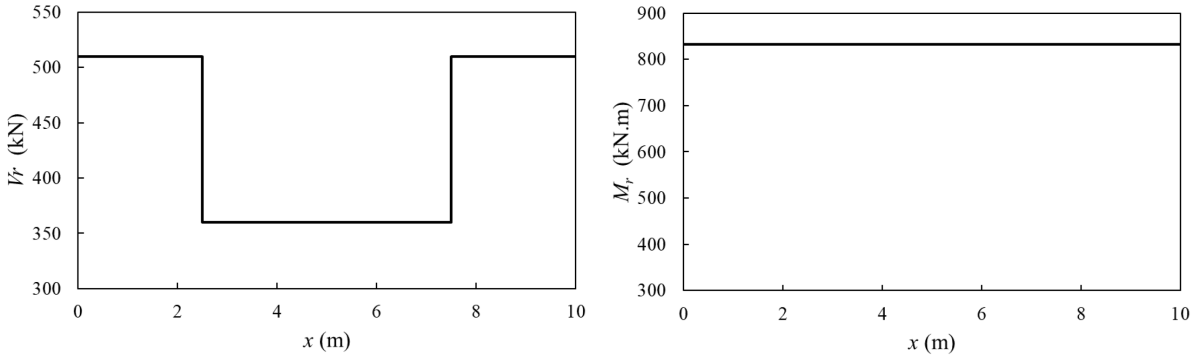

(a) Shear (b) Moment

Figure 18- The ultimate capacity of the undamaged RC girder

4.2 GENERATING ANALYTICAL MODEL

A simple analytical model has been developed in MATLAB® using one-dimensional fibers for reinforcements and three-dimensional fibers for concrete as shown in Figure 19. Fibers have been divided into three groups of "top", "bottom", and "side" fibers based on their locations (Figure 20). The moment of resistance was calculated using an iterative sectional analysis where the location of the neutral axis was determined to balance the coupled tension and compression forces on the section. The simplified method for calculating shear resistance was used as per CSA S6:19.

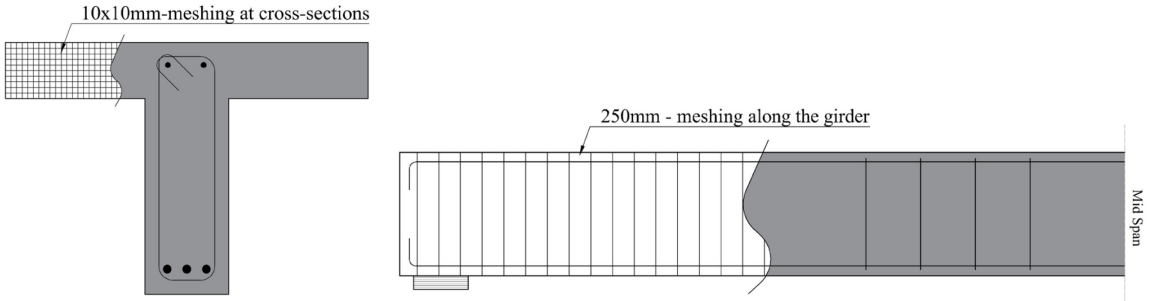

(a) Cross-section (b) Elevation view

Figure 19- Fiber model of the girder

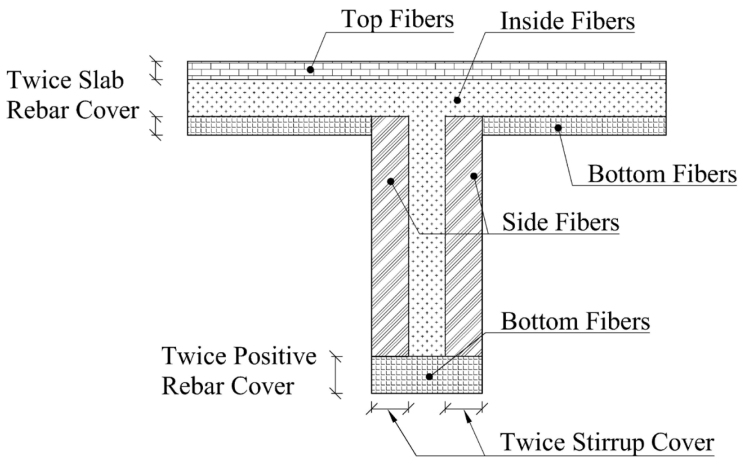

Figure 20- Fiber grouping based on their location in the cross-section

4.3 GENERATING RANDOM DAMAGE SCENARIOS

"*n*" random damage scenarios have been generated. For each scenario, a random element along the beam length is selected and assigned a random cracking severity. Then, cracking is assumed to progressively extend to the neighboring elements with decreasing severities. Figure 21 illustrates an example of the first six randomly generated damage scenarios. The minimum number of random models, "*n*", is a function of the acceptable level of accuracy and the convergence of the damage-performance function and could change based on the project. One could measure the accuracy of regression by calculating the coefficient of determination, R^2, or other similar means of data-fitting error measurement. In this case study, it was observed that increasing the number of samples (*n*) from 300 to 301 did not result in a change in the R^2 value up to three decimal points, indicating an acceptable level of accuracy. For comparison, the program always generates minor damage states at the first damage scenario.

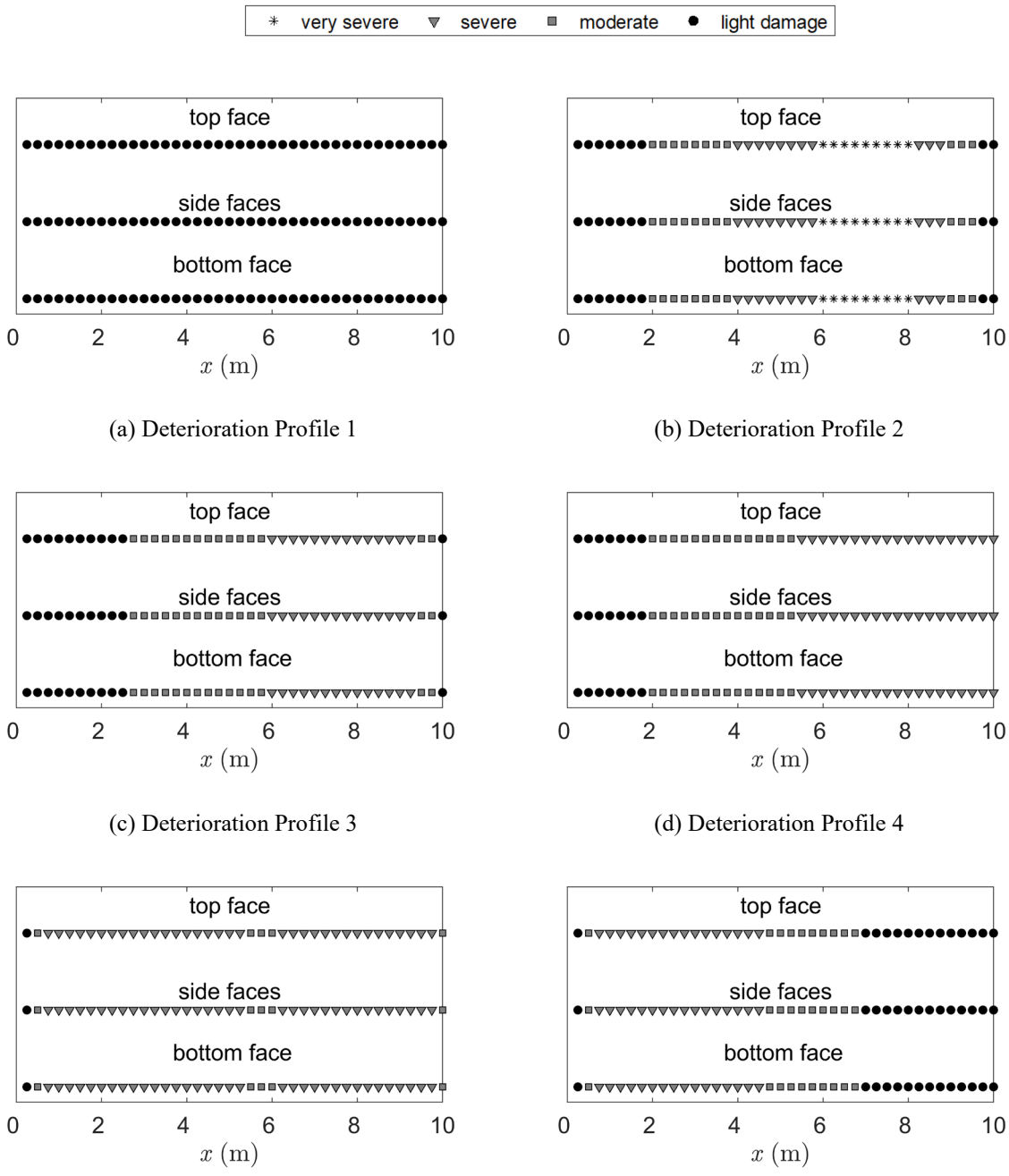

(a) Deterioration Profile 1

(b) Deterioration Profile 2

(c) Deterioration Profile 3

(d) Deterioration Profile 4

(e) Deterioration Profile 5

(f) Deterioration Profile 6

Figure 21- The first 6 random damage scenarios

4.4 MAPPING DAMAGE SCENARIOS TO STRUCTURAL PROPERTIES

The method described in section 3.5 has been used to map the linguistic descriptions of damage at each location to the structural material properties associated with that level of damage, considering four fuzzy cases of $\mu 0$ (best), $\mu 0$ (worst), $\mu 1$(best), and $\mu 1$ (worst) for each one. The assigned fuzzified material properties will be used in section 4.5 to analyze each randomly generated damaged girder.

4.5 ANALYZING DAMAGE SCENARIOS

This step deals with the analysis of each of the "*n*" randomly generated damaged girders and calculating their structural properties, including the ultimate shear and flexural resistances, and their vertical deflections. Analyzing these hypothetical randomly generated models serves as the basis for developing the performance-based charts in sections 4.7 and 4.8. Figures 22, 23, and 24 represent the analysis results, including shear and flexural resistances and deflections, for the first 6 randomly generated models, each providing 4 curves for each fuzzified case. One could see the impact of corrosion-induced damage on the structural performance of the girder. For instance, damage profile 2 shows very severe damage of all top, bottom, and side locations between $x = 6m$ and $x = 8m$, leading to 22% to 32% reduction in the ultimate shear resistance, and between 21% to 36% decrease in the moment capacity of the girder. The deflection, on the other hand, shows up to a 45% increase compared to the undamaged girder. It is worth noting that this study just considers the increase in deflection due to the change in the material properties, and other contributing factors, such as creep, are not reflected in the results. It should also be emphasized that while deflection is not typically utilized as a direct indicator of bridge deterioration in inspection procedures, the method for constructing deflection curves is discussed here for its

broader applicability.

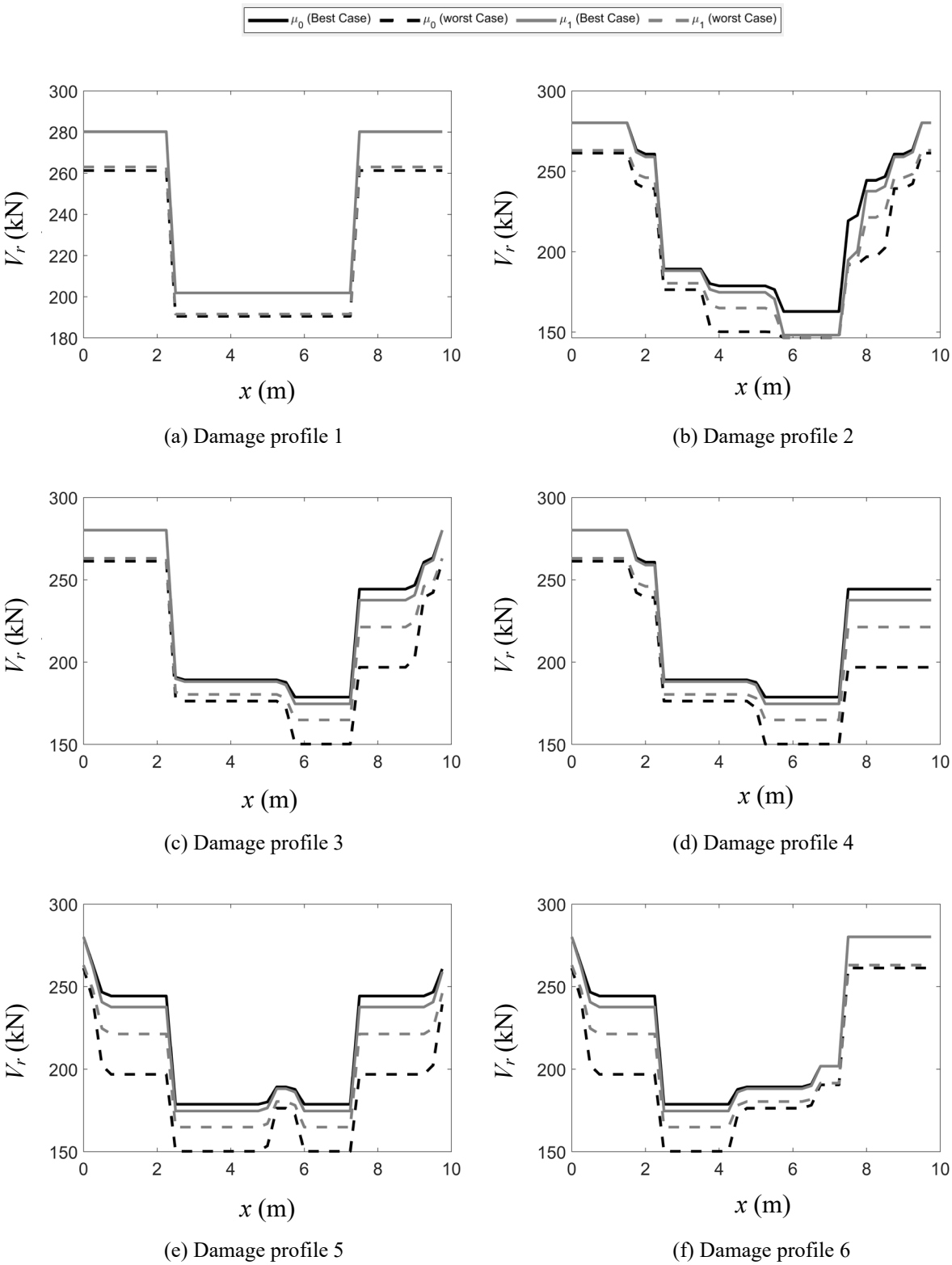

(a) Damage profile 1

(b) Damage profile 2

(c) Damage profile 3

(d) Damage profile 4

(e) Damage profile 5

(f) Damage profile 6

Figure 22- Shear capacities for the first 6 damage profiles

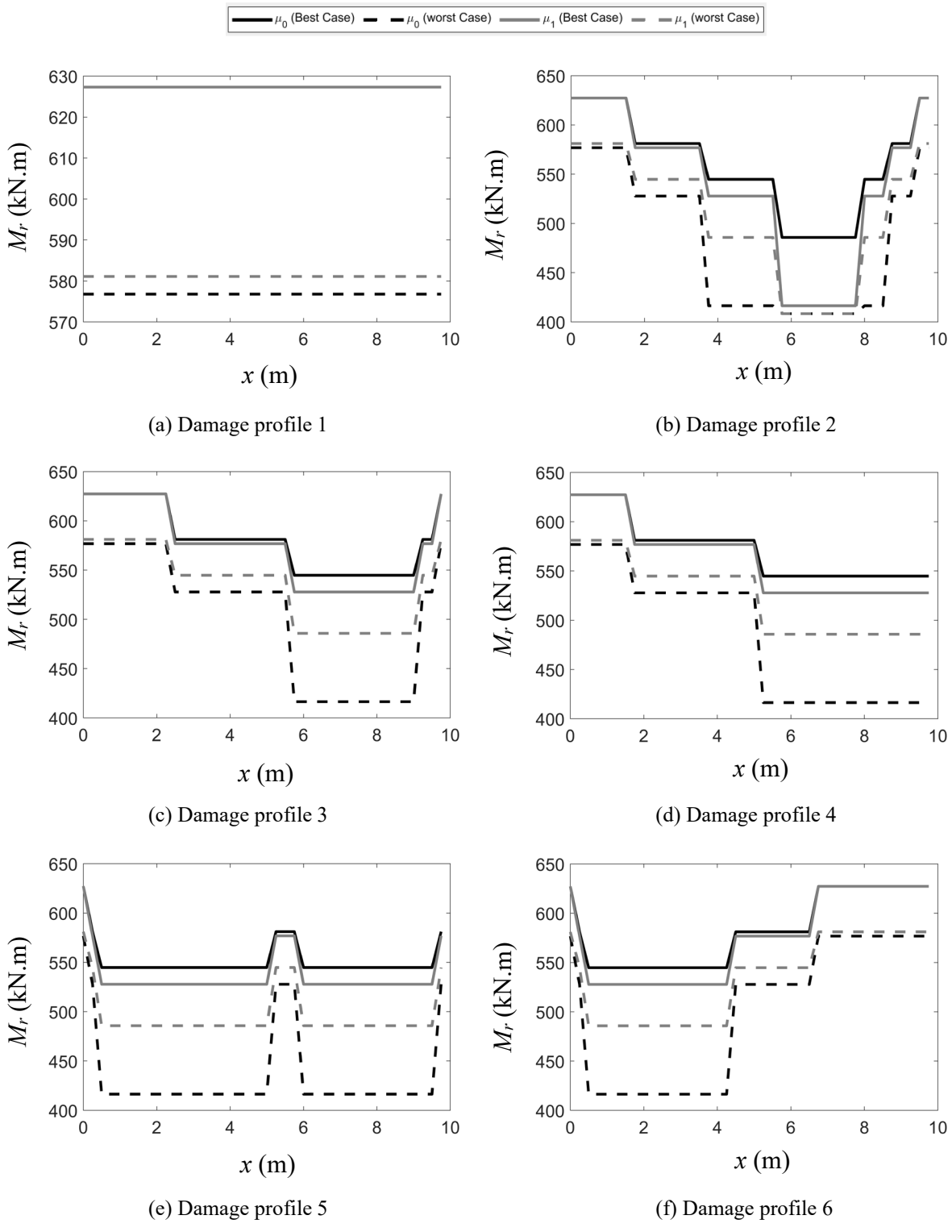

(a) Damage profile 1

(b) Damage profile 2

(c) Damage profile 3

(d) Damage profile 4

(e) Damage profile 5

(f) Damage profile 6

Figure 23- Flexural moment capacities for the first 6 damage profiles

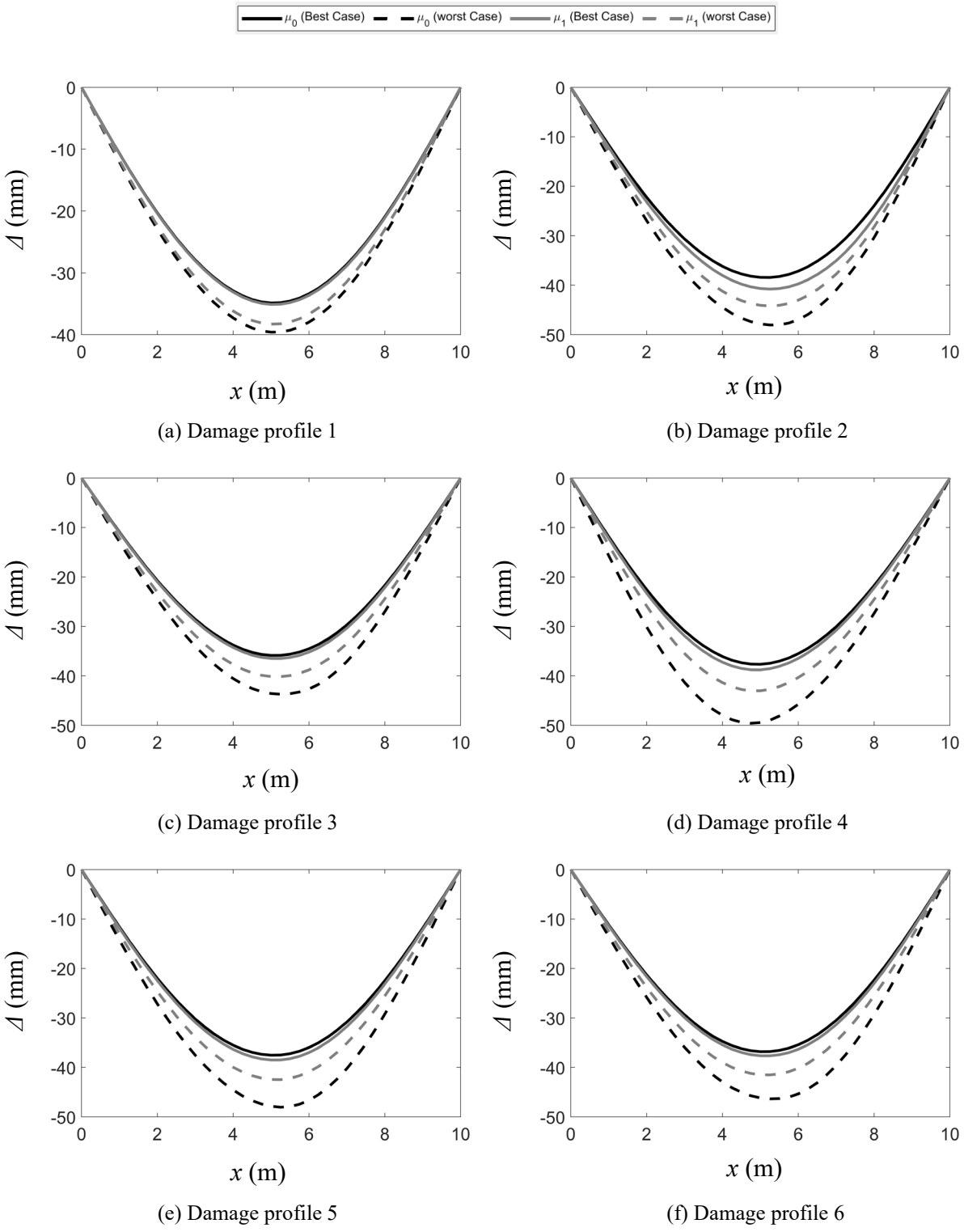

(a) Damage profile 1

(b) Damage profile 2

(c) Damage profile 3

(d) Damage profile 4

(e) Damage profile 5

(f) Damage profile 6

Figure 24- Deflections of the first 6 damage profiles

4.6 DEFUZZIFICATION

After generating the structural responses of the damaged girders, the results have been defuzzified using the centroid method and calculating the utilization ratios using equations (9) to (11). Figure 25 and Figure 26 represent the defuzzified utilization ratios for the first randomly generated damage models.

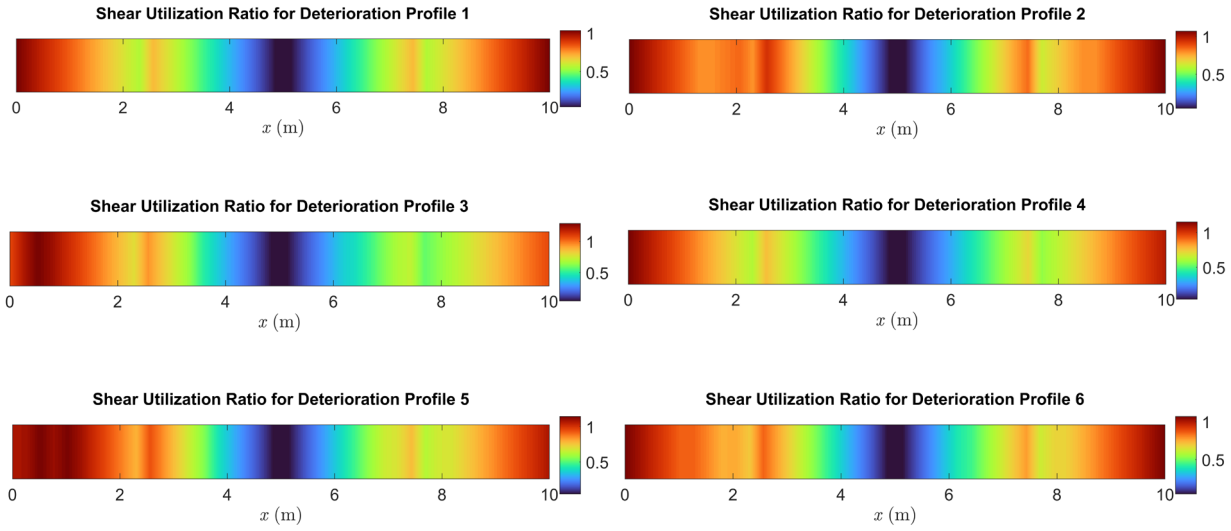

Figure 25- Defuzzified shear utilization ratios of the first 6 damage profile

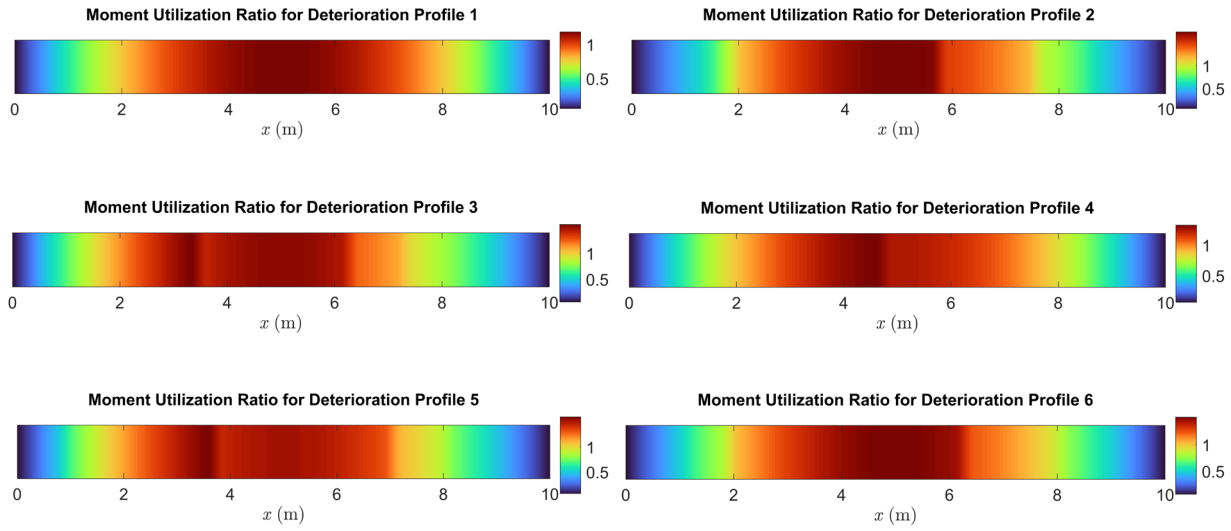

Figure 26- Defuzzified moment utilization ratios of the first 6 damage profile

4.7 STRENGTH-BASED CHARTS

The strength-based charts have been drawn using the method developed in Chapter 3. Figure 27 and Figure 28 represent the fuzzy shear and moment utilization ratios, respectively. Looking at Figure 27, one can find that very severe corrosion-induced damage "at" the critical section can lead to a utilization ratio of 1.25 to 1.52. On the other hand, very severe damage "near" the critical section has a less severe impact on the overall behavior of the structure, causing a utilization ratio of 1.1 to 1.4. severe damage far from the critical location cannot lead to utilization ratios more than 1.0, and hence, will not be a safety concern. One can find the relationship between the moment utilization ratios and the damage locations and severity by using Figure 28. For example, very severe damage "at" the critical location can lead to a moment utilization ratio of 1.55 to 1.85. Figure 29 provides the defuzzified version of the same results, leading to a more user-friendly format that can be readily employed by inspectors and engineers.

4.8 STIFFNESS-BASED CHARTS

Running the code for 300 randomly generated models, one could find the weights, W_{ij} as shown in Table 7 and then, the relationship between CI and DAF as shown in Figure 30 and Figure 31. The coefficient of determination, R^2, is more than 95% for most scenarios. Using the graphs provided along with the equation (16), the inspectors could estimate the increase in the displacement of the damaged girder with respect to its original condition.

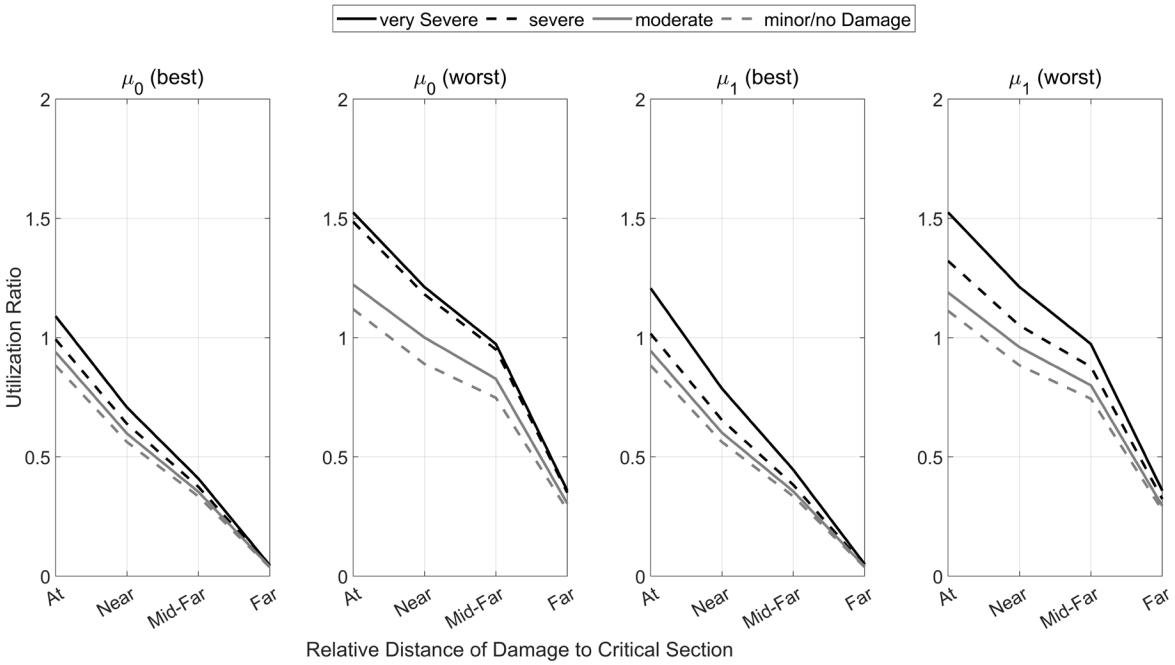

Figure 27- Shear utilization ratios as a function of damage location and severity

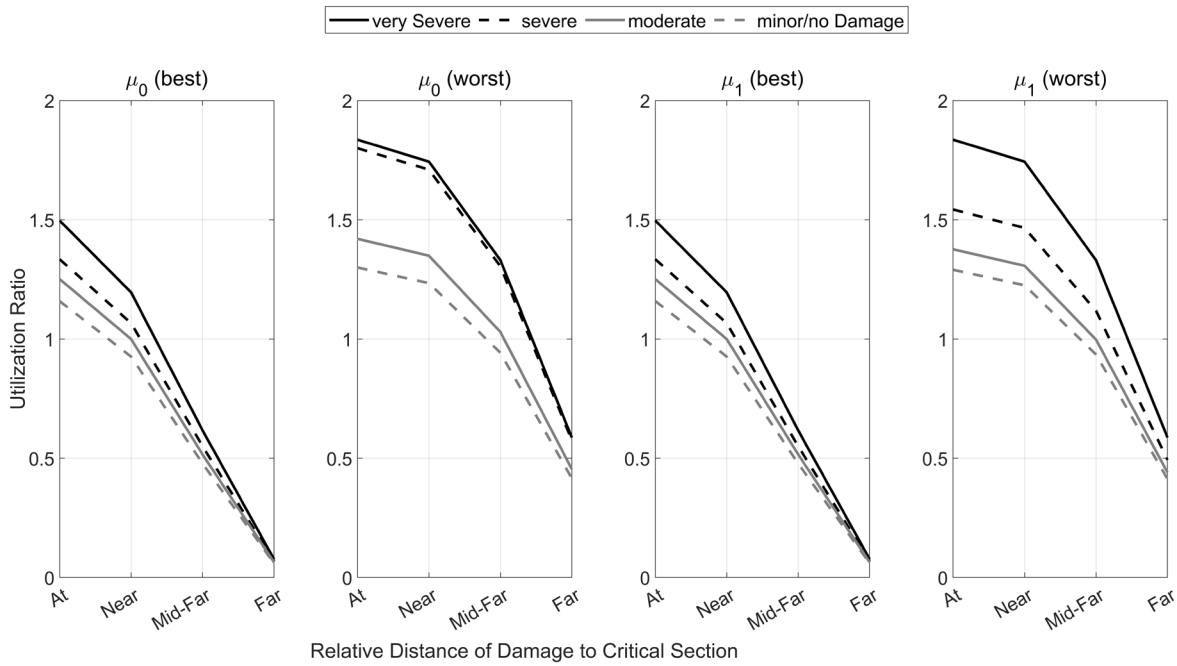

Figure 28- Moment utilization ratios as a function of damage location and severity

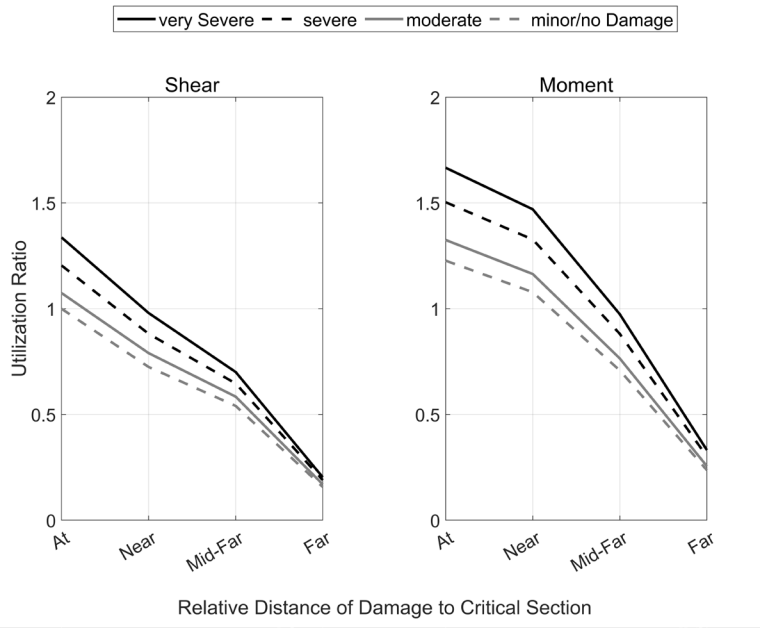

Figure 29- Defuzzified utilization ratios as a function of damage location and severity

Table 5- W_{ij} for corrosion-induced damaged girder

Severity	Location	
	Top End	Top Mid
Very Severe	0	0.85
Severe	0.45	0.90
Moderate	0.85	0.95
Light	1.00	1.00

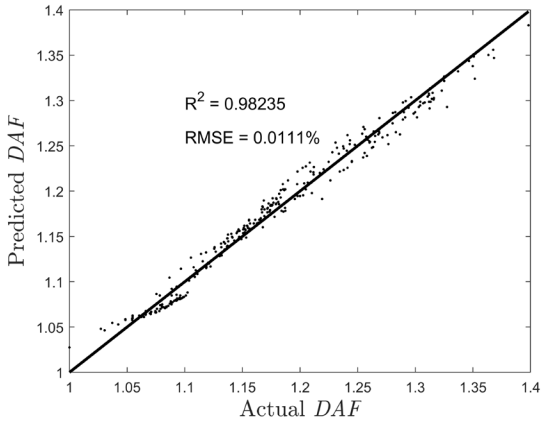

(a) $\mu 0$ (best)

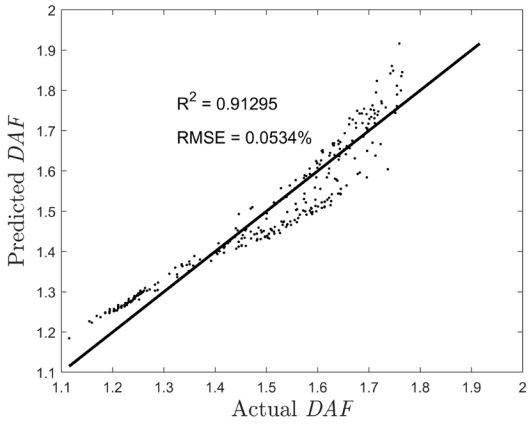

(b) $\mu 0$ (worst)

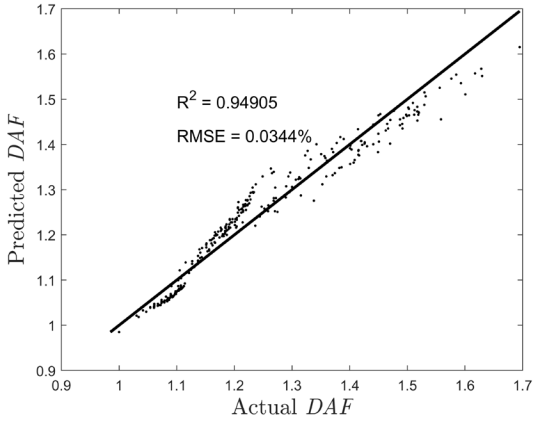

(c) $\mu 1$ (best)

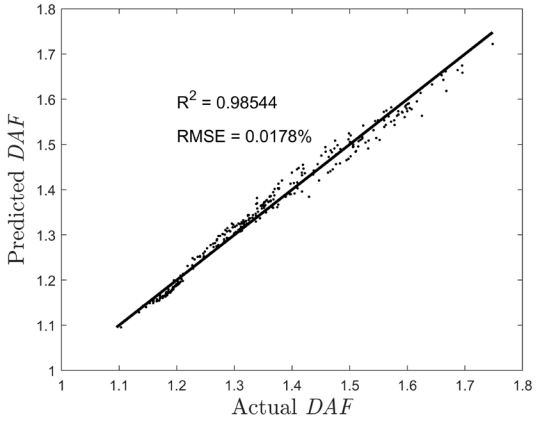

(d) $\mu 1$ (worst)

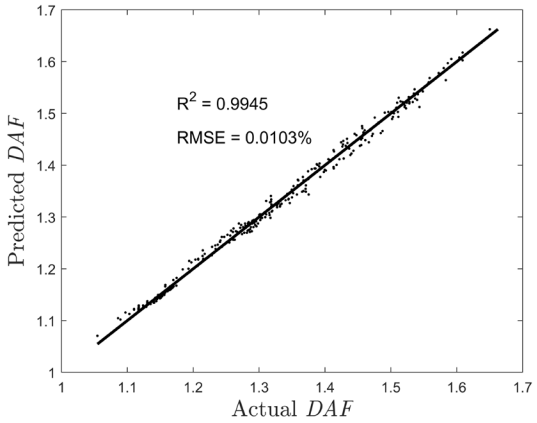

(e) Defuzzified

Figure 30- Predicted vs. actual Displacement Amplification Factor (*DAF*) for different fuzzy conditions

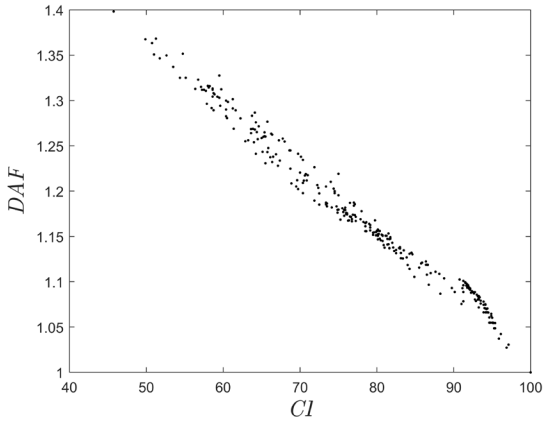

(a) $\mu 0$ (best)

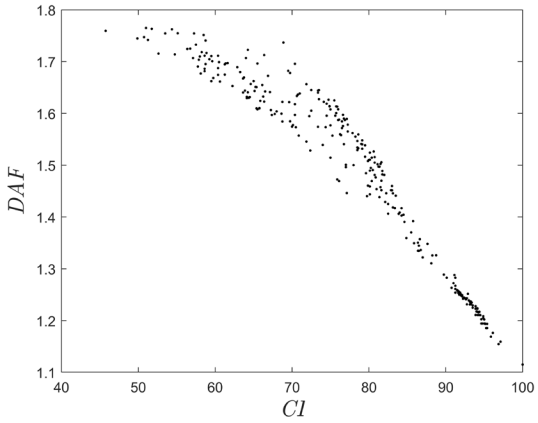

(b) $\mu 0$ (worst)

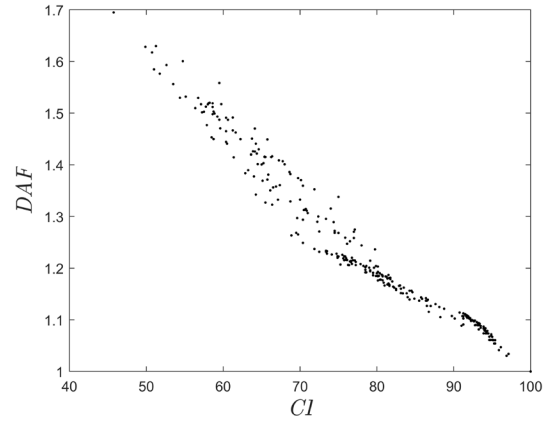

(c) $\mu 1$ (best)

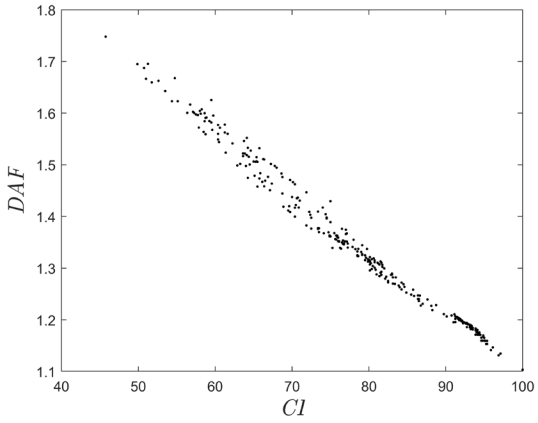

(d) $\mu 1$ (worst)

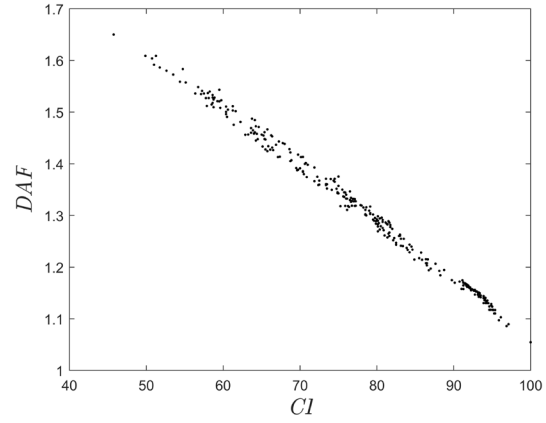

(e) Defuzzified

Figure 31- Displacement Amplification Factor (*DAF*) vs. Condition Index (*CI*)

CHAPTER 5 CASE STUDY: ASSESSING A DAMAGED PRESTRESSED CONCRETE BRIDGE GIRDER IN NOVA SCOTIA

5.1 GENERAL

In this chapter, the UPRS was utilized to produce structural performance charts and demonstrate its real-life application to assess the strength of an in-service bridge in Nova Scotia, Canada, shown in Figure 1 and Figure 2. The bridge suffered from extensive corrosion of prestressing strands, leading to high distress, extensive cracking, and spalling. In addition to studying the corrosion-induced damage, a scenario of ASR-induced damage has also been investigated.

The bridge consists of three spans of 13.7m, 18m, and 18m, respectively, with simply-supported AASHTO type (II) prestressed girders, and a 175mm-thick cast-in-place concrete deck slab working compositely with the girders. The girders consist of two tendon groups of bonded prestressing strands: one with a straight profile, and the other with a harped configuration, with pulling points at a distance of 6m from the seats. Figure 32 shows the cross-section and the elevation view of the girder chosen to be investigated. Table 6 represents the material properties according to the as-built drawings.

Table 6- Material properties of the PS girders

Concrete	$f'_c = 35\ MPa$
Prestressing strands	$f_{py}{}^{*} = 1765\ MPa$
(Low-relaxation 7-wire strands,	$f_{pu} = 1860\ MPa$
Grade 270)	
Shear reinforcements	$f_y = 400\ MPa$

* Minimum yielding strength at 1% elongation.

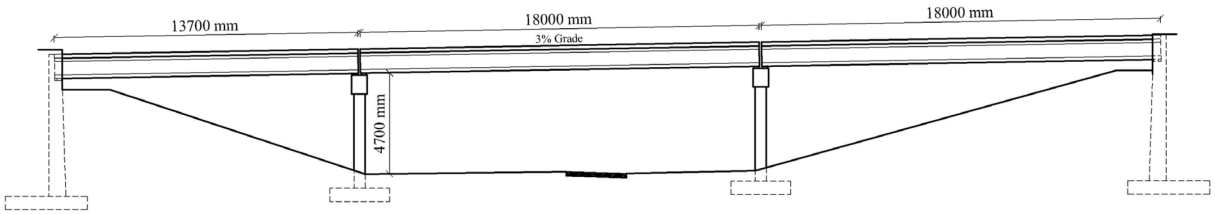

(a) Bridge elevation view

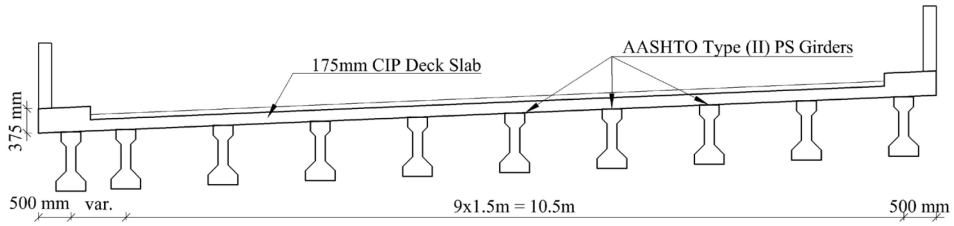

(b) Deck cross-section

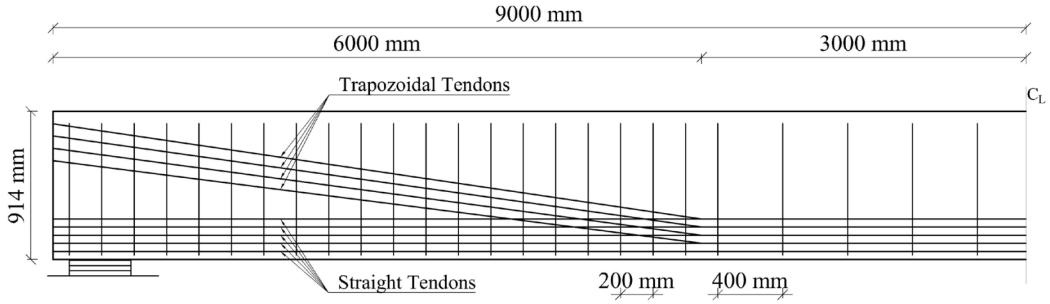

(c) Girder elevation view

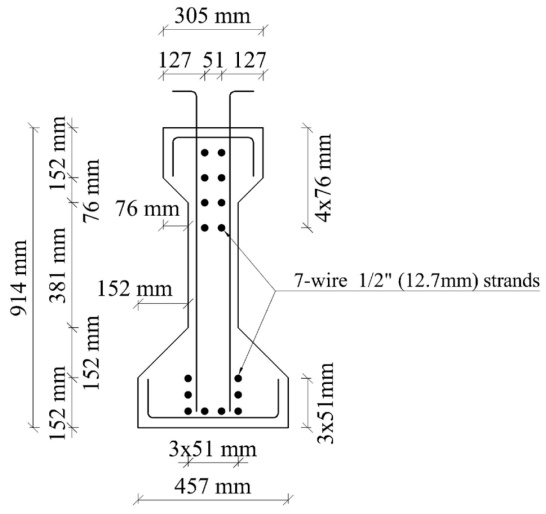

(d) Girder end section

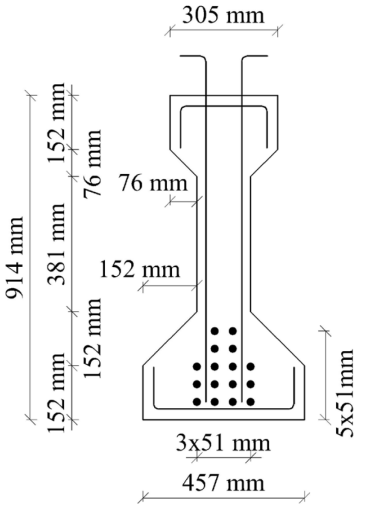

(e) Girder midspan section

Figure 32- Bridge Drawings

5.2 GENERATING ANALYTICAL MODEL

A MATLAB® code has been developed to incorporate prestressed concrete girders. Using this code, the girder has been analyzed and its structural properties, including the ultimate shear and moment resistances along the girder, as well as the deflection of the girder under service loads, have been calculated under CSA S6:19, considering the undamaged conditions. In this case, the cross-section has been divided into rectangular meshes with 20-by-20 mm dimensions. In the longitudinal direction, the girder has been divided into 20 segments, each having a length of 900mm. The cover elements have been identified, and named as bottom, side, and top covers according to their locations with respect to the girder's cross-section. The analytical model calculates the girder properties, at all damage scenarios, along the girder length. These properties, such as the moment of inertia, the cross-sectional area, as well as the material properties of the damaged girder discussed later in section 5.3, have been utilized to analyze the damaged girders as well as the undamaged ones.

5.3 GENERATING RANDOM DAMAGE SCENARIOS

Several random damage scenarios have been generated, with different starting points at the top, bottom, and side of the girder to represent damage to the negative, positive, and shear reinforcements, respectively (Abdelmaksoud, et. al., 2023; Salili, et. al., 2023). Each damage scenario starts at a randomly selected point, with a random intensity, and expands to its surrounding points. This process of analyzing a wide range of possible damage scenarios is the key to developing strength-based and stiffness-based performance charts. In this study, 300 random damage scenarios have been generated. Figure 33 shows the first 6 damage scenarios, while the first generated model is always with light damage for verification purposes.

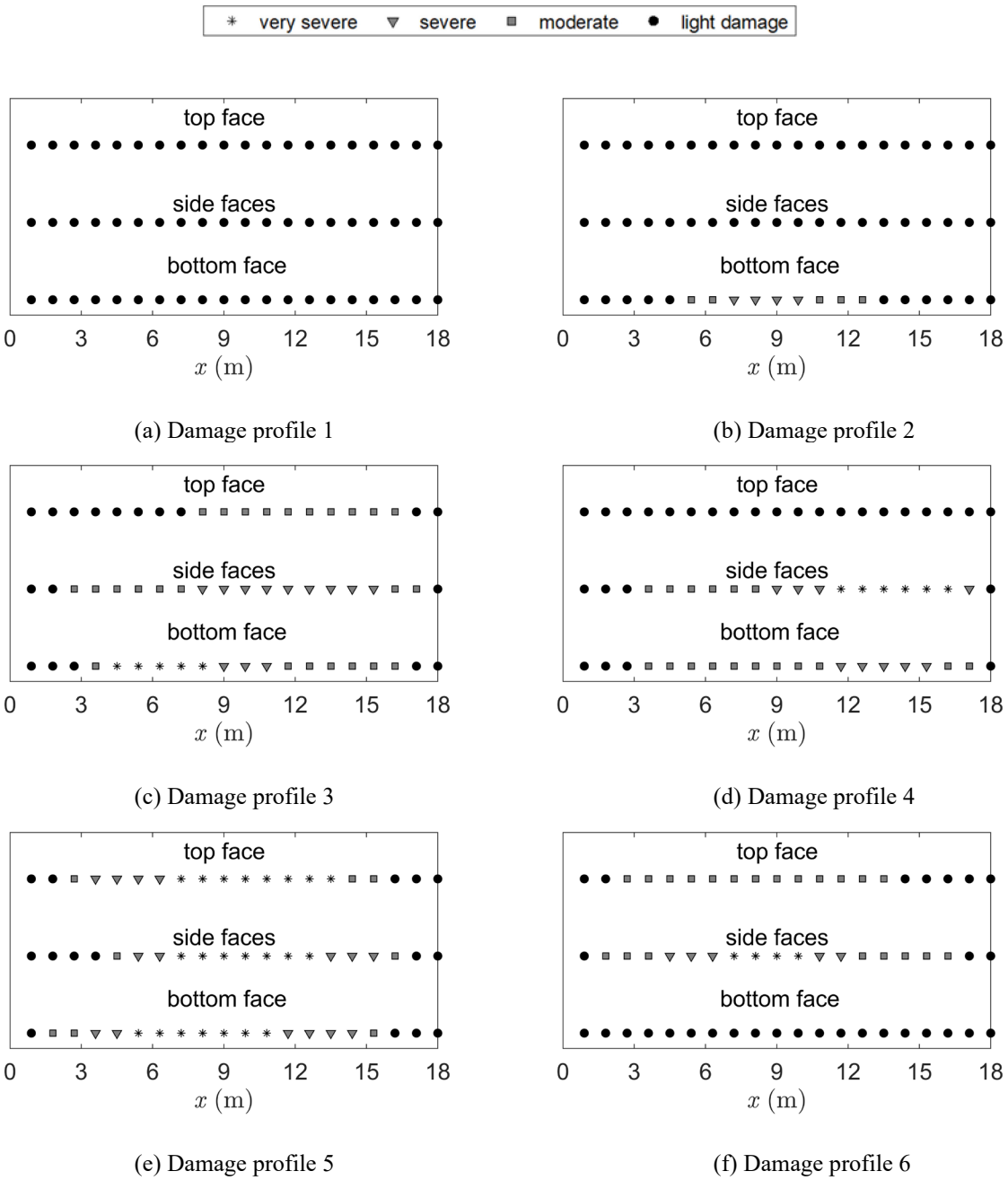

(a) Damage profile 1

(b) Damage profile 2

(c) Damage profile 3

(d) Damage profile 4

(e) Damage profile 5

(f) Damage profile 6

Figure 33- The first 6 random damage scenarios (corrosion)

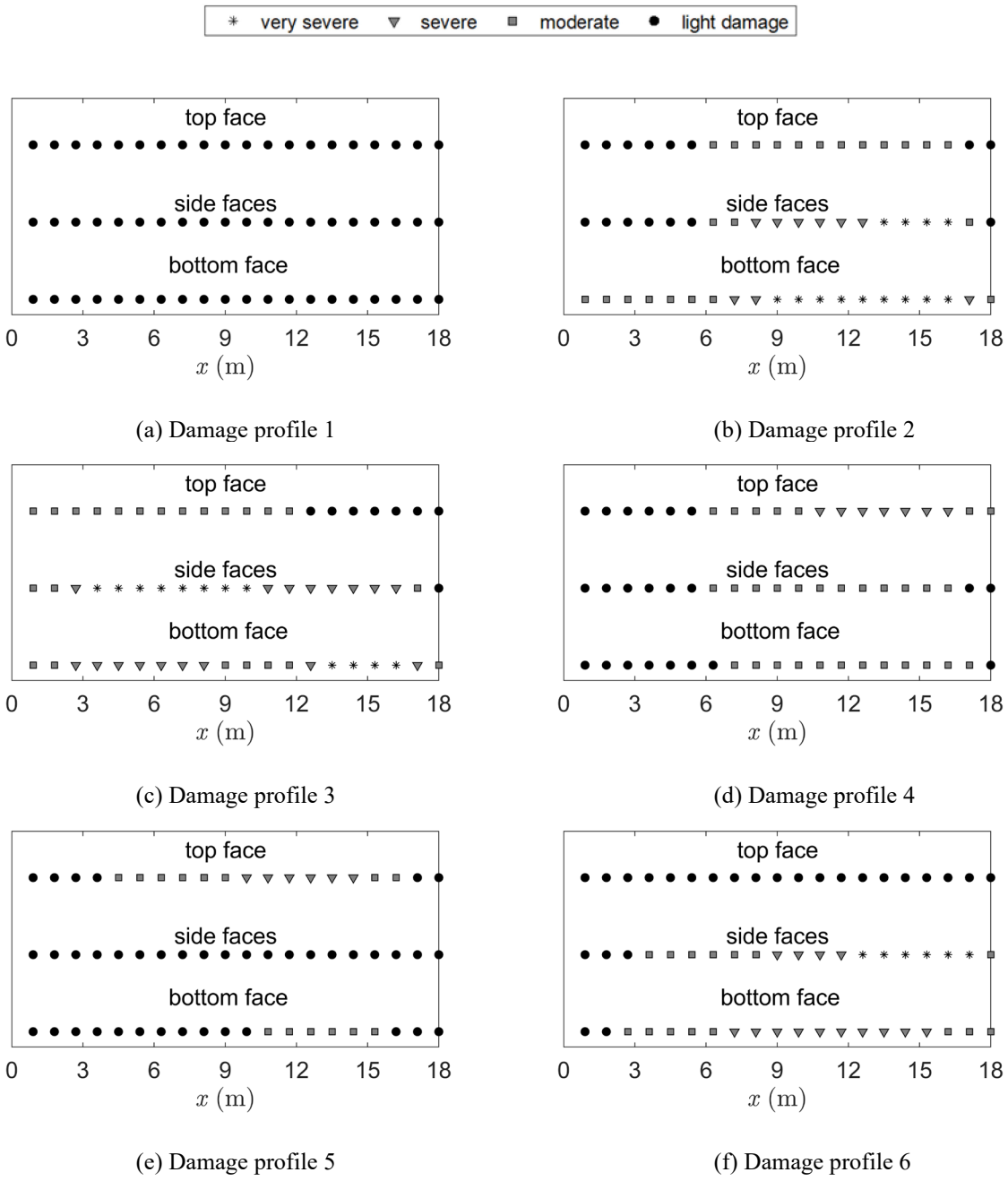

(a) Damage profile 1

(b) Damage profile 2

(c) Damage profile 3

(d) Damage profile 4

(e) Damage profile 5

(f) Damage profile 6

Figure 34- The first 6 random damage scenarios (ASR)

5.4 MAPPING DAMAGE SCENARIOS TO STRUCTURAL PROPERTIES

The damage scenarios have been mapped to the structural properties for two damage cases: (1) damage due to corrosion, and (2) damage due to ASR. The material degradation models along with the fuzzy logic model explained in Chapter 3 have been utilized for each damage model to map the damage severities into material properties for concrete, steel reinforcements, and prestressing strands, as well as the concrete-reinforcement bond loss. This process has been done for all random damage models generated in section 5.3. the analytical tool explained in section 5.2 has then been used to calculate the shear, moment, and deflection profiles of each damaged model. Figures 35 to 37 represent the ultimate shear and flexural resistances and the deflections along the girder length for the first 6 randomly generated corrosion-induced damaged models shown in Figure 33.

As an example, one could find very severe corrosion-induced damage happening around $x = 9\ m$ in Figure 33 (e), affecting the top, side, and bottom faces of the girder. This damage resulted in up to 32% reduction in shear capacity, and 28% to 47% reduction in flexural capacity of the girder, shown in Figure 35 (e) and Figure 36 (e), respectively. On the other hand, very severe ASR-induced damage in the bottom face of the girder between $x = 13\ m$ to $x = 16\ m$ in Figure 34 (b) resulted in up to 20% drop in shear capacity, and up to 5% reduction in flexural capacity, which is expected as ASR-induced damage in the bottom face affect the concrete properties, which has insignificant effect on the girder's flexural capacity and significant effect on the shear capacity. The change in deflection is shown in Figure 37 and Figure 40 for corrosion and ASR-induced damage scenarios, respectively, showing up to 50% for severely corrosion-induced damaged girders and up to 90% increase for severely ASR-induced damaged ones.

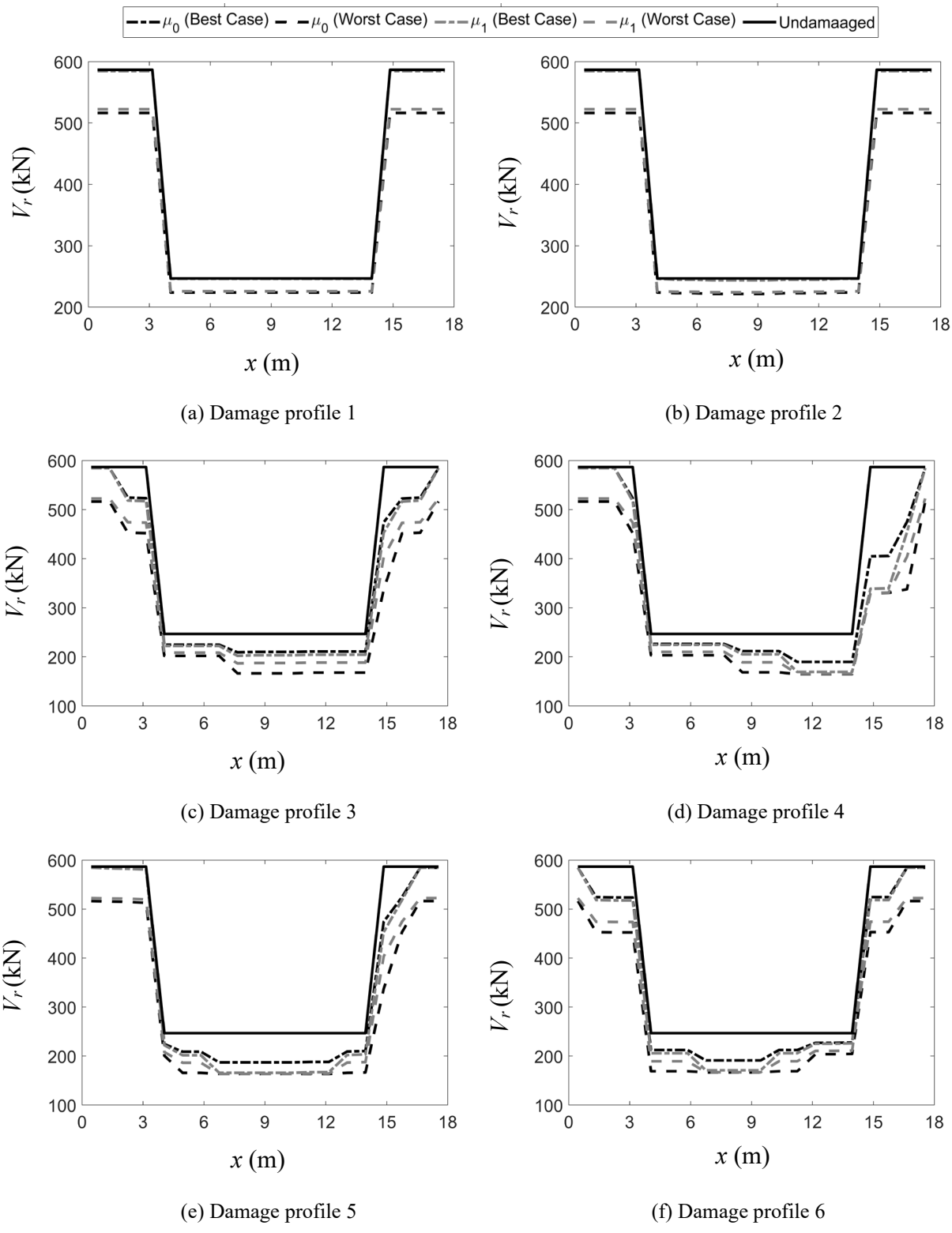

(a) Damage profile 1

(b) Damage profile 2

(c) Damage profile 3

(d) Damage profile 4

(e) Damage profile 5

(f) Damage profile 6

Figure 35- Ultimate shear capacity of undamaged and corrosion-damaged girders

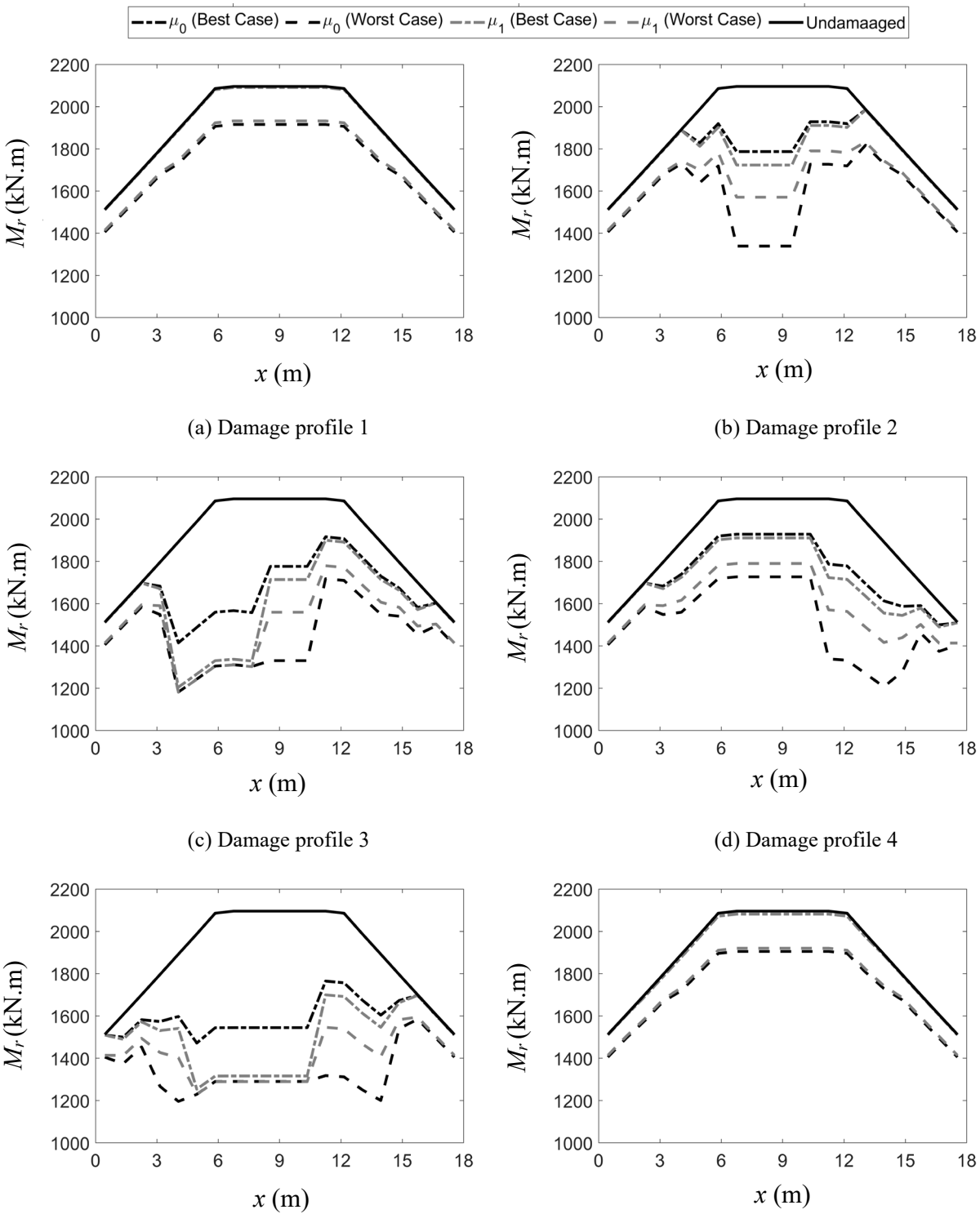

(a) Damage profile 1

(b) Damage profile 2

(c) Damage profile 3

(d) Damage profile 4

(e) Damage profile 5

(f) Damage profile 6

Figure 36- Ultimate moment capacity of undamaged and corrosion-damaged girders

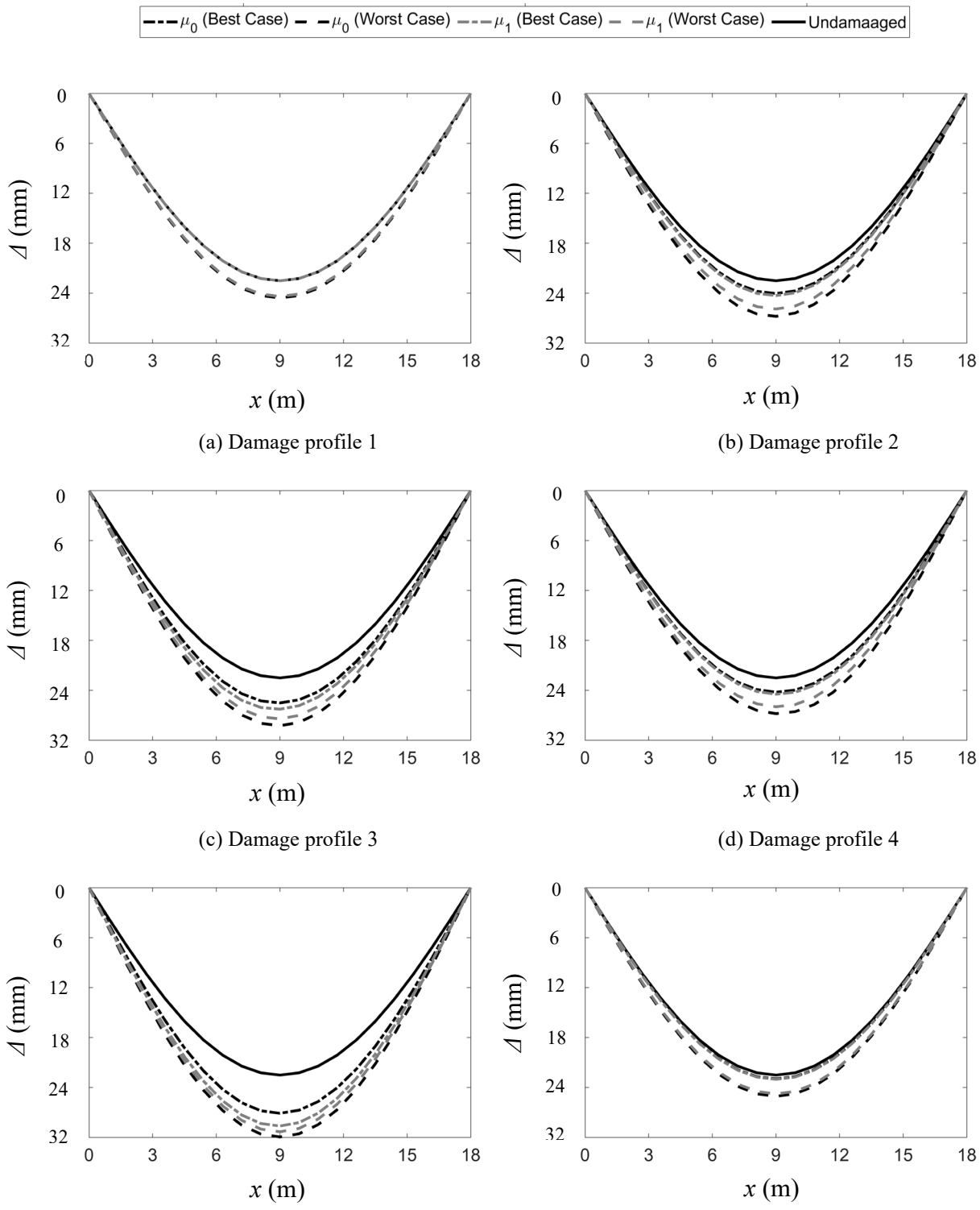

(a) Damage profile 1

(b) Damage profile 2

(c) Damage profile 3

(d) Damage profile 4

(e) Damage profile 5

(f) Damage profile 6

Figure 37- Deflection of undamaged and corrosion-damaged girders under service loads

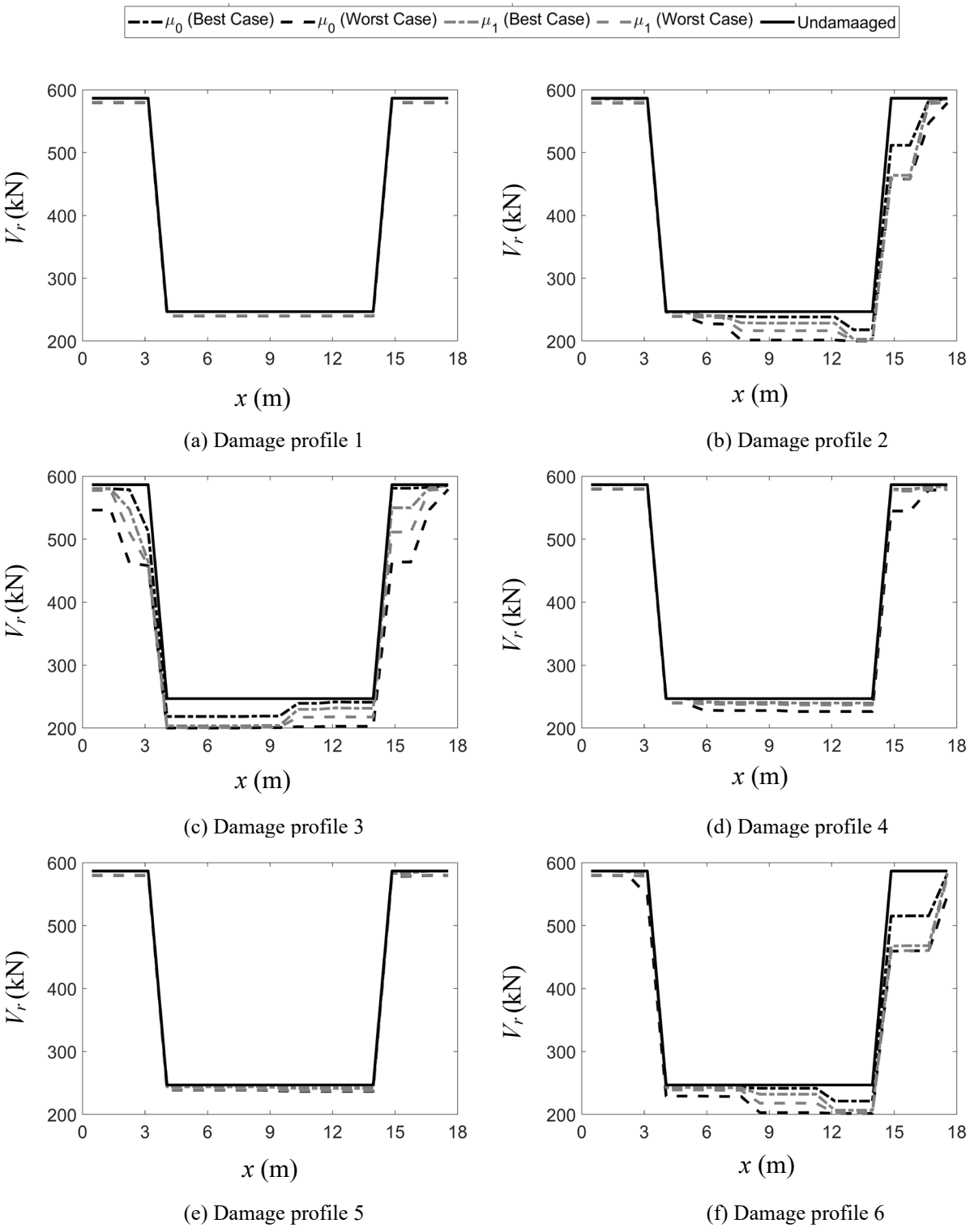

(a) Damage profile 1

(b) Damage profile 2

(c) Damage profile 3

(d) Damage profile 4

(e) Damage profile 5

(f) Damage profile 6

Figure 38- Ultimate shear capacity of undamaged and ASR-damaged girders

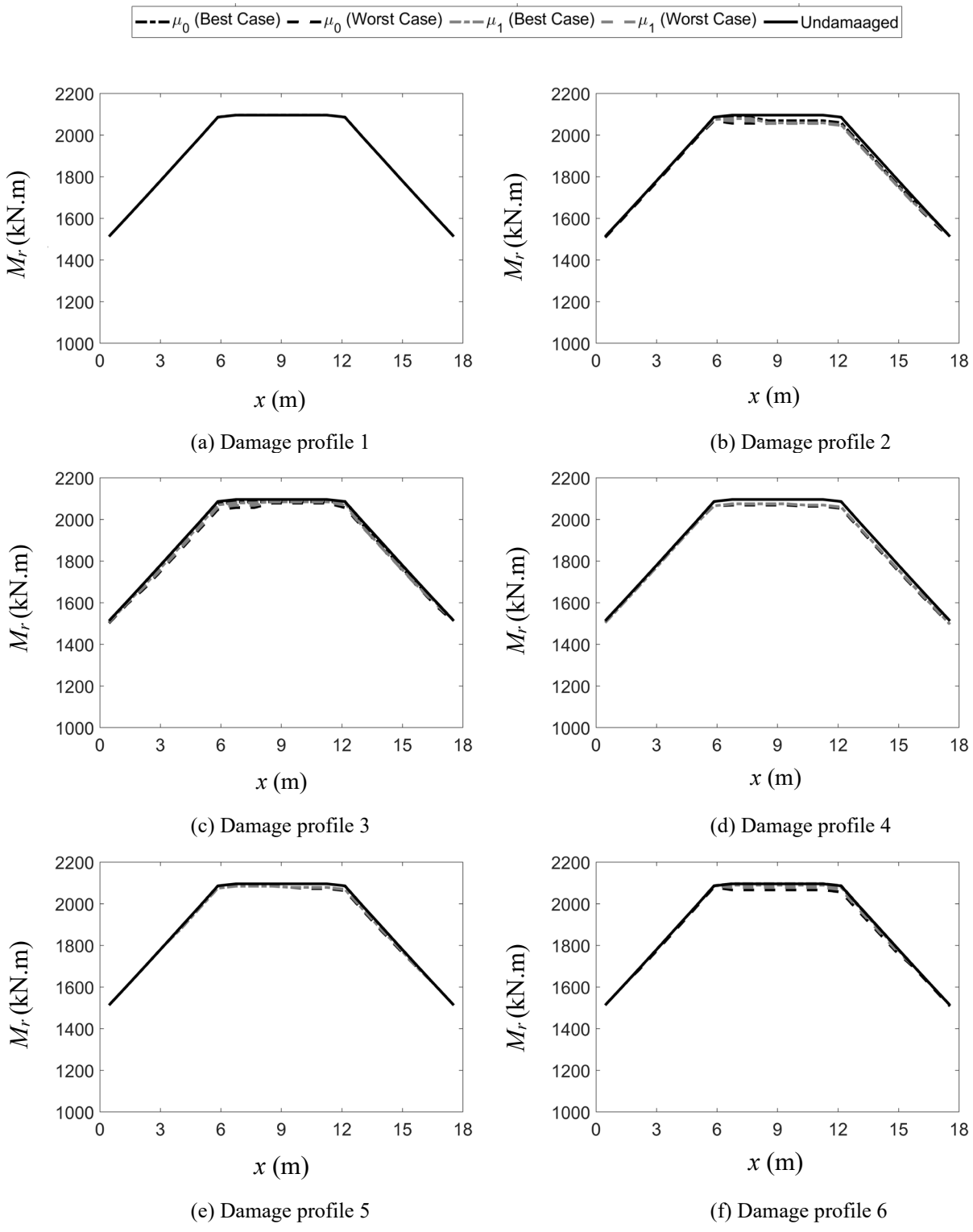

(a) Damage profile 1

(b) Damage profile 2

(c) Damage profile 3

(d) Damage profile 4

(e) Damage profile 5

(f) Damage profile 6

Figure 39- Ultimate moment capacity of undamaged and ASR-damaged girders

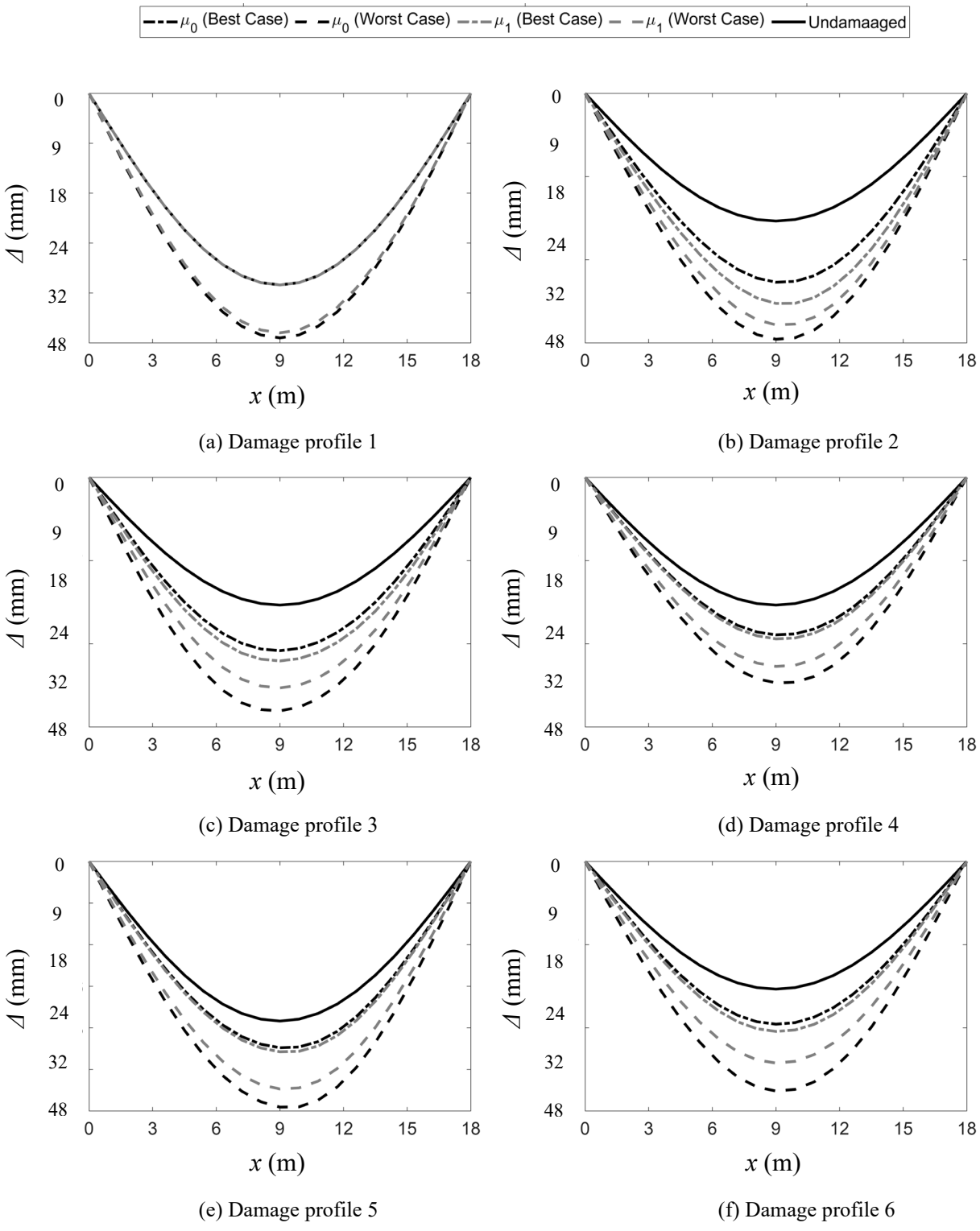

(a) Damage profile 1

(b) Damage profile 2

(c) Damage profile 3

(d) Damage profile 4

(e) Damage profile 5

(f) Damage profile 6

Figure 40- Deflection of undamaged and ASR-damaged girders under service loads

5.5 DEFUZZIFICATION

Figures 41 to 44 illustrate the ratio of defuzzified utilization ratios in damaged girders compared to those in undamaged ones. A ratio of one indicates the undamaged girder's capacity, with higher ratios signifying greater damage to the girder at the respective locations. The figures have been developed for two damage scenarios, namely: corrosion and ASR-induced damage conditions. For example, one could compare the changes in shear and flexural capacities shown in Figure 41 (e) and Figure 42 (e), respectively, and compare them to their associated damage profile, as well as the fuzzified shear and flexural introduced in Figure 35 and Figure 36, and see that very severe corrosion-induced damage distributed on all faces of the girder could lead to around 40% reduction in the girder's shear capacity (red zone) and more than 50% reduction in its flexural capacity (intense red zone). The same concept is true for defuzzified contours of ASR-induced damaged girders shown in Figure 43 and Figure 44, where very severe damage could lead to more than 20% reduction in shear capacity (damage profile 3), while the change in flexural capacity is less than 10% at all cases.

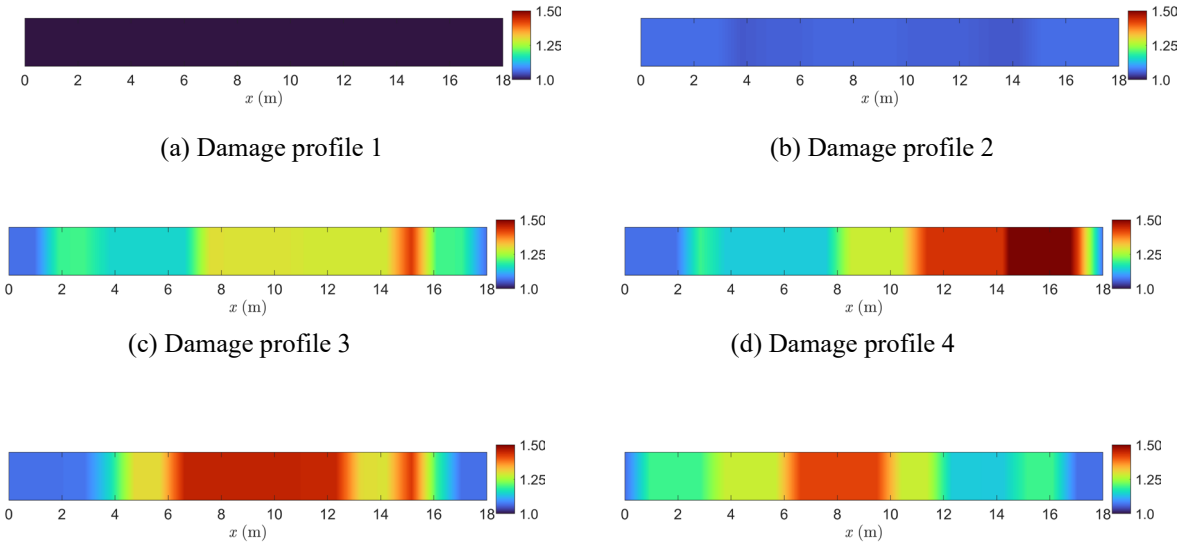

(a) Damage profile 1

(b) Damage profile 2

(c) Damage profile 3

(d) Damage profile 4

(e) Damage profile 5

(f) Damage profile 6

Figure 41- Shear amplification factors of corrosion-damaged girders

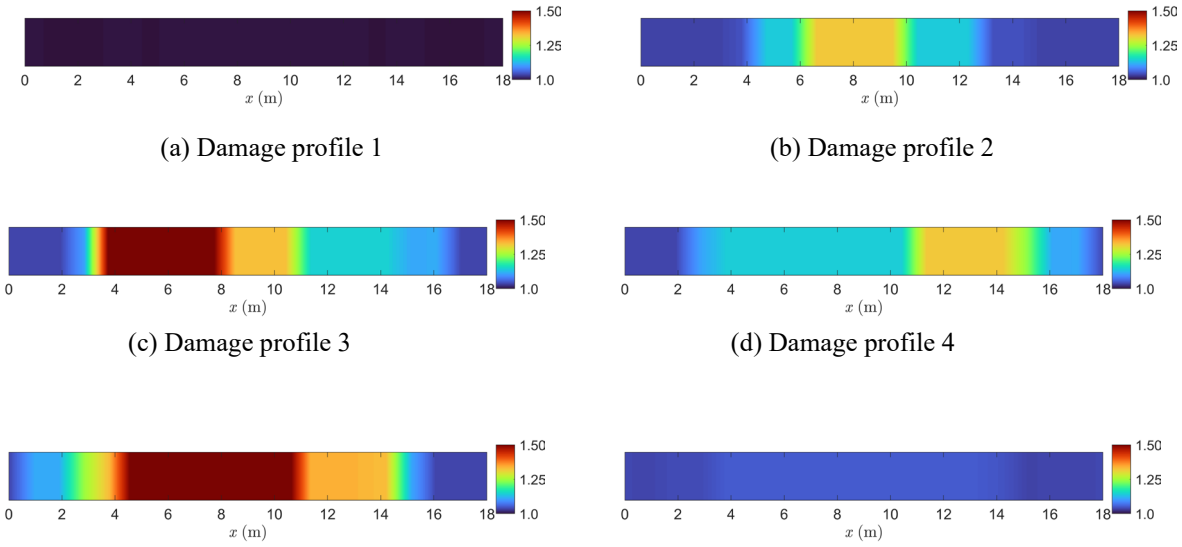

(a) Damage profile 1

(b) Damage profile 2

(c) Damage profile 3

(d) Damage profile 4

(e) Damage profile 5

(f) Damage profile 6

Figure 42- Moment amplification factors of corrosion-damaged girders

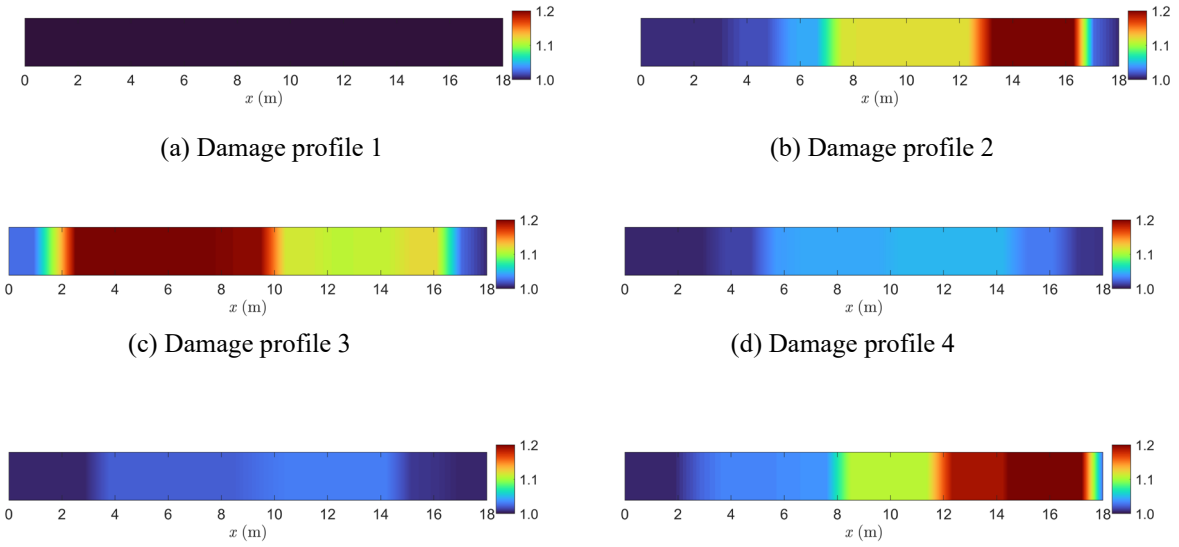

(a) Damage profile 1

(b) Damage profile 2

(c) Damage profile 3

(d) Damage profile 4

(e) Damage profile 5

(f) Damage profile 6

Figure 43- Shear amplification factors of ASR-damaged girders

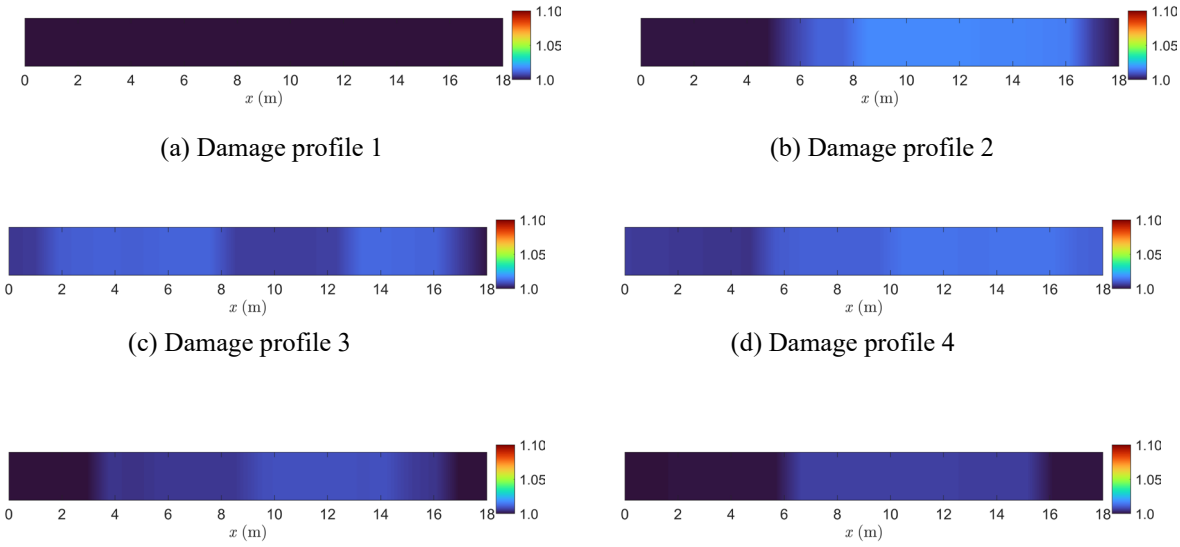

(a) Damage profile 1

(b) Damage profile 2

(c) Damage profile 3

(d) Damage profile 4

(e) Damage profile 5

(f) Damage profile 6

Figure 44- Moment amplification factors of ASR-damaged girders

5.6 STRENGTH-BASED CHARTS

In this section, the development of strength-based charts is discussed. To produce these charts, one should divide the damage scenarios into groups based on the damage locations (e.g., far, mid-far, near, and at the critical section) and the damage severity (e.g., very severe, severe, moderate, and light damage). Then, the envelope of the girder responses (in this case, the shear or flexural resistances) for each damage group have been calculated for four fuzzy cases, e.g., μ_0(best), μ_0(worst), μ_1 (best), μ_1 (worst). This procedure has been repeated twice for corrosion-induced damage, and ASR-induced damage, resulting in pairs of charts for the remaining shear and flexural capacities of the girder. Referring to Figure 45 and Figure 46 for corrosion-induced damage and Figure 47 and Figure 48 for ASR-induced damaged girder, one could get an estimate of the performance given the damage location and severity. In these figures, ND, L, M, S, and VS are the abbreviations for "No Damage", "Light Damage", "Moderate Damage", "Severe Damage", and "Very Severe Damage", respectively.

For example, Figure 45 shows that the corrosion "at the critical section" can result in reducing the ultimate shear resistance from 587 kN for the undamaged girder to a range between 325 kN to 410 kN for a "very severe" damage. Similarly, Figure 46 shows the downward trend of the ultimate flexural capacity of the girder, where a "very severe" damage "at the critical section" results in the reduction of the flexural capacity from 2,096 kN.m to 1,580 kN.m to 1,290 kN.m for the best and worst case scenarios, respectively. It is important to note that the shear and flexural capacity of the undamaged girder is not uniform. As a result, the undamaged values of shear and flexural capacities provided in these figures are not the same for different damage locations and need to be compared with themselves, and not with each other.

The charts for ASR-induced damaged girders could be used with the same approach. For example, Figure 47 shows a reduction in the shear capacity of the girder at the critical section from 578 kN for the undamaged case to a range between 460 kN and 520 kN, for the worst- and best-case scenarios. The effect of ASR on the flexural capacity is less severe, showing only a 1.6% to 2.8% reduction in the ultimate flexural capacity with very severe damage at the critical section.

Another way to represent the performance charts is to introduce *the Amplification of the Utilization Ratios,* which is the ratio between the undamaged girder's capacity at one location to the defuzzified values of the remaining damaged girder's capacities at the same location (refer to Figure 49 and Figure 50).

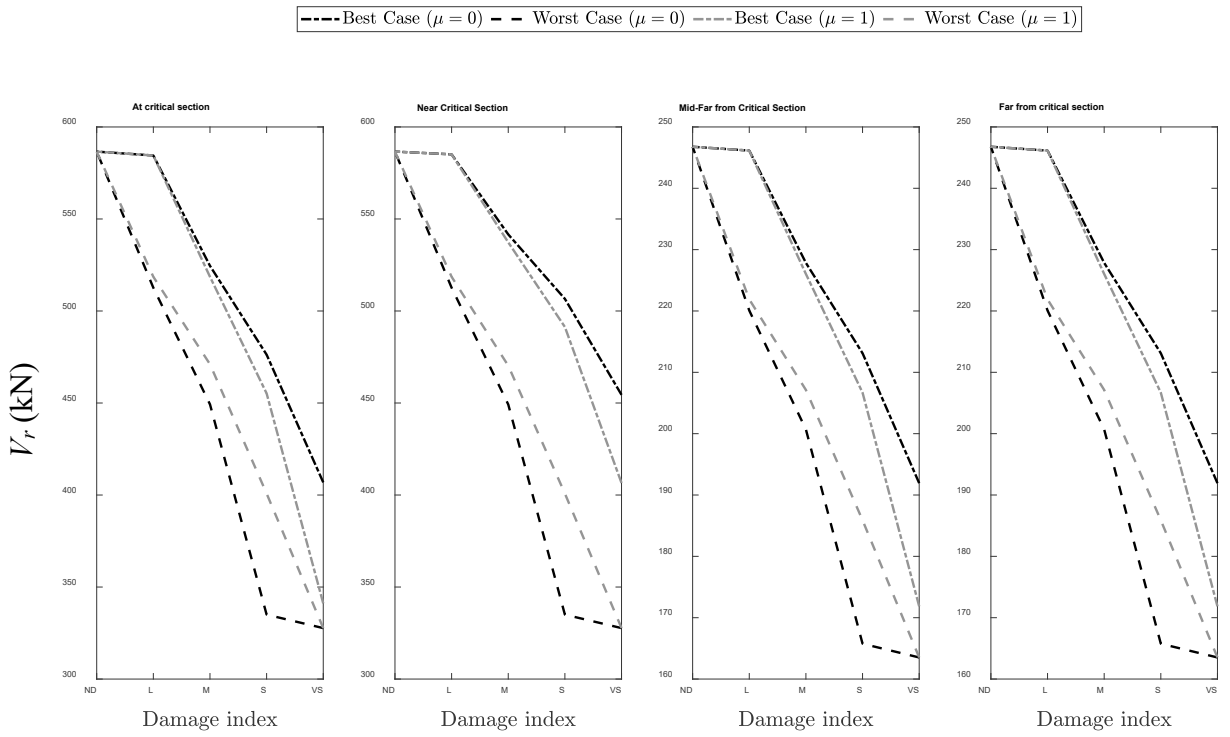

Figure 45- Shear capacity vs. Damage Indices (corrosion)

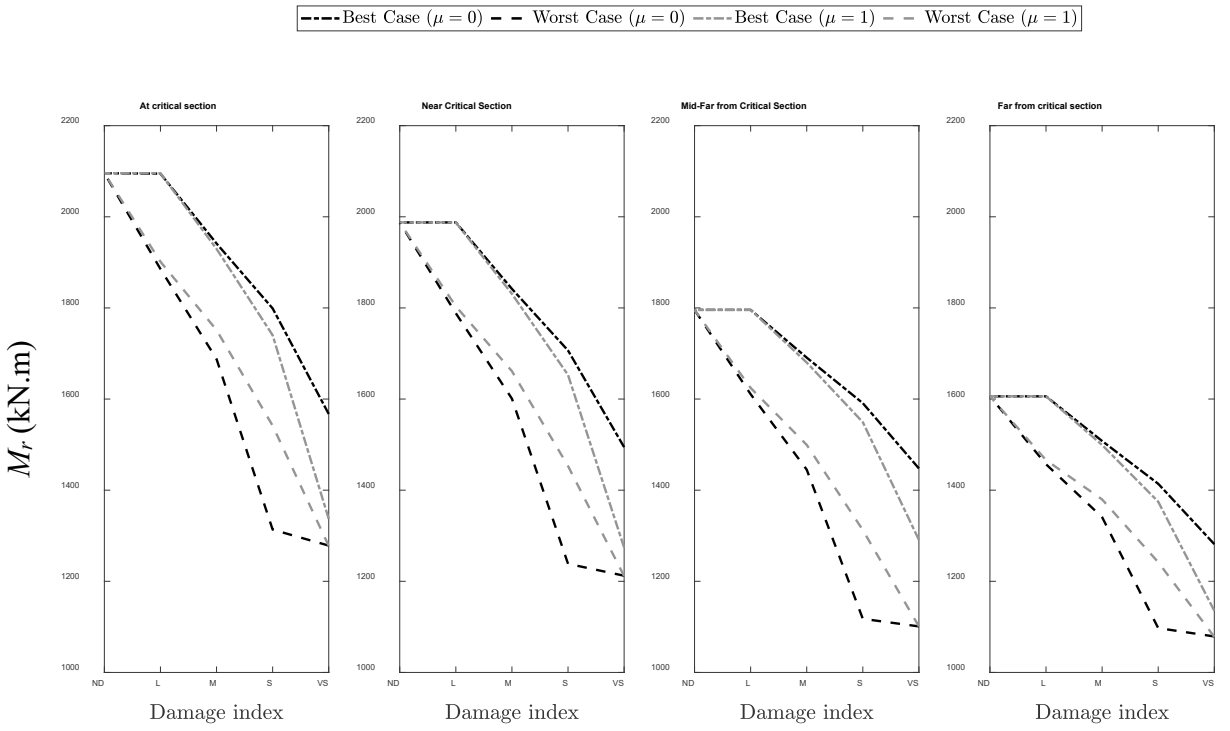

Figure 46- Moment capacity vs. Damage Indices (corrosion)

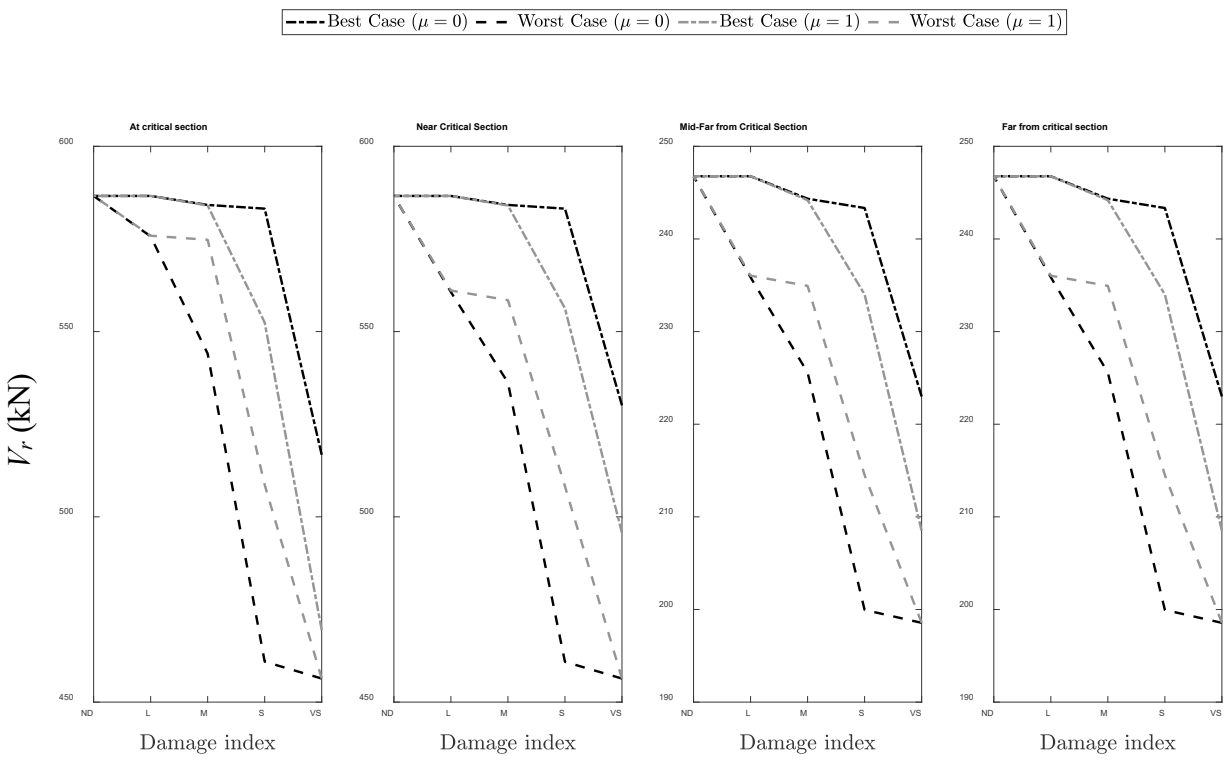

Figure 47- Shear capacity vs. Damage Indices (ASR)

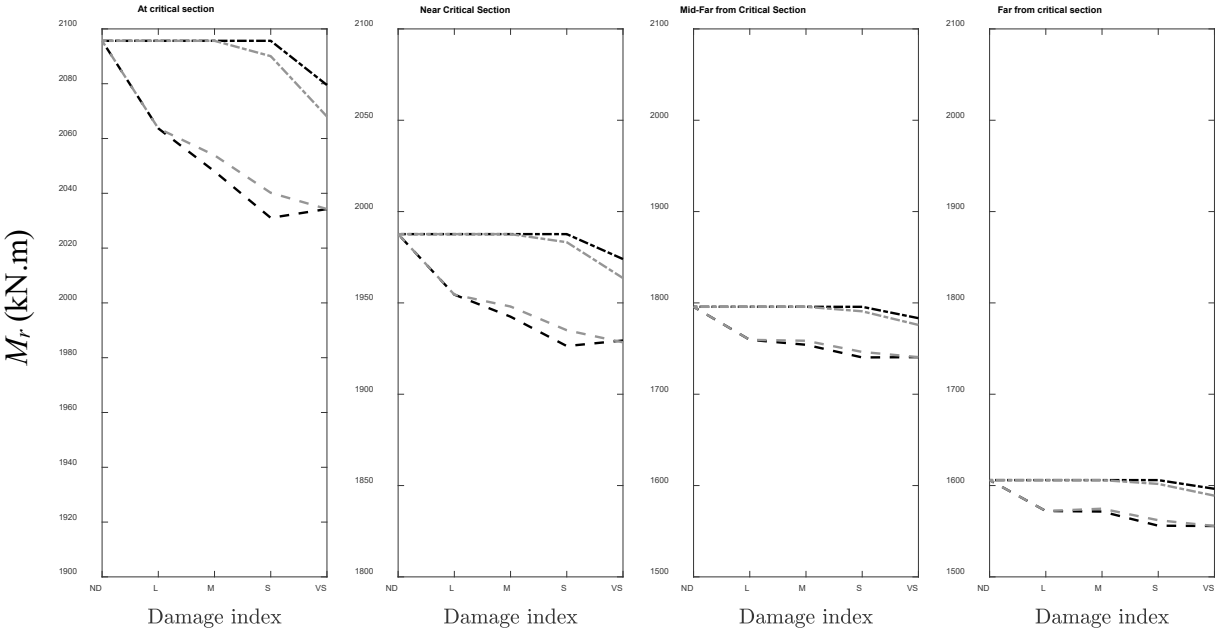

Figure 48- Moment capacity vs. Damage Indices (ASR)

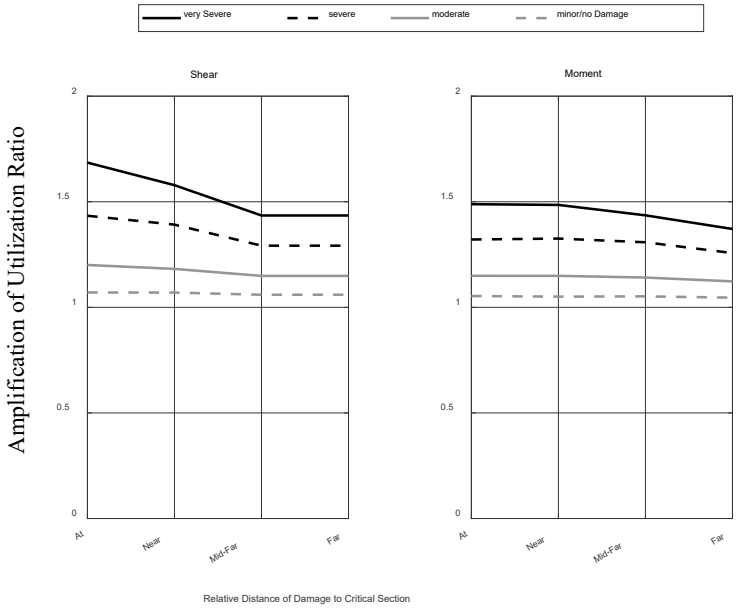

Figure 49- The amplification of the utilization ratios (corrosion)

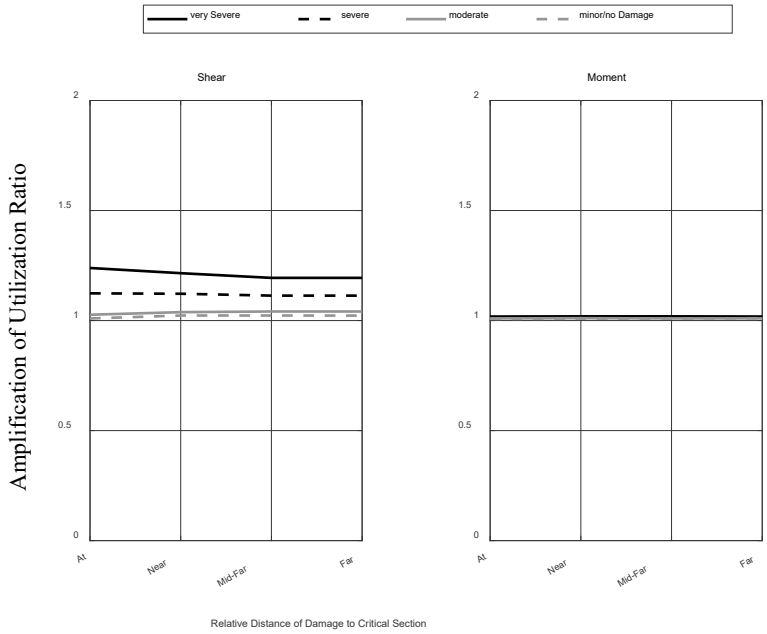

Figure 50- The amplification of the utilization ratios (ASR)

5.7 STIFFNESS-BASED CHARTS

Procedures described in section 3.7.2 have been conducted to develop the stiffness-based charts. With an iterative regression analysis, the weights for each location-severity pair of damage have been calculated (Eq. 22). This procedure has been repeated twice for corrosion-induced and ASR-induced damage. Table 7 represent the weights calculated for the corrosion-induced and ASR-induced cases, while the weights of the "at cross-section" and "no damage" have been set to unity to reduce the number of iterations. For the case of this study, one set of weights resulted in well-fitted graphs.

Table 7- W_{ij} for corrosion-induced and ASR-induced damaged girder

Severity	Location					
	Top End	Top Mid	Side End	Side Mid	Bottom End	Bottom Mid
Very Severe	0.7	0.4	0.8	0.7	0.7	0
Severe	0.75	0.55	0.85	0.75	0.85	0.20
Moderate	0.80	0.75	0.90	0.80	0.90	0.75
Light	0.90	0.85	0.95	0.90	1	1
No Damage	1	1	1	1	1	1

Using the weights, W_{ij}, one can calculate the displacement amplification factors, *DAF*, at each condition indices, *CI*, using equations (22) and (23). Figure 51 and Figure 52 represent *DAF* vs. *CI* of corrosion-induced and ASR-induced damage for the fuzzy cases, while Figure 53 illustrates the defuzzified version of those graphs. Although the graphs do not follow a similar pattern, one could use them to predict the range of *DAF* for a specific damage scenario. As an example, using Figure 53, one could estimate a range of *DAF* between 1.5 to 1.7 for $CI = 80$ for corrosion-induced cases. For ASR-induced cases, the estimated *DAF* range is 1.45 to 1.55 for the same *CI*.

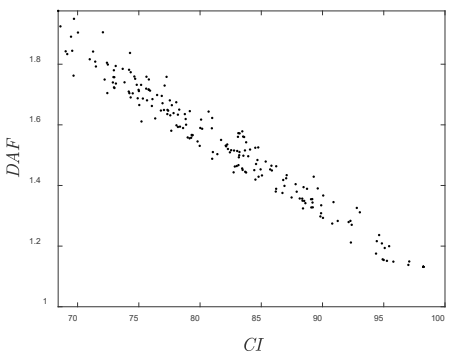

(a) *DAF* vs. *CI* for μ_0 (best)

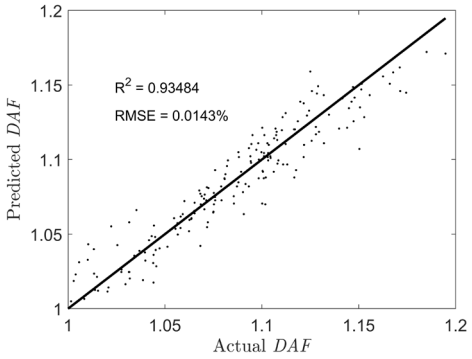

(b) Predicted vs. actual *DAF* for μ_0 (best)

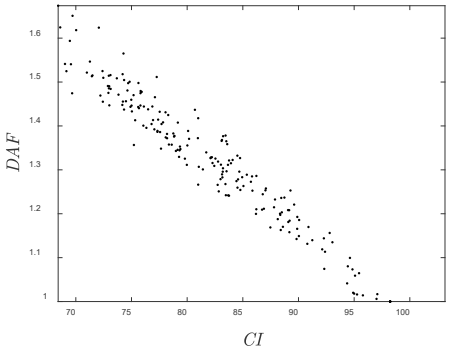

(c) *DAF* vs. *CI* for μ_0 (worst)

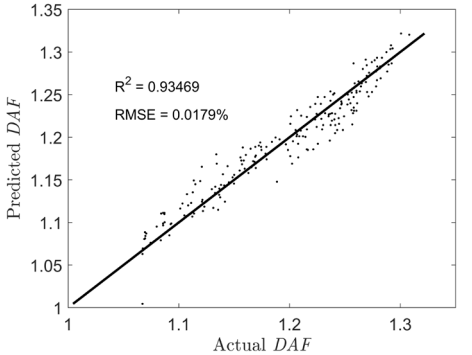

(d) Predicted vs. actual *DAF* for μ_0 (worst)

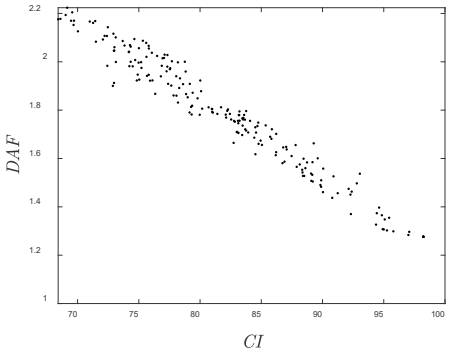

(e) *DAF* vs. *CI* for μ_1 (best)

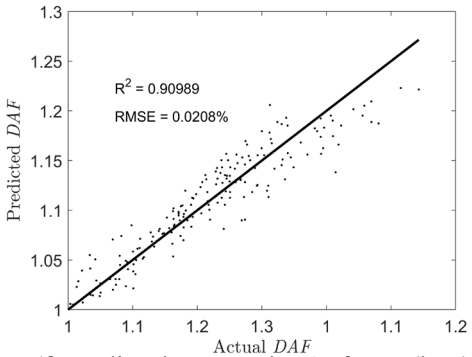

(f) Predicted vs. actual *DAF* for μ_1 (best)

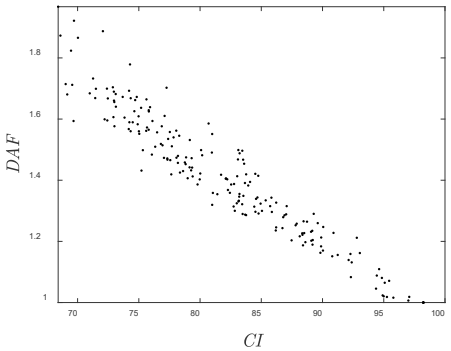

(g) *DAF* vs. *CI* for μ_1 (worst)

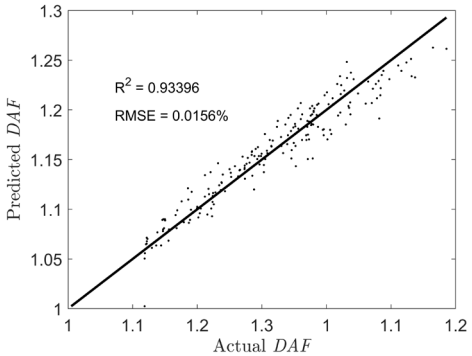

(h) Predicted vs. actual *DAF* for μ_1 (worst)

Figure 51- Predicted vs. Actual Displacement Amplification Factor (*DAF*) for different fuzzy conditions (Corrosion)

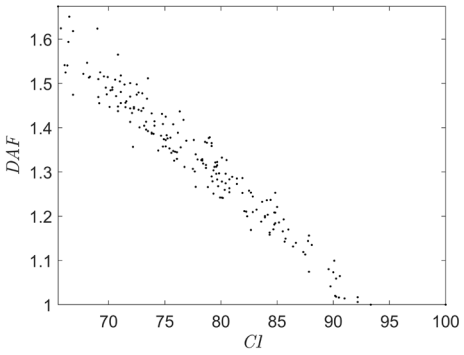

(a) *DAF* vs. *CI* for μ_0 (best)

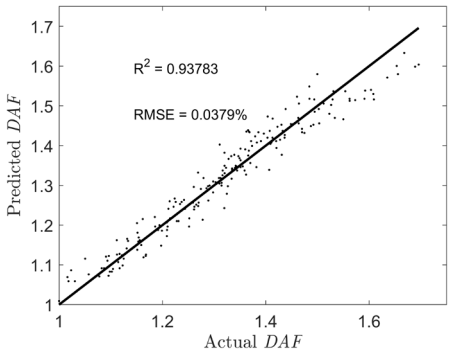

(b) Predicted vs. actual *DAF* for μ_0 (best)

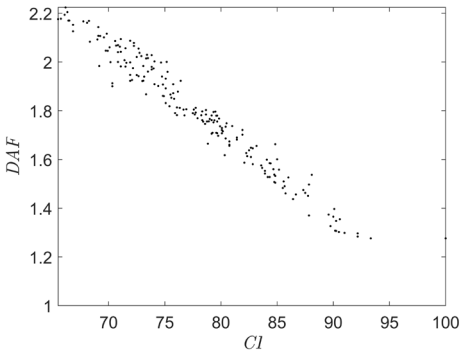

(c) *DAF* vs. *CI* for μ_0 (worst)

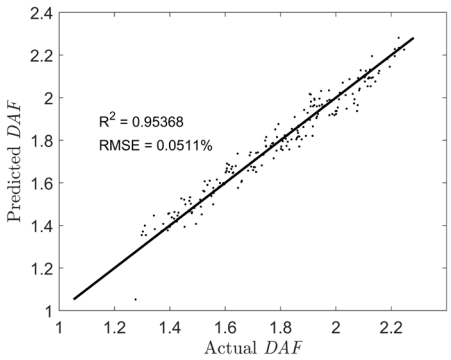

(d) Predicted vs. actual *DAF* for μ_0 (worst)

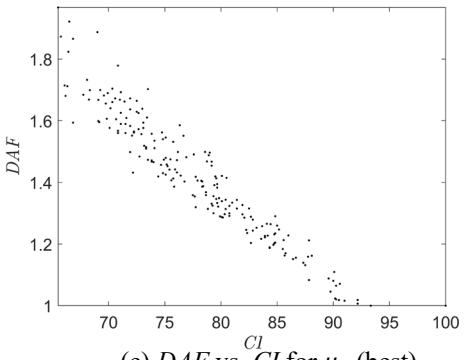

(e) *DAF* vs. *CI* for μ_1 (best)

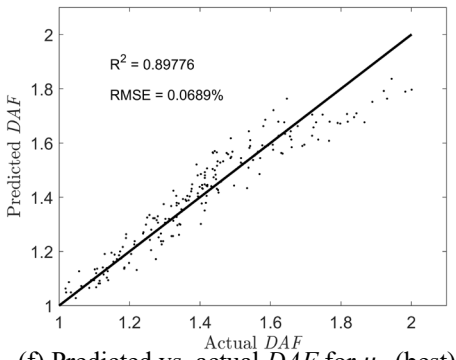

(f) Predicted vs. actual *DAF* for μ_1 (best)

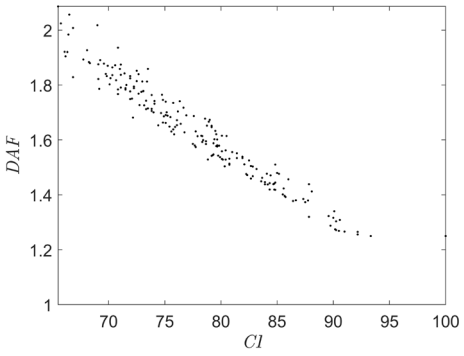

(g) *DAF* vs. *CI* for μ_1 (worst)

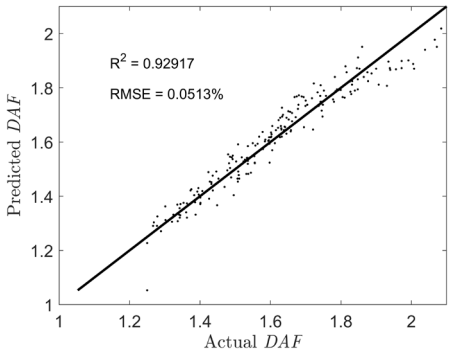

(h) Predicted vs. actual *DAF* for μ_1 (best)

Figure 52- Predicted vs. Actual Displacement Amplification Factors (*DAF*) for different fuzzy conditions (ASR)

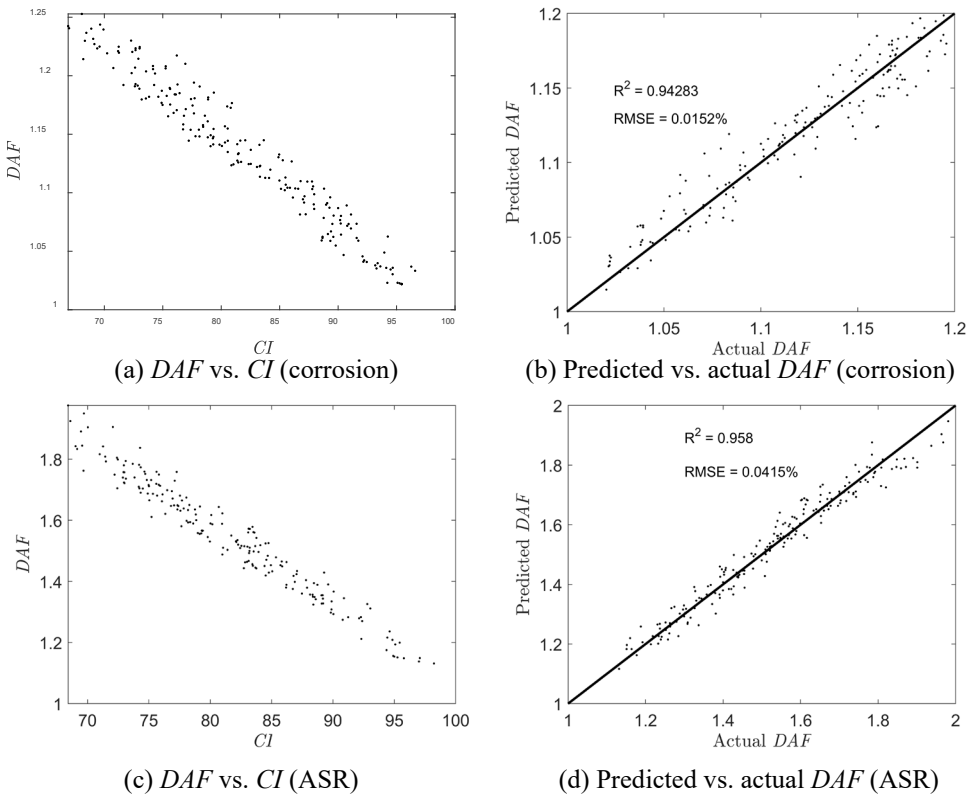

(a) *DAF* vs. *CI* (corrosion)

(b) Predicted vs. actual *DAF* (corrosion)

(c) *DAF* vs. *CI* (ASR)

(d) Predicted vs. actual *DAF* (ASR)

Figure 53- Predicted vs. Actual Displacement Amplification Factors (*DAF*) – Defuzzified

5.8 BRIDGE LOAD RATING BASED ON CSA S6:19

Bridge load rating is a process of calculating the weight of trucks that are allowed to pass safely over the bridge, without causing distress to the bridge, or danger to the other users of the road. CSA S6:19 suggests calculating the Live Load Capacity Factors (LLCF) for three levels of evaluations (levels 1, 2, and 3), and based on three vehicles. A level 1 evaluation shall be carried out if the bridge is required to carry CL1-*W* trucks, known as vehicle trains. Similarly, level 2 and level 3 evaluations are necessary if the bridge is to carry CL2-*W* (two-axle vehicles) or CL3-*W* (single-unit vehicles), respectively, where *W* shall be taken as 625 kN unless a regulatory body authorizes users lesser or more values. In this study, *W* is considered equal to 625 kN. Figure 54 shows the tuck and the lane loading for evaluation as of Chapter 14 of CSA S6. LLCF for ultimate limit states shall be calculated as follows:

$$F = \frac{UR_r - \sum \alpha_D D - \sum \alpha_A A}{\alpha_L L(1+I_D)} \quad (24)$$

where,

A= Force effects due to additional loads (creep, shrinkage, etc.)

D = Dead loads

L = Live loads

R_r= Ultimate resistance of the member

U = Resistance adjustment factor

I_D = Dynamic load allowance

α_A = Load factor for force effects due to additional loads (creep, shrinkage, etc.)

α_D = Load factor for force effects due to dead loads

α_L = Load factor for force effects due to live loads

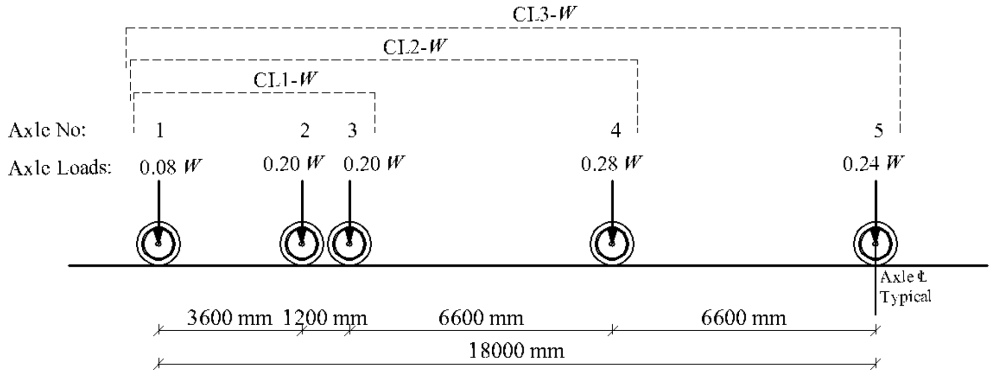

(a) CL-W truck Loading

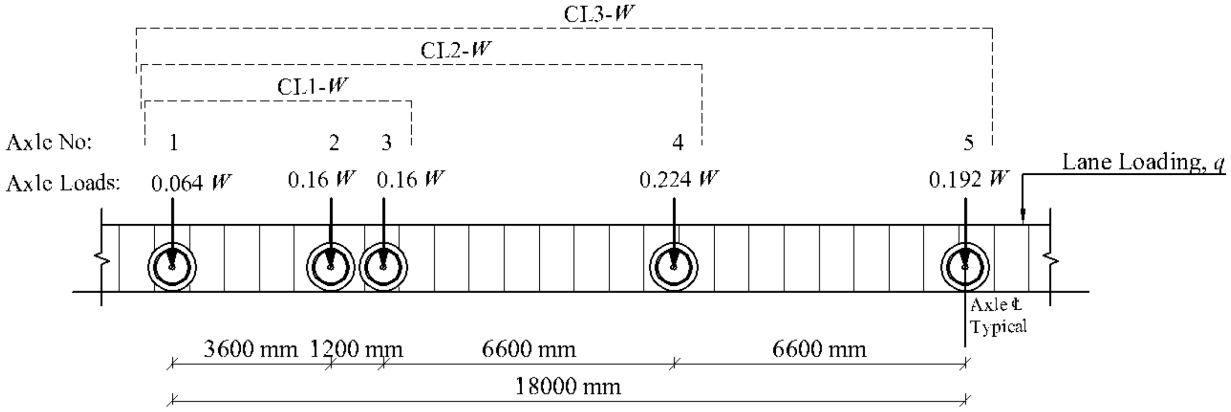

(b) CL-W lane loading

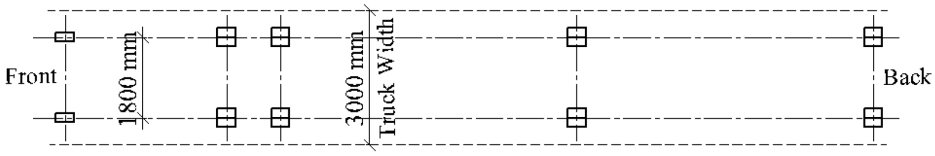

(c) CL-W loading plan view

Figure 54- CL-*W* truck and lane loadings (CSA S6:19)

The parameters used in the evaluation procedure have been presented in Table 8. One could calculate the ultimate girder's resistance, R_r, based on the method described in this study to consider the damaged conditions. The inspection of the girder shown in Figure 1 and Figure 2 indicated very severe damage to the bottom portion of the girder and severe damage to the side of

the girder, at most of the length of the girder under consideration. Based on these field results, one could use Figure 49 and Figure 50 to calculate the amplification of the utilization ratios for the shear and moment load effects and calculate the *LLCF*s based on the existing condition of the girder. An *LLCF* of less than one indicates that the girder's capacity is insufficient to tolerate the design truck loads (refer to Figure 55 and Figure 56 showing the *LLCF* based on the shear failure and the moment failure mechanisms).

Figure 55 shows the *LLCF* results based on the shear failure mechanism considering very severe (VS) damage at and near the critical section, and severe (S) damage at other sections at the side face of the girder. As can be seen, the *LLCF* is 0.33, 0.34, and 0.49 for CL1-625, CL2-625, and CL3-625, respectively. Figure 56, on the other hand, shows the *LLCF*s for the moment failure mechanism, with a minimum of 0.37, 0.31, and 0.28 for CL1-625, CL2-625, and CL3-625, respectively. The results show that a VS corrosion at the critical section for shear (at the start and end of the girder) and moment (around the midspan) could make the bridge incapable of carrying the loads of normal vehicles.

Table 8- Design parameters as of CSA S6:19- Chapters 3 and 14

Item	**Shear**	**Moment**
System Behavior Category	S2	S2
Element Behavior Category	E2	E3
Inspection Level	INSP2	INSP2
Traffic Type	Normal Traffic	
Type of Analysis	Sophisticated	
Reliability index, β	3.25	3.00
Dead (1) load factor, α_{D1}	1.08	1.07
Dead (2) load factor, α_{D2}	1.16	1.14
Dead (3) load factor, α_{D3}	1.40	1.35
Live load factor, α_L	1.56	1.49
Resistance adjustment factor, U		
Dynamic load allowance, I_D	0.25 or 0.30 based on the number of CL-W axles considered	
Max. number of design lanes, n	3	
Lane width, w_l (mm)	3’650	
Multiple loaded lanes reduction factor	$\begin{cases} 1.0 & (\text{if } n = 1) \\ 0.9 & (\text{if } n = 2) \\ 0.8 & (\text{if } n = 3) \end{cases}$	

Disclaimer: The analysis in Chapter 5 is based on simplified assumptions and limited available field data, which may not fully represent real-world conditions. Those limitations could affect the conclusions. A more detailed and refined analysis, incorporating additional parameters and more accurate inspection, may lead to different findings.

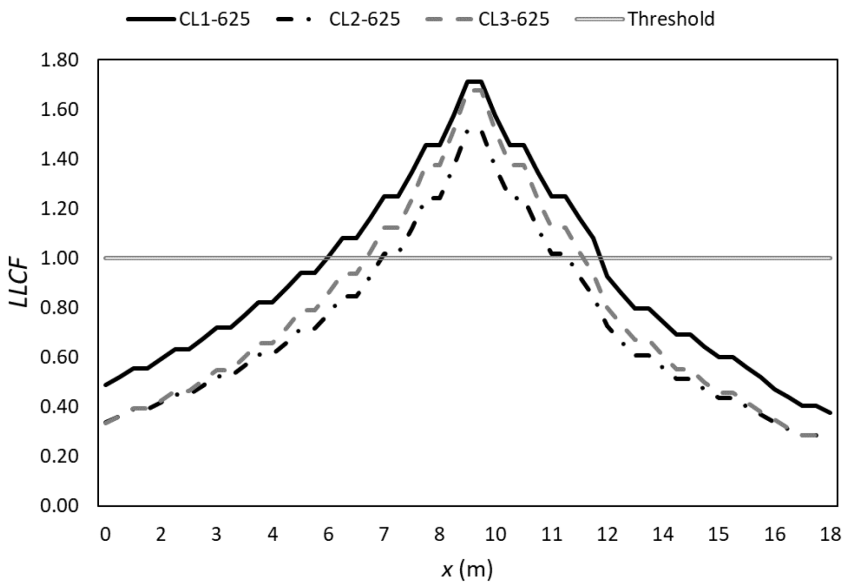

Figure 55- *LLCF* of the damaged girder calculated based on the shear failure

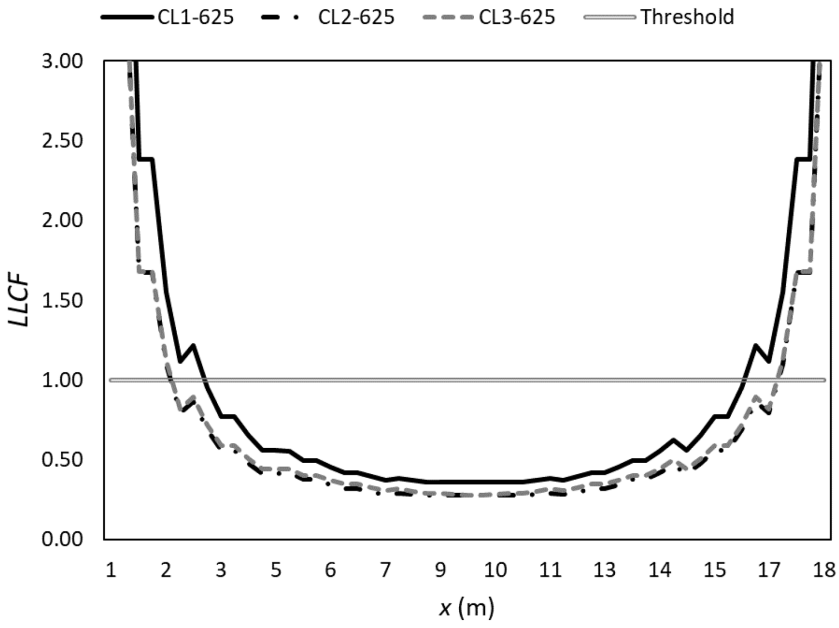

Figure 56- *LLCF* of the damaged girder calculated based on the moment failure

CHAPTER 6 CONCLUSIONS AND RECOMMENDATIONS

6.1 SUMMARY AND CONCLUSIONS

This study introduces a pioneering performance rating system tailored for deteriorating structures, called the universal performance rating system (UPRS). It leverages fuzzy logic theory to yield quantitative measurements of a structure's current performance, utilizing only visual inspection data. Visual inspection of existing structures provides valuable data such as the damage severity and location. These valuable data could just lead to some judgmental linguistic descriptions of the condition of the structure if remained unprocessed (e.g., moderate, or severe defects). The proposed UPRS processes the qualitative measurements common in visual inspections using a numerical-fuzzy approach and provides the decision-makers with numerical representations of the remaining performance of the structure, helping them to identify the defects, and decide on the next steps necessary for the assessment of the structure. By applying this methodology, the uncertainties associated with visual inspection methods, and the decision-making after that, will be minimized. The proposed methodology comprises the following key steps:

Step 1. Establishing structural performance criteria relevant to the structure under evaluation.

Step 2. Developing relevant material degradation models.

Step 3. Developing a fuzzy logic model capable of translating descriptive damage conditions to numerical values of material properties.

Step 4. Generating randomized damage scenarios (i.e., deterioration patterns) based on the properties of the undamaged structure.

Step 5. Conducting a fuzzy-numerical analysis based on the material degradation models to

evaluate the performance of each damage scenario.

Step 6. Developing fuzzy and defuzzified strength and stiffness-based performance charts to establish relationships between the pair of damage location and severity and the remaining performance of the structure.

The developed methodology has been applied to two illustrative examples: (a) an RC bridge girder designed according to CSA S6:19 suffered from corrosion, and (b) an existing bridge in NS, Canada including AASHTO type (II) PS concrete girders suffered from corrosion and ASR. For each example, the strength and stiffness-based performance charts have been developed relating the location and severity of damage to the remaining performance of the structure. In the first example, the shear and moment utilization ratios of the RC girder at the critical section have changed from less than unity to 1.35 and 1.6, respectively, for very severe damage, showing the probability of distress and failure. In this example, the displacement amplification factor, which represents the ratio of the maximum displacements of the damaged girder to an undamaged one, increased from unity for undamaged conditions to more than 1.60 for $CI = 45$. For the second example, very severe corrosion-induced damage at the critical location increased the amplification of utilization ratios of shear and moment to 1.6 and 1.5, respectively. Those ratios have been 1.25 and 1.03 in the case of ASR-induced damage for the shear and moment, respectively, showing that ASR mostly affected the shear resistance of the girder. Corrosion-induced and ASR-induced damage caused the deflection to increase by 25% and 85% compared to the undamaged conditions, indicating that ASR affects the deflection more than corrosion does.

6.2 RECOMMENDED FUTURE RESEARCH

The scope of this study focused on utilizing UPRS on concrete bridge superstructures. To further advance this research field, the following areas of future investigations are recommended:

- *Application to Various Structural Systems:* Future studies could explore the adaptability of the proposed framework to a wider range of structures and construction materials, including but not limited to offshore structures, buildings, and industrial facilities. Adapting the framework to various structural types would necessitate an extensive examination of the unique challenges posed by each.
- *Application to Various Damage Mechanisms*: The research focused on environmentally driven deterioration mechanisms, such as corrosion and ASR. Expanding the framework to cover structures subjected to various forms of damage, such as fire, seismic events, and overloading, would be a valuable avenue for future research. Each type of damage introduces unique challenges and considerations in assessing structural performance. Investigating these cases would make the system more versatile and applicable to a broader spectrum of structures and scenarios.
- *Exploring Different Analysis Techniques*: While this research primarily utilizes linear analysis methods, future research could delve into nonlinear analysis approaches. Nonlinear analyses can offer more accurate capacity estimation for the ultimate and serviceability limit states of deteriorated structures under various loading conditions and deterioration patterns, enhancing the framework's robustness and versatility.
- *Integration with Advanced Inspection Techniques*: To further enhance the applicability of the performance rating system, future research should explore the integration of advanced inspection techniques. This includes incorporating technologies like ground-penetrating

radar (GPR) to detect hidden damages not observable through traditional visual inspection. The fusion of fuzzy-logic analysis with other inspection techniques could add to the comprehensiveness and accuracy of current structural assessment methods.

BIBLIOGRAPHY

AASHTO Bridge Element Inspection Guide Manual (2010).

Abdelmaksoud, A.M., Balomenos, G.P. and Becker, T.C. (2021) 'Parameterized Logistic Models for Bridge Inspection and Maintenance Scheduling', *Journal of Bridge Engineering*, 26(10). Available at: https://doi.org/10.1061/(asce)be.1943-5592.0001774.

Abdelmaksoud, A.M., Balomenos, G.P. and Becker, T.C. (2022) 'Fuzzy-Logistic Models for Incorporating Epistemic Uncertainty in Bridge Management Decisions', *ASCE-ASME Journal of Risk and Uncertainty in Engineering Systems, Part A: Civil Engineering*, 8(3). Available at: https://doi.org/10.1061/ajrua6.0001247.

Abdelmaksoud, A.M., Becker, T.C. and Balomenos, G.P. (2023) 'Fuzzy-logic framework for updating the seismic fragility of deteriorating bridges via visual inspections', *Soil Dynamics and Earthquake Engineering*, 173. Available at: https://doi.org/10.1016/j.soildyn.2023.108105.

ACI Committee 201. and American Concrete Institute. (2008) *Guide for conducting a visual inspection of concrete in service*. American Concrete Institute.

ACI Committee 201. and American Concrete Institute. (2008) *Guide for conducting a visual inspection of concrete in service*. American Concrete Institute.

El Aghoury, I.M. and Galal, K. (2014) 'Corrosion-Fatigue Strain-Life Model for Steel Bridge Girders under Various Weathering Conditions', *Journal of Structural Engineering*, 140(6). Available at: https://doi.org/10.1061/(asce)st.1943-541x.0000992.

Ahmed, S.F.U. *et al.* (2006) 'Assessment of corrosion-induced damage and its effect on the structural behavior of RC beams containing supplementary cementitious materials', *Progress in Structural Engineering and Materials*, 8(2), pp. 69–77. Available at: https://doi.org/10.1002/pse.214.

Andrade, C. *et al.* (2016) 'Estimating corrosion attack in reinforced concrete by means of crack opening', *Structural Concrete*, 17(4), pp. 533–540. Available at: https://doi.org/10.1002/suco.201500114.

Andrić, J.M. and Lu, D.G. (2016) 'Risk assessment of bridges under multiple hazards in operation period', *Safety Science*, 83, pp. 80–92. Available at: https://doi.org/10.1016/j.ssci.2015.11.001.

Azad, A.K., Ahmad, S. and Al-Gohi, B.H.A. (2010) 'Flexural strength of corroded reinforced concrete beams', *Magazine of Concrete Research*, 62(6), pp. 405–414. Available at: https://doi.org/10.1680/macr.2010.62.6.405.

Azad, A.K., Ahmad, S. and Asher, S.A. (2007) 'Residual Strength of Corrosion-Damaged Reinforced Concrete Beams', *ACI MATERIALS JOURNAL*, 104(05), pp. 40–50.

Bridge Inspection & Maintenance System BIM Bridge Inspection and Maintenance (2008).

Bridge Inspection Field Manual Minnesota Department of Transportation. 2.0 (2016). Minnesota Department of Transportation.

Bridge Inspection Manual; Structures, Marine and Transportation (2010). Public Works and Government Services Canada.

Brown, C.B. *et al.* (1983) *FUZZY SETS AND STRUCTURAL ENGINEERING*.

Building bridges that span a lifetime; https://nrc.canada.ca/en/stories/building-bridges-span-lifetime (2015) *Government of Canada*.

Cabrera, J.G. (1996) *Deterioration of Concrete Due to Reinforcement Steel Corrosion*, *Cement & Concrete Composites*.

Chakraverty, S. *et al.* (2019) *Concepts of Soft Computing Fuzzy and ANN with Programming*. Singapore: Springer.

Cho, H.C. *et al.* (2017) 'Fire damage assessment of reinforced concrete structures using fuzzy theory', *Applied Sciences (Switzerland)*, 7(5). Available at: https://doi.org/10.3390/app7050518.

Coronelli, D. and Gambarova, P. (2004) 'Structural Assessment of Corroded Reinforced Concrete Beams: Modeling Guidelines', *JOURNAL OF STRUCTURAL ENGINEERING*, 130(8), pp. 1214–1224. Available at: https://doi.org/10.1061/ASCE0733-94452004130:81214.

Coronelli, D. and Gambarova, P. (no date) 'Structural Assessment of Corroded Reinforced Concrete Beams: Modeling Guidelines'. Available at: https://doi.org/10.1061/ASCE0733-94452004130:81214.

CSA Group (2019) *Canadian Highway Bridge Design Code (CSA-S6:19)*. Canadian Standards Association.

Dai, L. *et al.* (2015) 'A global model for corrosion-induced cracking in prestressed concrete structures', *Engineering Failure Analysis*, 62, pp. 263–275. Available at: https://doi.org/10.1016/j.engfailanal.2016.01.013.

Dai, L. *et al.* (2019) 'Flexural Capacity Prediction of Corroded Prestressed Concrete Beams Incorporating Bond Degradation', *Journal of Aerospace Engineering*, 32(4). Available at: https://doi.org/10.1061/(asce)as.1943-5525.0001022.

Design of concrete structures (CSA A23.3:19) (2019). Canadian Standards Association (CSA) . Available at: www.csagroup.org/legal.

Desnerck, P., Lees, J.M. and Morley, C.T. (2015) 'Bond behaviour of reinforcing bars in cracked concrete', *Construction and Building Materials*, 94, pp. 126–136. Available at: https://doi.org/10.1016/j.conbuildmat.2015.06.043.

Diab, S.H., Soliman, A.M. and Nokken, M.R. (2020) 'Changes in mechanical properties and durability indices of concrete undergoing ASR expansion', *Construction and Building Materials*, 251. Available at: https://doi.org/10.1016/j.conbuildmat.2020.118951.

Du, Y.G., Clark, L.A. and Chan, A.H.C. (2005) *Residual capacity of corroded reinforcing bars*.

Esposito, R. *et al.* (2016) 'Influence of the Alkali-Silica Reaction on the Mechanical Degradation of Concrete', *Journal of Materials in Civil Engineering*, 28(6). Available at: https://doi.org/10.1061/(asce)mt.1943-5533.0001486.

Feng, Q., Visintin, P. and Oehlers, D.J. (2016) 'Deterioration of bond-slip due to corrosion of steel reinforcement in reinforced concrete', *Magazine of Concrete Research*, 68(15), pp. 768–781. Available at: https://doi.org/10.1680/jmacr.15.00217.

Five Year Highway Improvement Plan, 2023-2024 Edition (2023). Province of Nova Scotia.

Ghanooni-Bagha, M. *et al.* (2016) 'Corrosion-induced reduction in compressive strength of self-compacting concretes containing mineral admixtures', *Construction and Building*

Materials, 113, pp. 221–228. Available at: https://doi.org/10.1016/j.conbuildmat.2016.03.046.

Google Map (Barington Street over 111 Highway Overpass), M99J+X4Q Halifax, Nova Scotia (2021).

Gopinath, S., Murthy, A.R. and Iyer, N.R. (2011) *Nonlinear Finite Element Analysis of RC Structures Incorporating Corrosion Effects*, *CMC*. Available at: https://www.researchgate.net/publication/274065782.

Huang, R. and Yang, C.C. (1997) 'Condition Assessment of Reinforced Concrete Beams Relative to Reinforcement Corrosion', *Cement and Concrete Composites*, 19, pp. 131–137.

Islam, M.S. and Ghafouri, N. (2014) 'Relation of ASR-induced expansion and compressive strength of concrete', *Materials and Structures*, 48, pp. 4055–4066.

Jeon, C.H. *et al.* (2019) 'Equivalent material model of corroded prestressing steel strand', *Journal of Materials Research and Technology*. Elsevier Editora Ltda, pp. 2450–2460. Available at: https://doi.org/10.1016/j.jmrt.2019.02.010.

Jnaid, F. and Aboutaha, R.S. (2016) 'Residual flexural strength of corroded reinforced concrete beams', *Engineering Structures*, 119, pp. 198–216. Available at: https://doi.org/10.1016/j.engstruct.2016.04.018.

Jones, A.E.K. and Clark, L.A. (1998) 'The effects of ASR on the properties of concrete and the implications for assessment', *Engineering structures*, 20(9), pp. 785–791.

Karthik, M.M., Mander, J.B. and Hurlebaus, S. (2020) 'Simulating behaviour of large reinforced concrete beam-column joints subject to ASR/DEF deterioration and influence of

corrosion', *Engineering Structures*, 222. Available at: https://doi.org/10.1016/j.engstruct.2020.111064.

Kongshaug, S.S. *et al.* (2020) 'Experimental investigation of ASR-affected concrete – The influence of uniaxial loading on the evolution of mechanical properties, expansion and damage indices', *Construction and Building Materials*, 245. Available at: https://doi.org/10.1016/j.conbuildmat.2020.118384.

Lindgård, J. *et al.* (2012) 'Alkali-silica reactions (ASR): Literature review on parameters influencing laboratory performance testing', *Cement and Concrete Research*, pp. 223–243. Available at: https://doi.org/10.1016/j.cemconres.2011.10.004.

Lu, Z.-H., Li, F. and Zhao, Y.-G. (2016) 'An Investigation of Degradation of Mechanical Behaviour of Prestressing Strands Subjected to Chloride Attacking', in *International Conference on the Durability of Concrete Structures*.

Luo, J., Asamoto, S. and Nagai, K. (2022) 'An analytical investigation of bond deterioration between rebar and ASR/DEF-damaged concrete with and without stirrup confinement using 3D RBSM', *Construction and Building Materials*, 351. Available at: https://doi.org/10.1016/j.conbuildmat.2022.128923.

Marano, G.C. and Quaranta, G. (2008) 'Fuzzy-based robust structural optimization', *International Journal of Solids and Structures*, 45(11–12), pp. 3544–3557. Available at: https://doi.org/10.1016/j.ijsolstr.2008.02.016.

Markiz, N. and Jrade, A. (2018) 'INTEGRATING FUZZY-LOGIC DECISION SUPPORT WITH A BRIDGE INFORMATION MANAGEMENT SYSTEM (BRIMS) AT THE

CONCEPTUAL STAGE OF BRIDGE DESIGN', *Journal of Information Technology in Construction*, 23, pp. 92–121. Available at: http://www.itcon.org/2018/5.

Meyyappaq, L. *et al.* (no date) *Fuzzy-Neuro System for Bridge Health Monitoring*.

Michael D.A. Thomas, Kevin J. Folliard and Benoit Fournier (2013) *Methods for Preventing ASR in New Construction Results of Field Exposure Sites December 2013*.

Mitra, G. *et al.* (2010) 'Condition Assessment of Corrosion-Distressed Reinforced Concrete Buildings Using Fuzzy Logic'. Available at: https://doi.org/10.1061/ASCECF.1943-5509.0000137.

Mohammadi, A., Ghiasvand, E. and Nili, M. (2020) 'Relation between mechanical properties of concrete and alkali-silica reaction (ASR); a review', *Construction and Building Materials*. Elsevier Ltd. Available at: https://doi.org/10.1016/j.conbuildmat.2020.119567.

Nieto-Morote, A. and Ruz-Vila, F. (2011) 'A fuzzy approach to construction project risk assessment', *International Journal of Project Management*, 29(2), pp. 220–231. Available at: https://doi.org/10.1016/j.ijproman.2010.02.002.

Nürnberger, U. (2002) 'Corrosion induced failure mechanisms of prestressing steel', *Materials and Corrosion*, 53(8), pp. 591–601. Available at: https://doi.org/10.1002/1521-4176(200208)53:8<591::AID-MACO591>3.0.CO;2-X.

Omar, T., Nehdi, M.L. and Zayed, T. (2017) 'Integrated Condition Rating Model for Reinforced Concrete Bridge Decks', *Journal of Performance of Constructed Facilities*, 31(5). Available at: https://doi.org/10.1061/(asce)cf.1943-5509.0001084.

Ontario Data Catalogue, Bridge Condition (2021). Available at: https://data.ontario.ca/dataset/bridge-conditions (Accessed: 26 October 2023).

Oudah, Fadi. 'Time-dependent reliability-based charts to evaluate the structural safety of RC wharf decks exposed to corrosion and freeze-thaw effect.' *Engineering Structures* 283 (2023): 115887.

Parulekar, Y.M. *et al.* (2020) 'Performance Assessment of Corroded Reinforced Concrete Structure Considering Bond Deterioration', *Journal of Performance of Constructed Facilities*, 34(2). Available at: https://doi.org/10.1061/(asce)cf.1943-5509.0001411.

Peng, J. *et al.* (2022) 'Prediction and optimization of the flexural behavior of corroded concrete beams using adaptive neuro fuzzy inference system', *Structures*, 43, pp. 200–208. Available at: https://doi.org/10.1016/j.istruc.2022.06.043.

Salili, S., Abdelmaksoud, A. and Oudah, F. (2023) 'A Universal Performance-Based Rating System for Existing Structures via Fuzzy Logic: A General Framework', in. Moncton: Canadian Society for Civil En- gineering 2023 Annual Meeting (CSCE 2023). Available at: https://www.researchgate.net/publication/371599431.

Sanchez, L.F.M. *et al.* (2016) 'Practical use of the Stiffness Damage Test (SDT) for assessing damage in concrete infrastructure affected by alkali-silica reaction', *Construction and Building Materials*, 125, pp. 1178–1188. Available at: https://doi.org/10.1016/j.conbuildmat.2016.08.101.

Sanchez, L.F.M. *et al.* (2017) 'Overall assessment of Alkali-Aggregate Reaction (AAR) in concretes presenting different strengths and incorporating a wide range of reactive aggregate types and natures', *Cement and Concrete Research*, 93, pp. 17–31. Available at: https://doi.org/10.1016/j.cemconres.2016.12.001.

Shayanfar, M.A., Barkhordari, M.A. and Ghanooni-Bagha, M. (2016) 'Effect of longitudinal rebar corrosion on the compressive strength reduction of concrete in reinforced concrete structure', *Advances in Structural Engineering*, 19(6), pp. 897–907. Available at: https://doi.org/10.1177/1369433216630367.

Siddiquee, K. and Shahria Alam, M. (2017) 'Highway bridge infrastructure in the province of British Columbia (BC), Canada', *Infrastructures*, 2(2). Available at: https://doi.org/10.3390/infrastructures2020007.

Steware, M.G. and Rosowsky, D. V (1998) 'STRUCTURAL SAFETY AND SERVICEABILITY OF CONCRETE BRIDGES SUBJECT TO CORROSION', *JOURNAL OF INFRASTRUCTURE SYSTEMS*, 4(4), pp. 146–155.

Tahershamsi, M. *et al.* (2017) 'Investigating correlations between crack width, corrosion level and anchorage capacity', *Structure and Infrastructure Engineering*, 13(10), pp. 1294–1307. Available at: https://doi.org/10.1080/15732479.2016.1263673.

Tee, A.B., Bowman, M.D. and Sinha, K.C. (1988) *Application of Fuzzy Logic to Condition Assessment of Concrete Slab Bridges*.

THE MANUAL FOR BRIDGE EVALUATION (2018). Available at: www.transportation.org.

Thomas, M.D.A. *et al.* (2011) *Alkali-Silica Reactivity Field Identification Handbook*.

Vereecken, E. *et al.* (2021) 'Assessment of corroded prestressed and posttensioned concrete structures: A review', *Structural Concrete*, 22(5), pp. 2556–2580. Available at: https://doi.org/10.1002/suco.202100050.

Wang, L. *et al.* (2013) 'Probabilistic Analysis of Corrosion of Reinforcement in RC Bridges Considering Fuzziness and Randomness', *Journal of Structural Engineering*, 139(9), pp. 1529–1540. Available at: https://doi.org/10.1061/(asce)st.1943-541x.0000738.

Wang, L. *et al.* (2017) 'Failure analysis of corroded PC beams under flexural load considering bond degradation', *Engineering Failure Analysis*, 73, pp. 11–24. Available at: https://doi.org/10.1016/j.engfailanal.2016.12.004.

Wang, L. *et al.* (2019) 'Concrete cracking prediction under combined prestress and strand corrosion', *Structure and Infrastructure Engineering*, 15(3), pp. 285–295. Available at: https://doi.org/10.1080/15732479.2018.1550519.

Washer, G. (2001) *Reliability of Visual Inspection for Highway Bridges, Volume I: Final Report*. Available at: http://www.tfhrc.gov/hnr20/nde/home.htm.

Wu, Y. and Nürnberger, U. (2009) 'Corrosion-technical properties of high-strength stainless steels for the application in prestressed concrete structures', *Materials and Corrosion*, 60(10), pp. 771–780. Available at: https://doi.org/10.1002/maco.200905279.

Yuan, W., Guo, A. and Li, H. (2020) 'Equivalent elastic modulus of reinforcement to consider bond-slip effects of coastal bridge piers with non-uniform corrosion', *Engineering Structures*, 210. Available at: https://doi.org/10.1016/j.engstruct.2020.110382.

Zadeh, L.A. (1965) 'Fuzzy Sets', *Information and Control*, 8, pp. 338–353.

Zahedi, A., F M Sanchez, L. and Noël, M. (2022) 'Appraisal of visual inspection techniques to understand and describe ASR-induced development under distinct confinement conditions', *Construction and Building Materials*, 323. Available at: https://doi.org/10.1016/j.conbuildmat.2022.126549.

Zambon, I. *et al.* (2019) 'Condition prediction of existing concrete bridges as a combination of visual inspection and analytical models of deterioration', *Applied Sciences (Switzerland)*, 9(1). Available at: https://doi.org/10.3390/app9010148.

Zhang, X. *et al.* (2017) 'Flexural behavior of bonded post-tensioned concrete beams under strand corrosion', *Nuclear Engineering and Design*, 313, pp. 414–424. Available at: https://doi.org/10.1016/j.nucengdes.2017.01.004.

Zhang, Y. *et al.* (2019) 'Corrosion-fatigue evaluation of uncoated weathering steel bridges', *Applied Sciences (Switzerland)*, 9(17). Available at: https://doi.org/10.3390/app9173461.

Zhychkovska, O. (2020) *Effect of Alkali-Silica Reaction (ASR) on Steel-Concrete Bond*. University of Toronto. Available at: https://hdl.handle.net/1807/101053 (Accessed: 30 September 2023).